TABLE OF CONTENTS

Page

LIST OF TABLES

Page

LIST OF FIGURES

LIST OF ABREVIATIONS

AC	Alternating current
Al_2O_3	Aluminum oxide or Alumina
AlN	Aluminium nitride
BDS	Broadband dielectric spectroscopy
BN	Boron nitride
CNT	Carbon nanotubes
DC	Direct current
DMA	Dynamic mechanical analysis
DSC	Differential scanning calorimetry
E	Electric field
FTIR	Fourier transformed infrared spectroscopy
GO	Graphene oxide
HDPE	High density polyethylene
HRSEM	High resolution scanning electron microscopy
HV	High voltage
HVAC	High voltage alternating current
HVDC	High voltage direct current
LDPE	Low density polyethylene
MA	Maleic anhydride
MgO	Magnesium oxide
MMT	Montmorillonite
MWS	Maxwell Wagner Sillars (polarization)
PE	Polyethylene
PEB	Poly(ethylene-co-butylene)
PEO	Polyethylene oxide
PMMA	Poly(methyl methacrylate)
POE	Polyolefin elastomer
POSS	Polyhedral oligomeric silsesquioxane
PP	Polypropylene

PS	Polystyrene
SAOS	Small amplitude oscillatory shear
SAXS	Small angle X-ray scattering
SBR	Styrene-butadiene rubber
SEBS	Polystyrene-b-poly(ethylene-co-butylene)-b-polystyrene
Si3N4	Silicon nitride
SiC	Silicon carbide
SiO_2	Silicon dioxide or Silica
TEM	Transmission electron microscopy
TiO_2	Titanium oxide
VFT	Vogel Fulcher Tammann equation
XLPE	Crosslinked polyethylene
ZnO	Zinc oxide

LIST OF SYMBOLS

G’	Storage modulus
G’’	Loss modulus
t	Thickness
T	Temperature
tanδ	Loss tangent or dissipation factor in BDS measurements
T_g	Glass Transition
T_{gi}	Interfacial Glass Transition
W_a	Wetting coefficient
δ	Surface tension
Δε	Dielectric strength
ε	Complex dielectric permittivity
ε’	Real part of dielectric permittivity
ε’’	Imaginary part of dielectric permittivity
η*	Complex viscosity
λ	Thermal conductivity
σ	Conductivity modulus
σ’	Real part of complex conductivity
τ	Relaxation time
ω	Angular frequency

CHAPTER 1:

INTRODUCTION

1.1 Overview and research problem

Insulating systems are a very important part of any high voltage (HV) apparatus and require well design and adequate reliability. An interesting example is the insulating materials that are being used in high voltage power cables for transmitting power over long distances. They are constantly subjected to increasing electrical and thermal stresses as the demand for electricity increases worldwide. New power cables require more durable insulation to meet the growing operating voltages and power ratings. To address this urgent need a huge amount of research has been conducted in recent decades to develop new reliable and cost-effective insulating materials for HV cables. This has led to the introduction of nanocomposites as potential candidates to replace the existing insulating materials, known as "Nanodielectrics" (Lewis 1994, Cao, Irwin et al. 2004, Tanaka 2005, Fréchette, Reed et al. 2006).

Current insulating materials used in HV power cables suffer from some drawbacks. In HV alternating current (HVAC) systems, XLPE or cross-linked polyethylene is the main choice due to its excellent electrical properties and thermo-mechanical stability even at elevated temperatures. However, crosslinking makes XLPE a thermoset material and therefore not recyclable which has recently raised a lot of concerns from the environmental point of view (Lawson 2013). Also, XLPE has shown to have serious issues when used in HV Direct current (HVDC) systems, i.e. the accumulation of space charges, which has led to industry sticking with older technologies such as paper-oil cables with a lot of disadvantages including cost of fabrication, installation and repair (Mazzanti and Marzinotto 2013).

1.2 Motivations

Nanodielectrics, mostly polymers reinforced with inorganic nanoparticles, are believed to feature promising properties as insulating materials in both HVAC and HVDC systems, despite the fact that their reliability and reproducibility massively depend on the quality of the dispersion of nanoparticles which is a challenging task to achieve (Fréchette, Larocque et al. 2008, Kindersberger, Tanaka et al. 2011, David and Fréchette 2013). During nanocomposite processing, the inorganic nanoparticles tend to form agglomerations due to their incompatibility with the organic polymers. This reduces the potential benefits of the nanoscale reinforcement and affects the suggested/proved abilities of nanodielectrics to enhance the functional properties (David and Fréchette 2013). Numerous attempts have been done by researchers to resolve and prevent the agglomeration of nanoparticles. Most popular techniques include addition of compatibilizer (Reichert, Nitz et al. 2000, Wang, Choi et al. 2001, Garcıa-López, Picazo et al. 2003, Hasegawa and Usuki 2004), functionalization of the surface of nanoparticles (Wu, Wu et al. 2008, Liu, Wang et al. 2009), and in situ polymerization or synthesis of nanoparticles (Shin, Simon et al. 2003, Fim, Basso et al. 2013, Hakim, Nekoomanesh et al. 2018).

A new approach in this regards is to selectively accommodate nanoparticles in a template matrix to control their quality of the dispersion and their spatial distribution. In particular, an immiscible blend as the matrix would offer the possibility to disperse the nanofiller according to its micrometric morphology and guide them towards final locations based on the affinity between nanoparticles and different phases in the blend matrix (Ray, Pouliot et al. 2004, Elias, Fenouillot et al. 2007, Elias, Fenouillot et al. 2008, Graziano, Jaffer et al. 2018). Thanks to their tunable microstructure, it is possible to selectively locate and disperse nanoparticles within the immiscible blend matrix and improve certain physical properties when the base materials are properly selected and processed.

1.3 Objectives

This Ph.D. project focuses on introducing novel polymeric materials with the help of nanotechnology in the aim of producing novel nanodielectrics for HV insulation systems and tailoring their functional properties in correlation with their microstructures. The new materials must be recyclable, have the ability to be easily processed and meet all the requirements for HV applications.

Low-density polyethylene (LDPE) and polypropylene (PP) were chosen as the base polymers due to their excellent electrical properties to produce advance nanodielectrics incorporating a natural clay, montmorillonite, as the nanoreinforcement. Attempts have been made to further modify the microstructure of such nanodielectrics via incorporating a compatibilizer and forming a blend matrix to host the nanofiller. In particular, two industrial grades of polystyrene-b-poly(ethylene-co-butylene)-b-polystyrene (SEBS) have been used to form a co-continuous blend with either LDPE or PP to finely tune the dispersion and localization of the nanofiller. SEBS provides good level of electrical properties while is available commercially. It is consisted of two polystyrene PS endblocks within a hydrogenated polybutadiene midblock matrix, known as poly(ethylene-co-butylene) PEB. The rubbery midblock of SEBS has a similar structure as to the main chain of both LDPE and PP indicating an expected good level of compatibility. Melt mixing via extrusion was chosen as the main technique to prepare the nanodielectrics as it is the only viable approach in the industry. Within the framework of this research, it is expected that the obtained nanodielectrics possess enhanced electrical performance while having good thermo-mechanical properties.

1.4 Methodology

From the material point of view, this PhD project covers binary nanocomposites based on LDPE and PP incorporating different loadings of nanoclay. Blends of SEBS with LDPE and PP were used to accommodate certain loadings of clay. Also, the effect of a well-known compatibilizer on the microstructure and performance of LDPE/clay nanocomposites has been evaluated.

A co-rotating twin-screw extruder was used to process the materials. Extrusion is the most common process in manufacturing plastics in industry. A premixed polyolefin-based masterbatch presumably containing 50% organomodified montmorillonite was used as the source of the nanofiller, which was direct fed into the extruder along with the polymer powder to be diluted to the desired concentrations. Thus, series of LDPE/clay and PP/clay nanocomposites are achieved. the same procedure was used to create nanocomposite with compatibilizer. To Produce blend nanocomposites equivalent amounts of SEBS and total polyolefin were fed into the extruder to ensure that the co-continuous structure would be achieved. All the obtained pellets were then press-molded in an electrically heated hydraulic press into thin plates for characterization.

The microstructure of all the prepared nanocomposites were investigated using Scanning Electron Microscopy and Transmission Electron Microscopy. The degree of dispersion of clay was evaluated through X-ray diffraction. The dielectric performance was assessed by means of broadband dielectric spectroscopy, short-term AC and DC breakdown strength, space charge measurement and electrical conductivity.

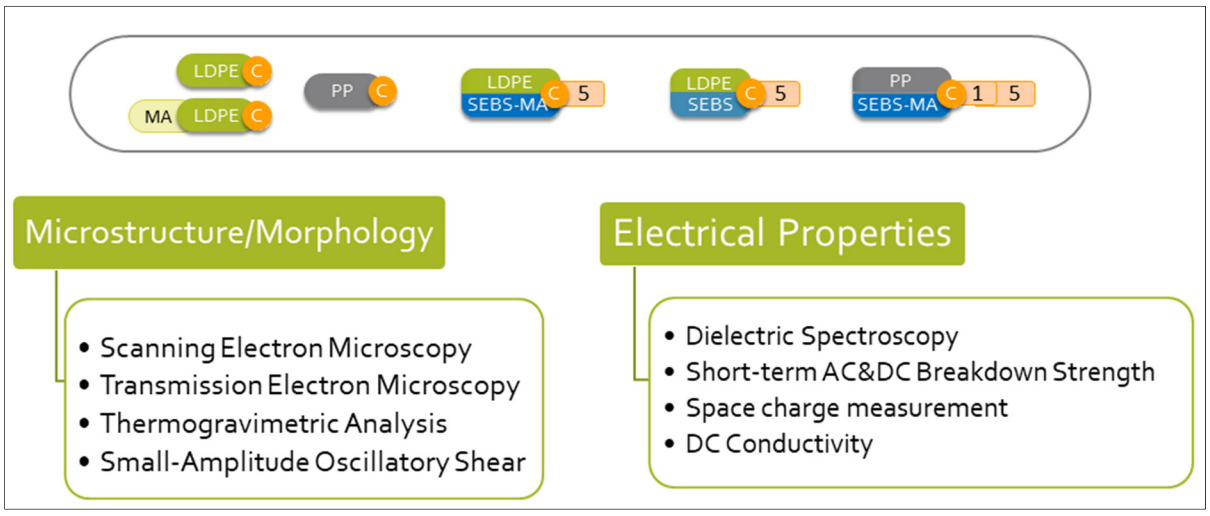

Figure 1-1 Materials and characterization methods employed in this study

1.5 Thesis Organization

This thesis in divided into 6 chapters consisting of an introduction and a brief literature review followed by 4 other chapters representing the outcome articles that are either published, accepted or submitted to related international journals.

In the first paper (chapter 3) the evolution of morphology and short-term breakdown strength of clay-containing LDPE blends and nanocomposites have been discussed. Nanoclay's dispersion/distribution states and its effect on development of co-continuous morphology of LDPE/SEBS blends are fully addressed. Also the improvement mechanism of nanoclay on breakdown strength of nanocomposites is explained.

In chapter 4 (paper 2) charge transport and accumulation in LDPE/clay nanocomposites are discussed. A correlation of DC conductivity and space charge measurements is used to have a general view towards charge trapping and transfer within the materials.

Chapter 5 (paper 3) provides an in-depth evaluation of the dielectric spectra of clay-containing LDPE blends and nanocomposites. When necessary, the spectra are fitted to theoretical models to more clarify the outcomes.

In chapter 6 (paper 4) the morphology and electrical properties of blends and nanocomposites based on PP are investigated. Finally, conclusions and recommendations for future works are provided following the last chapter.

CHAPTER 2

POLYOLEFIN NANOCOMPOSITES FOR HV INSULATIONS

2.1 Transmission of electric energy

The main objective of the power system is to provide electrical energy from power source to the consumers in a safe and reliable way at the lowest possible cost (Figure 2-1). The bulk movement of electrical energy from a generating site, usually in remote areas, to an electrical substation near cities is called the electric power transmission. This is possible with the help of interconnected lines facilitating this movement known as a transmission network. The electrical energy received in HV substation is then transferred to customers through local wiring known as electric power distribution. The combined transmission and distribution network is known as the "power grid".

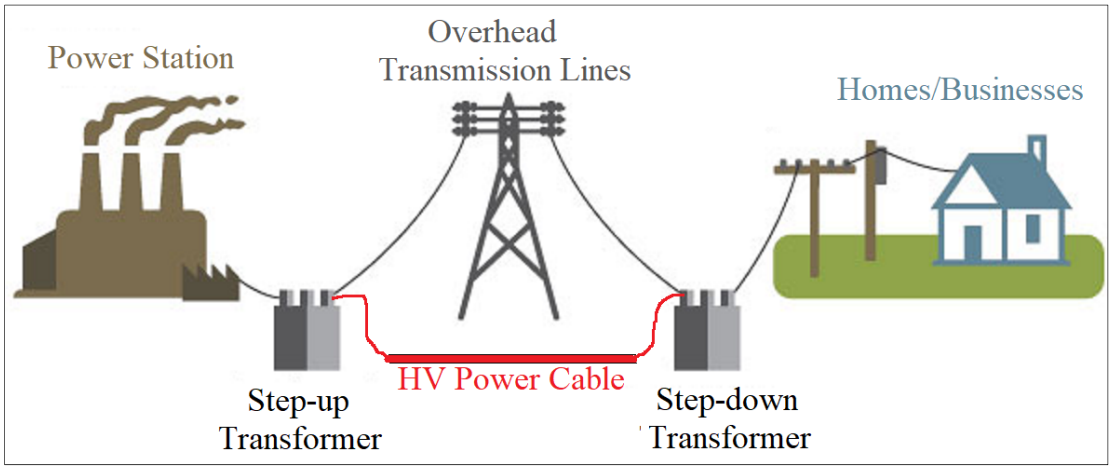

Figure 2-1 Electricity generation and transmission

The electrical distribution systems were somewhat fully developed during the twentieth century by connecting the consumers and generators using national and international grids. Despite the development, the current electrical transmission network needs to be strengthened

to transmit huge amounts of power long distances across continents. In North America, the power grid is highly integrated as there are over 35 electric transmission interconnections between the Canadian and US power systems. This integration is set to continue expanding, with multiple cross-border transmission projects currently being developed.

Throughout the grid, electricity is being transmitted at high voltages (>115 kV) to reduce the energy loss. The two main means of HV transmission are overhead and underground power transmission lines. HV overhead transmission lines are a reliable, low-cost, easily maintained and established method to transport bulk electricity across long distances. Their conductors (aluminum or copper) are not covered by insulation and are, therefore, exposed and vulnerable to adverse weather conditions.

Figure 2-2 Thick underground cable next to smaller overhead conductor
(Photo courtesy of Georgia Transmission Corporation)

Underground cables, on the other hand, take up less right-of-way, have lower visibility, and are less affected by weather conditions. However, costs of insulated cable and excavation are much higher. Also, faults take longer time to locate and repair. The cable lines are attractive for crossing wide metropolitan areas or long distances in the open sea. The focus in this work is on the advances in insulating materials used in HV underground cables.

The use of HV power cable is increasing in recent years. Increasing of population of urban areas in industrialized countries has led to the increasing of energy consumption where the use of power cable is the only viable option. Power cables eliminate the environmental problems that are associated with the overhead transmission lines. Many developing countries have changed their power system network to meet the increasing of demand by using power cables. Also, parts of the existing power cable networks have reached the end of their lifetime and need to be replaced.

2.1.1 Extruded HV power cables

A cable includes a conductor and insulation, and is suitable for being run underground or underwater. High voltage power cable has a common design, independent of its operating voltage and frequency. Basically it consists of the conductor, the insulation, the inner and outer semi-conductive screens, earthed metallic screen and protection sheath that form long concentric cylinder. Figure 2-3 shows a common design of a high voltage cable.

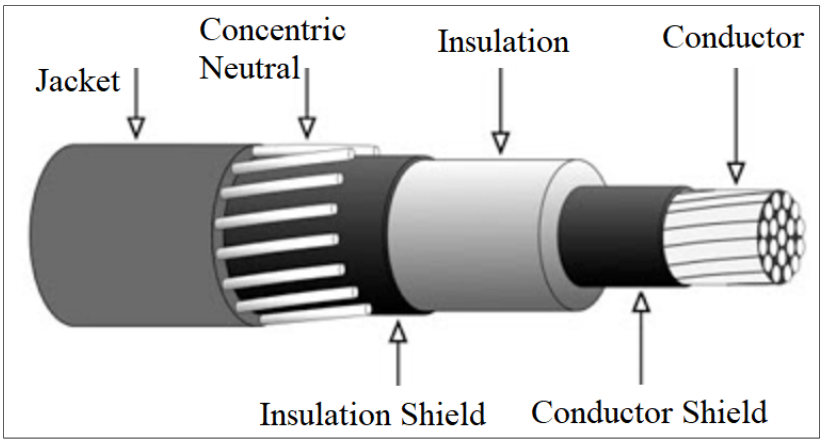

Figure 2-3 Common design elements of high voltage cable
(from www.openelectrical.org)

The insulation is the most critical part in cable structure due its crucial task to withstand a long term electrical stress during the service life of the cable. The use of extruded synthetic insulation in single layer construction is increasing due to its advantages in relatively easy

processing and handling of this insulation. This insulation can be selected to have 10% lower dielectric losses than cellulosic paper, higher intrinsic breakdown strength four times as high as impregnated paper insulation (Ryan 2001). The disadvantage is that a single defect can produce large influence on the whole insulation due to its homogeneity of this type of insulation (Ryan 2001).

2.1.2 HVAC versus HVDC systems

The first high voltage transmission line goes back to 1882, thanks to Thomas Edison, when a 45-km High-voltage direct-current (HVDC) link was constructed to connect Miesbach and Munich using rotating DC machines at each end. Later on, alternating-current generation, transmission, and utilization started to be dominant (Long and Nilsson 2007). They were realized to be more favorable because of benefitting from efficient and easy-to-manufacture transformers instead of high cost convertors that are necessary in DC lines. Voltage conversion in AC systems is simply via AC transformers achieved with low losses and little maintenance that allows high power and insulation levels within one single unit. Therefore, shortly after AC technology was introduced, it was accepted as the only feasible technology for generation, transmission, and distribution of electrical energy (Siemens 2011).

However, the inductive and capacitive elements of cables limit the transmission distance of AC transmission links. There are induced loss in all parts of AC cables. Also direct connection between two AC systems with different frequencies is not possible. Whereas HVDC transmission lines have no range limit, can be directly connected, and their only loss is the ohmic loss in conductor.

Nonetheless, the differences between extruded cables designed for a HVAC system and those designed for a HVDC system are negligible and the same structural components are required. Under the AC current, the insulation layer will experience electrical stress according to (Krueger 1991):

$$\boldsymbol{E(x) = \frac{U}{\left[x.\ln\left(\frac{R}{r}\right)\right]}} \quad (1\text{-}1)$$

Where U is the operating voltage, R and r are the external and internal radius of insulation and x is the radius of the insulation where the electrical stress is determined by the equation above. Therefore, there is an electric field distribution within the insulation of a HVAC cable.

In HVDC cables, the electric field is temperature and time dependent and is determined by the local electrical resistance and thus by the electrical resistivity/conductivity of the insulation. This means that if the DC insulation resistivity were constant with temperature and electric field, then the field distribution in an HVDC cable would be identical to that of an HVAC cable of the same geometry (Mazzanti and Marzinotto 2013). Moreover, the phenomena of field inversion and space-charge accumulation are the cause of a significant distortion of the electric field with respect to the capacitive field distribution typical of AC cables.

2.1.3 Insulating materials for HV cables

Apart from mechanical stability and extrudability, a dielectric to be chosen for realizing the insulation of both HVAC and HVDC cables should have high breakdown strength and lowest possible thermal resistivity. HVAC cable insulation must show low losses, while in HVDC systems low space charge retention properties are important.

Most of the cable insulation materials for both AC and DC applications are based on polyethylene (PE). PE is a semicrystalline polymer that has good electrical properties (low dielectric constant, low dielectric loss, and high breakdown strength) together with other desirable properties such as mechanical toughness and flexibility, good resistance to chemicals, easy processing, and low cost. Its main drawback is the low melting temperature. This restricts the maximum operation temperature to 75°C. To improve this property, PE is cross-linked (XLPE). Crosslinking increases maximum operation temperature to 90°C, the emergency temperature to 130°C, and the short-circuit maximum temperature to 250°C. Crosslinking also

increases impact strength, dimensional stability, tensile strength, thermal properties, chemical resistance, and it improves electrical properties, aging, and solvent resistance of polyethylene. However, crosslinking makes XLPE a thermoset polymer, therefore non-recyclable. This is a drawback that cannot be easily tolerated nowadays as the trend is that the environmental issues must be addressed. In addition, the cross-linking by-products within XLPE can create an irregular distribution of the dielectric stress and often cause the formation and growth of storage centers of space charge that remains trapped within the dielectric.

Attempts to use XLPE for HVDC cables were not successful, as it tends to accumulate space charge over time. For this reason, at present most HVDC installations in service all over the world use paper–oil insulated cable, mostly mass impregnated non-draining (MIND) whose insulation is pure cellulose paper impregnated with oil and resin, since these cable systems have shown very high service reliability and good resistance towards space charge accumulation (Ildstad, Sletbak et al. 2004). However, paper–oil insulated cables have operational limitations (service temperature and installation length) and environmental issues. They also have a rather complex and expensive manufacturing process.

It is obvious that there is a need for improvement in the insulating materials used for both high voltage AC and DC power cables. To meet the environmental issues, the material of choice for insulation layer must be recyclable. This can easily be satisfied by extruded cables having a thermoplastic as the insulation layer. Apart from adequate mechanical flexibility, in all applications high breakdown strength, low thermal resistivity and low moisture absorption are needed. In the case of HVAC cable insulation, the amount of energy loss must be as low as possible, while in HVDC systems low space charge retention properties are important.

Therefore, this project aims to introduce a new formulation for HV cable insulating materials based on extrudable thermoplastic polymers, while improving their electrical properties by modifying the polymer via blending or by incorporating nano-reinforcements.

2.2 Polymer nanocomposites as the insulating materials for HV cables

2.2.1 Nanotechnology: Nanocomposites

Nanotechnology is a science that pursues knowledge and control of matter at scales ranging roughly from 1 to 100 nanometers, where unique phenomena generate new or improved physical, chemical, biological properties. Nanocomposites permit to obtain a combination of properties not achievable in the traditional composites. The main difference from the traditional composites is that the filler dimensions in the latter are above 1 μm while in the former the particles are in the order of 10 nm; furthermore, the filler loading required for an acceptable performance is typically an order of magnitude less in the nanocomposites.

To obtain the desired behavior it is necessary to have control over the size and distribution of the fillers and to understand the role of the interfaces between constituents that are chemically and structurally different. Due to the high surface area of the nanostructures, the strong interaction between the organic and inorganic phases permits to obtain an improved reinforcement of the polymer matrix, and so the nanocomposites exhibit unique properties.

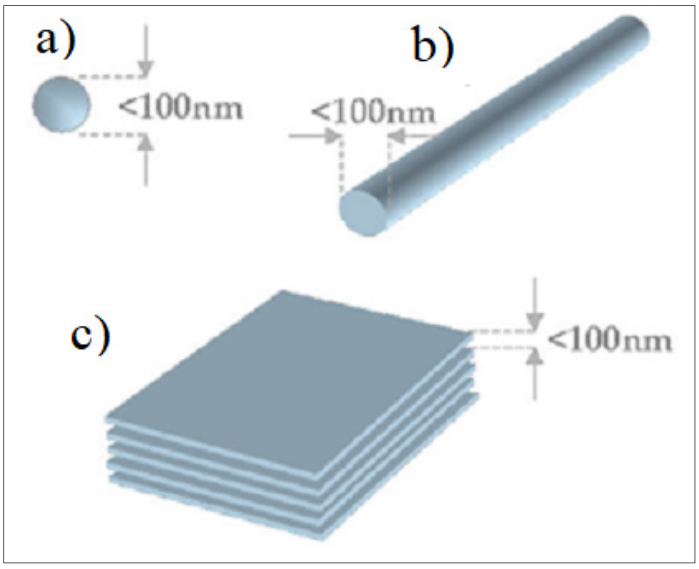

Figure 2-4 Nanoparticles' geometrical representation
a) iso-dimensional, b) nanotubes and c) layered crystals.

The particles to be dispersed could be, as represented in Figure 2-4, iso-dimensional when the three dimensions are in the order of nanometers, e.g. spherical silica nanoparticles, nanotubes or whiskers when two dimensions are on the nanometer scale, e.g. carbon nanotubes, cellulose whiskers, and particles in the form of sheets, such as layered crystals or clays.

2.2.2 Nanodielectrics: nanocomposites tuned for HV applications

The term "Nanodielectric", short for nanometric dielectric, is assigned to a multicomponent dielectric processing nanostructures, the presence of which lead to changes in one or several of its dielectric properties (Lewis 1994). An important category of nanodielectrics are polymer nanocomposites. Nowadays, it is well-established that electrical properties of polymers can be significantly enhanced, as will be discussed later, upon addition of specific nanoparticles. Thus, nanodielectrics have gained attention for dielectric application including HV insulation (Fréchette, Reed et al. 2006, Fréchette, Larocque et al. 2008).

The extend of improvement in electrical properties of polymer nanocomposites, however, is hugely affected by the dispersion/distribution of nanoreinforcement and its interfacial area with the polymer matrix. Although these parameters are interrelated, the quality of interfacial area is also dependent to the nanoparticle size/area and their compatibility with the polymer host making it hard to predict the electrical properties of these specific materials. Nonetheless, several models have been introduced to describe the interfacial region in nanocomposites (Schönhals and Kremer 2003, Tanaka 2005, Zou, Fothergill et al. 2007, Pitsa and Danikas 2011).

Different types of nanometric filler particles have been used to prepare nanodielectrics. Metal oxide nanoparticles (MgO, Al_2O_3, SiO_2, TiO_2, ZnO, …) have been shown to significantly alter the electrical properties of polymers, even in very low concentration. Improvement in breakdown strength and voltage endurance has been seen upon addition of some metal oxide nanoparticles into polymers (Ishimoto, Tanaka et al. 2008, David and Fréchette 2013). Also it is reported that metal oxide nanoparticles will reduce the mobility of charge carriers in the

polymer matrix resulting in an overall reduction of the electrical conductivity and space charge accumulation (Fleming, Pawlowski et al. 2005, Murakami, Okuzumi et al. 2010, Milliere, Makasheva et al. 2014, Park, Kwon et al. 2014, Du, Li et al. 2017, Wang, Wu et al. 2017).

Another interesting category of nanoparticles in this regards are nitride and carbide nanoparticles including silicon nitride (Si_3N_4), aluminium nitride (AlN), boron nitride (BN) and silicon carbide (SiC). They show high thermal conductivities and are mostly tuned for electrical applications such as HV insulation systems and HV accessories (Huang, Jiang et al. 2011).

Finally, anisotropic nanoparticles have also been used for HV applications such as graphene oxide (GO) and graphene (Deshmukh, Ahamed et al. 2015, Mancinelli, Fabiani et al. 2015, Fabiani, Camprini et al. 2017), BN nanotubes and nanosheets (Golberg, Bando et al. 2010, Song, Wang et al. 2012, Heid, Fréchette et al. 2015), as well as nanoclay (Tomer, Polizos et al. 2011, Zazoum, David et al. 2014, David, Zazoum et al. 2015, Ghosh, Rahman et al. 2016). The anisotropy usually results in unique properties in preferential directions when purposefully aligned. In particular, nanoclay with layered structure and the ability to be easily dispersed is a great candidate for HV applications. More details about nanoclay and clay-containing polymer nanocomposites are discussed in the following sections.

2.2.3 Nanoclay

As defined by the Clay Mineral Society, clay is a "naturally occurring material composed primarily of fine-grained minerals, which is generally plastic at appropriate water contents and will harden when dried" (Guggenheim and Martin 1995). Smectite clays are the most used in nanocomposites as the inorganic particles especially montmorillonite. The crystal structure of layered silicates is built up of two tetrahedral sheets and one octahedral sheet. The structure 2:1 layered silicates are shown in Figure 2-5. The thickness of each layer is around 1 nm and the lateral dimension may vary from 30 nm to several microns. The layers are placed on the

top of each other's forming stacks. These stacked layers have a van der Waals gap between layers, which is called the interlayer or gallery.

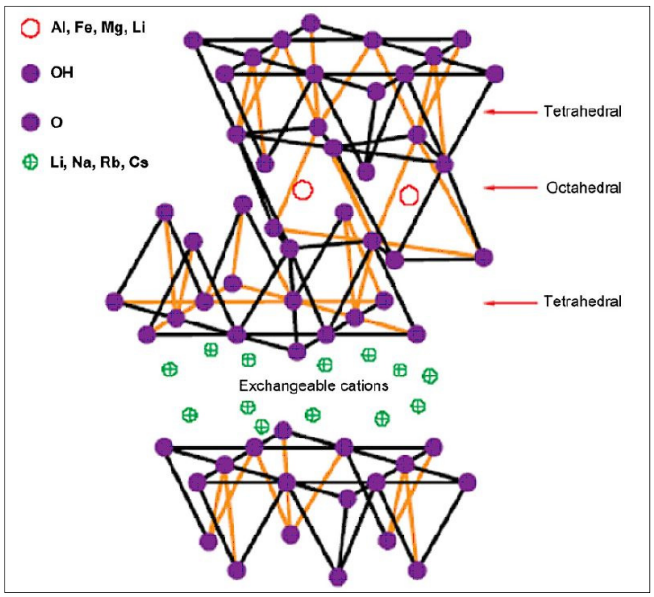

Figure 2-5 Crystal structure of 2:1 layered silicates
Reproduced from (Beyer 2002)

Layered silicates have two particular characteristics that make them perfect for mixing with polymers to prepare polymer nanoclay nanocomposites. The first characteristic is the dispersion of layered silicates into individual layers in the polymer matrix and the second is the finely tuned surface made through cation exchange reactions with organic and inorganic cations. Both characteristics are dependent on each other, since the dispersion of layered silicate in a particular polymer is related to the interlayer cation (Ray and Okamoto 2003). Due to their hydrophilic nature and to be able to mix them with non-polar polymers, layered clays usually undergo an organic treatment on the surface to obtain satisfactory dispersion. The organic treatment is most of the time based on quaternary ammonium salts in a variety of chain lengths (Powell and Beall 2007, Choudalakis and Gotsis 2009).

2.2.4 Clay-containing polymer nanocomposites

The polymer layered silicates nanocomposites have been widely studied, and have shown markedly improved mechanical, thermal, and electrical properties compared to pure polymer or conventional, microscale (Ray and Okamoto 2003). Due to their high aspect ratio, the addition of clay in polymers can act as reinforcement in the same way as glass fiber or microscale inorganic nanofiller. Thus clay-containing polymer nanocomposites are expected to have unique characteristics.

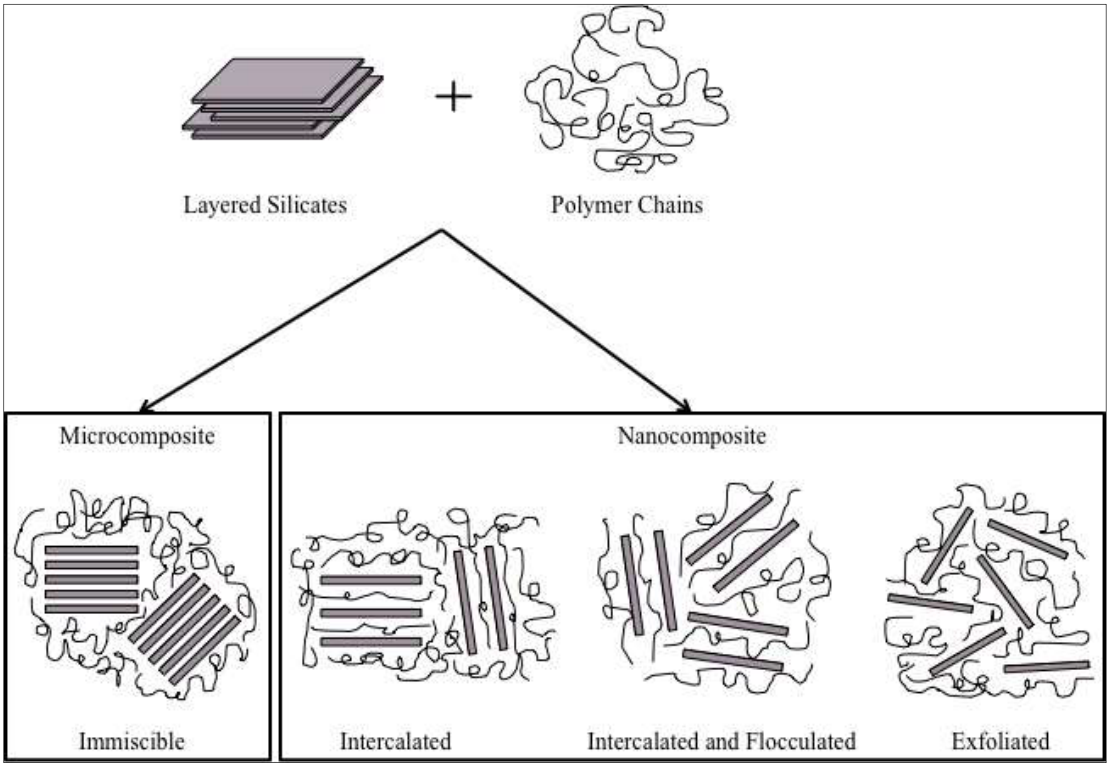

Figure 2-6 Different structures of polymer layered silicates (PLS) nanocomposite, reproduced from (Albdiry, Yousif et al. 2013)

With regards to preparation, depending on the nature of the components and the method of preparation three main types of composites may be obtained as illustrated in Figure 2-6. In an *intercalated* structure, polymer chains intercalate between the layered structures of the clay and effectively expand the distance between the layers. Polymer chains penetrate inside the

galleries of layered silicates and make a “crystallographically regular fashion” structure. A *flocculated* structure conceptually is similar to an intercalated one; however, in this structure silicate layers become flocculated due to the hydroxilated edge-edge interaction. The last type is the *exfoliated* structure in which layered silicates are separated to their individual layers. The layers disperse continuously in the polymer matrix at random orientation and have an average distance with a value that is dependent on the amount of nanoclay loading.

2.2.5 Preparation methods of polymer/clay nanocomposite

Three main methods are generally available for preparation of polymer layered silicate nanocomposites. The differences between these methods are the result of the initial materials and the processing techniques used (Manias, Touny et al. 2001, Ray and Okamoto 2003, Albdiry, Yousif et al. 2013) :

Intercalation of polymer or pre-polymer from solution: Polymer or prepolymer is dissolved in a solvent (e.g. water, chloroform or toluene), which is appropriate for the dispersion of the silicate layers. The polymer chains intercalate into the interlayer silicates in the solution phase and remain in the intercalated structure after removal form the solvent. This method is limited to a limited number of polymers, which have a suitable and available solvent that is also suitable for the clay. It is useful for producing polymer nanocomposites with little or no polarity. However, this method is not commercially viable because of high cost of solvent recovery, making it environmentally unfriendly.

In situ intercalative polymerization method: In this method, the silicate layers disperse within the liquid monomer or monomer solution. The polymerization process can be initiated by heat or radiation, suitable initiator or fixed catalyst, which leads to the formation of an exfoliated structure. Most factors, including the requirement for separate production lines or major changes to existing production facilities, limit the commercialization of this method.

Melt intercalation method: Structurally, polymer/layered silicates are prepared under annealing polymer glass transition or melting temperature conditions, as well as shear mixing. Above their softening point polymer chains move easily, and can intercalate between silicate layers. In Figure 2-7, a schematic of the melt intercalation method is shown. This preparation method is environmentally friendly and economically favorable compared to other methods because of the absence of solvents in this technique. In addition, evidence suggests that a conventional processing technique, such as the twin-screw extruder, is an effective way for the dispersion of layered silicates within the polymer (Vaia and Giannelis 1997). A range of nanocomposite structures, from intercalated to exfoliated, can be obtained by this method.

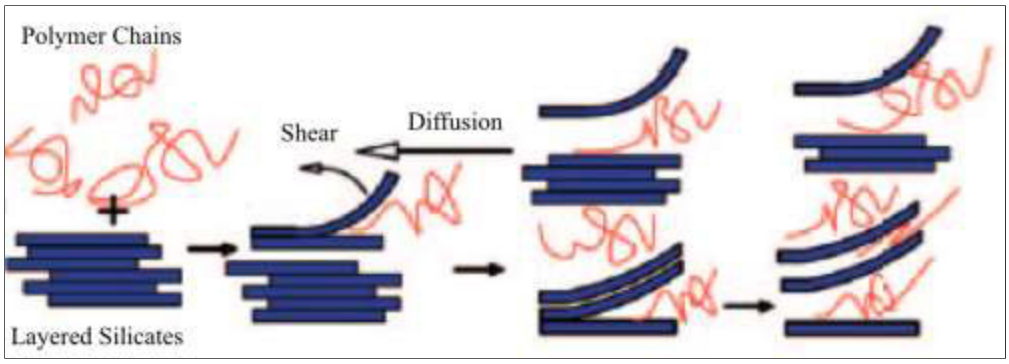

Figure 2-7 Schematic of melt intercalation method
reproduced from (Ray and Okamoto 2003)

2.2.6 Effect of nanoclay on electrical properties of polymers

Extensive research has been carried out on clay nanocomposites. Clay-containing nanocomposites have already been used in many applications and the processes to achieve organically modified clays are well-developed. Clay dispersion in polymer materials has shown to improve fundamental properties including mechanical properties (Lan and Pinnavaia 1994), thermal properties (Messersmith and Giannelis 1994) and electrical insulation properties (Lee and Lin 2006). Clay dispersion can impart new functional properties in polymer materials such as gas barrier (Yano, Usuki et al. 1993) and flame resistance (Zhu, Morgan et al. 2001).

They are also reported to have enhanced dielectric properties, i.e. higher breakdown strength comparing to the neat polymer. This is possible thanks to the high aspect ratio and surface area that increase the tortuosity and scattering opposing the flow of charge carriers, especially when clay layers are oriented (Tomer, Polizos et al. 2011, David, Fréchette et al. 2013, Zazoum, David et al. 2014). Clay nanocomposites have also shown to have higher resistance to PD erosion than the base polymer (Kozako, Fuse et al. 2004) and delay electrical treeing propagation .

On the other hand, other important electrical properties of clay-containing nanocomposites such space charge accumulation have not been fully discussed. In this work, a comprehensive look will be given to the electrical properties of clay containing nanocomposites based on LDPE and PP including evaluating the dielectric spectra, the role of thickness in breakdown strength, dc conductivity and space charge accumulation.

2.3 Modified matrix: polymer blends

Modification of polymer matrix via blending is now a new trend to improve the dielectric and breakdown behavior of semi-crystalline polymers. This enhancement could be as a result of modification of the structure ordering and crystallinity of the polymer. Here the polymer blends and their morphology are briefly reviewed. At the end, readers will be introduced to SEBS, polystyrene-b-poly(ethylene-co-butylene)-b-polystyrene, as an excellent candidate to form a blend with polyolefin.

2.3.1 Polymer blends classification

A polymer blend is a mixture of two or more polymers that have been blended together to create a new material with different physical properties (Paul and Newman 1978). All-important performance properties can be improved by blend systems. Notable among the properties are flow, mechanical strength, thermal stability, and cost. From the morphological point of view, polymer blends can be classified into two main categories:

Miscible polymer blend, a polymer blend that is homogenous at a microscopic scale (i.e., achieving a state of equilibrium at a molecular level).

Immiscible polymer blend, a polymer blend that is at a phase-separated state of mixing at a molecular level with the composition of the separated phases pure or identical to the pure components prior to blending. This is the most common case of polymer blends due to the fact that most polymers are immiscible.

The morphologies of the miscible and immiscible polymer blends are distinct from each other. The miscible polymer blends exhibit single phase morphology. In an immiscible blend, two phases are present: the discrete phase (domain), which is lower in concentration, and the continuous phase, which is higher in concentration. In some cases, the two phases may not have a well-defined boundary (partially miscible). Each component of the blend penetrates the other phase at a molecular level. The molecular mixing that occurs at the interface of a partially miscible two-phase blend can stabilize the domains and improve the interfacial adhesion.

In this project, we are interested in the immiscible type of polymer blends, since their multiphase nature and controllable morphology works in the favor of being a good choice to help dispersing nanoparticles inside the polyolefin matrix. To achieve that, the interfacial chemistry and the dispersed phase morphology must be well-controlled. In particular, the control of the morphology of the dispersed phase under melt-processing conditions is of great importance due to the increasing interest in using melt compounding techniques in the mixing and dispersion of polymers.

2.3.2 Morphology of immiscible polymer blends

As multiphase materials, the properties of immiscible polymer blends are considerably influenced by their phase structure. The final morphology of a polymer blend prepared by melt mixing is a result of the complex relationships of inner and outer parameters. Besides the

chemical structure and rheological properties of pure components or blend composition as inner parameters, applied flow field or temperature as outer factors influence the morphology development to great extent. Therefore, by changing the composition of the blend or processing conditions it is possible to obtain materials with morphologies of different types (Robeson 2007).

Generally, the vast majority of immiscible polymer blends can be classified as a blend with either dispersed (droplet/matrix) or co-continuous morphology, as shown schematically in Figure 2-8. If the amount of component A is low, it forms a dispersed particles surrounded by a matrix of component B. Increasing the amount of phase A, the size of the dispersed domains grows and approaching the threshold of geometric percolation the first continuous structures appear. The morphology is considered co-continuous when both of the phases are fully continuous. With a further increase in the concentration of A, the structures of phase B disintegrate and finally the phases invert and A forms the matrix of the blend and B the dispersed phase.

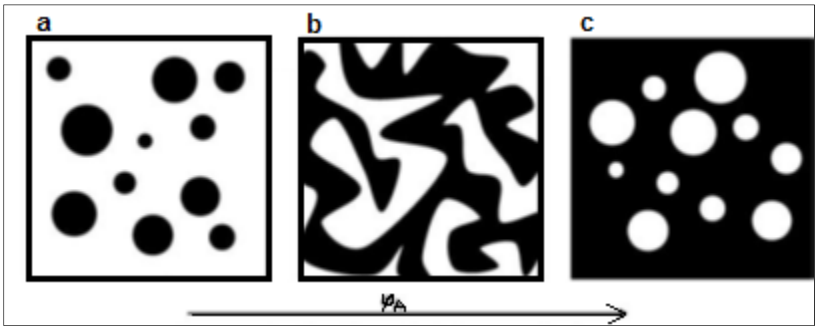

Figure 2-8 Basic types of phase structures in polymer blends

In order to minimize the free surface energy of the system, the dispersed particles tend to achieve a spherical shape. However, many anisotropic particle shapes, such as ellipsoids, fibrils or platelets, can be observed in polymer blends as the final morphology is often quenched immediately after melt processing. Thus, any particles deformed by the shear and/or elongational stresses applied in the mixing devices are solidified before they can regain an energetically favorable spherical shape.

2.3.2.1 Morphology development during melt processing

Most of polymer blends are produced by melt-mixing from powders or pellets of pure components. In the initial stage of mixing the original, typically millimeter-sized solid particles are heated and sheared, and during melting the size of the domains decreases into the micro range. In this early mixing stage, the pellets in contact with the hot walls of a processing device are exposed to high shear stresses and disintegrate into thin sheets or ribbons (Scott and Macosko 1995). Subsequently, as the thickness of these sheets decreases in the micrometer range, the interfacial forces become important and holes are formed in the sheets. These lacey structures then break up into irregularly shaped particles, which in turn break up further or relax into near-spherical particles. This mechanism leads to a rapid decrease in the dispersed particle sizes during the first few minutes of mixing.

After the initial stage of mixing the domain size decreases only slightly such that, after some time, the phase structure no longer shows any changes. In this steady state time interval, the morphology is stable until thermal degradation alters the rheological properties of polymers considerably. The morphology development during mixing is a result of the competition between droplet deformation and break-up on one side, and droplet coalescence on the other side (Fortelný, Kovář et al. 1996). In steady-state mixing these two processes are in dynamic equilibrium, and this determines the final shape and size of the phase domains.

Another process influencing blend morphology is the coalescence of the dispersed particles. In contrast to droplet break-up, coalescence leads to an increase in droplet size and a coarsening of the phase structure. It is a consequence of the collision of droplets having different velocities. When two droplets approach each other, they begin to deform due to the axial force, and at the same time the matrix film between the particles is squeezed out. If the critical distance between the particles is reached, the matrix film ruptures and the droplets merge.

Overall, the development of the final morphology is a consequence of complex relationships between the viscosity and elasticity of the components, the processing conditions, the chemical

structure of the components, and the blend composition. Therefore, it is difficult to predict the shape, size and spatial arrangement of the phases.

2.3.3 SEBS to form blend with polyolefin

An interesting type of polymers are block copolymers. A block copolymer molecule contains two or more polymer chains attached at their ends. They can have different types of morphology (i.e. diblock, triblock …) depending on composition, thermodynamical affinity between components, rheological properties of phases, and history of processing conditions (Carastan, Amurin et al. 2013). When one block has a glass-transition temperature (T_g) above ambient temperature and one below ambient temperature, the result is a micrometric mixture of hard and soft parts known as thermoplastic elastomers. This especial type of block copolymers behaves as a rubber at ambient conditions, but can be molded at high temperatures due to the presence of the glassy domains that act as physical cross-links. Thermoplastic elastomers can also be used as a host template for nanofillers. In fact, both immiscible blends and block copolymers constitute self-ordered structures with controllable morphologies offering various possibilities to disperse nanofillers, nanoclay platelets in our case, based on the affinity of the selected nano-charge to one phase or another.

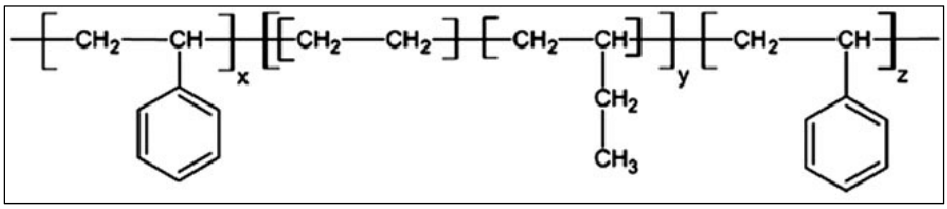

Figure 2-9 Chemical Structure of SEBS

One interesting type of triblock copolymers is SEBS which is composed of polystyrene blocks at both ends and a rubber block at the middle. It is a thermoplastic elastomer that combines advantages of both rubbery and plastic materials. It features self-assembled nanodomains and exhibits excellent mechanical properties combining both the thermoplastic and the elastomer behaviors (Holden, Kricheldorf et al. 2004, Balsamo, Lorenzo et al. 2006, Carastan, Amurin

et al. 2013). The polystyrene end-blocks form domains that act as multifunctional junction points to give an elastomeric network and the cross-links are formed by a physical rather than a chemical process (Figure 2-9). Thus, at room temperature, the material behaves as a conventional vulcanized elastomer, but when it is heated, the domains soften, the network loses its strength and eventually the block copolymer can flow; the changes experienced by the material upon heating are completely reversible (Legge 1987).

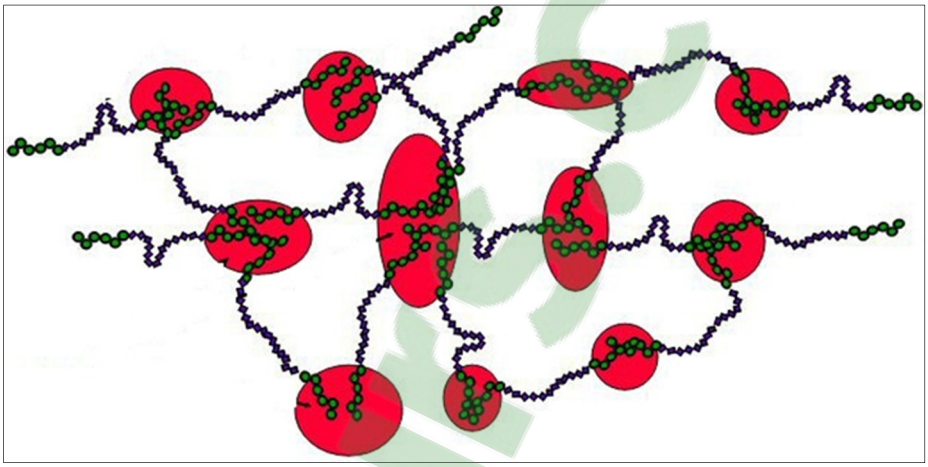

Figure 2-10 Domain Structure of SEBS (from www.eastman.com)

When making a blend, SEBS is a great choice. Its hydrogenated polybutadiene midblock has a similar structure to LDPE and PP ensuring a good compatibility with polyolefins (Agari, Ueda et al. 1993). Also the relatively polar aromatic rings of PS block provide chemical affinity to some inorganic nanoparticles such as nanoclays (Carastan, Amurin et al. 2014, Kuester, Barra et al. 2016). SEBS and SEBS grafted maleic anhydride (SEBS-MA) can compensate for decreased toughness of clay-containing nanocomposites, especially based on PP, while maintaining the improved electrical properties. Apart from water treeing retardant agent (Ma, Jiang et al. 2010, Liu, Mhetar et al. 2011) and dielectric elastomer actuators (Mc Carthy, Risse et al. 2009, Kofod, Risse et al. 2011, Stoyanov, Kollosche et al. 2011), SEBS is now gaining attention as a recyclable polymer to form blend with polyolefin as insulating materials for HV applications, especially for HV cable insulation (Zhang, Zha et al. 2017).

In this work, two grades of SEBS have been used to modify the morphology of clay containing nanocomposites based on LDPE and PP. It is expected that SEBS and the resultant immiscible blend will act as a template matrix to control the dispersion/distribution of nanoclay and therefore directly affect the electrical properties of those nanocomposites.

CHAPTER 3

ARTICLE 1: ELECTRICAL BREAKDOWN PROPERTIES OF CLAY-BASED LDPE BLENDS AND NANOCOMPOSITES

M. Eesaee[1], E. David[1], N.R. Demarquette[1], Davide Fabiani[2]

[1] Mechanical Engineering Department, École de Technologie Supérieure, Montréal, QC, Canada
[2] Department of Electrical, Electronic, and Information Engineering, University of Bologna, Bologna, Italy

This article has been published in:
Journal of Nanomaterials, Volume 2018, 11 January 2018, Article ID 7921725
https://doi.org/10.1155/2018/7921725

Abstract

Microstructure and electrical breakdown properties of blends and nanocomposites based on low-density polyethylene (LDPE) have been discussed. A series of LDPE nanocomposites containing different amount of organomodified montmorillonite (clay) with and without compatibilizer have been prepared by means of melt compounding. Two sets of blends of LDPE with two grades of Styrene-Ethylene-Butylene-Styrene block copolymers have been prepared to form cocontinuous structure and host the nanoreinforcement. A high degree of dispersion of oriented clay was observed through X-ray diffraction, scanning, and transmission electron microscopy. This was confirmed by the solid-like behavior of storage modulus in low frequencies in rheological measurement results. An alteration in the morphology of blends was witnessed upon addition of clay where the transportation phenomenon to the copolymer phase

resulted in a downsizing on the domain size of the constituents of the immiscible blends. The AC breakdown strength of nanocomposites significantly increased when clay was incorporated. The partially exfoliated and intercalated clay platelets are believed to distribute the electric stress and prolong the breakdown time by creating a tortuous path for charge carriers. However, the incorporation of clay has been shown to diminish the DC breakdown strength of nanocomposites, mostly due to the thermal instability brought by clay.

Keywords: Electrical breakdown strength, polymer blend, nanocomposite, clay, block copolymer

3.1 Introduction

It has been more than eight decades that synthetic polymers have been used as solid electrical insulating materials because of their excellent dielectric properties, the most important of which is the high dielectric breakdown strength. When a dielectric is subjected to a rising voltage, with a high enough applied electrical field the electrical pressure will eventually overcome the insulating material and electrical charge carriers will flow. Current flow behavior through an insulator is not linear as in conductors and practically no electrons will flow below a certain threshold level, above which current will gain sufficient kinetic energy and forcibly runs through the material. Electrons will multiply as a result of the ionization of the collision process, electronic conduction takes place and breakdown occurs. This mechanism is known as avalanche process (Zeller, Pfluger et al. 1984, Kao 2004) and the dielectric strength is defined as the highest voltage the insulator withstands before breakdown divided by its thickness. However, this is not the only known mechanism and breakdown may occur in advance of electron avalanche by insulation melting due to temperature rise (thermal breakdown), enhanced electric stress when the insulation thickness is mechanically reduced (electromechanical breakdown) or due to partial discharge (Dissado and Fothergill 1992, Zakrevskii, Sudar et al. 2003, Blythe and Bloor 2005, Tanaka 2016). In reality the mechanism of dielectric breakdown is more complicated in many polymers and pre-existing discontinuities also contribute to the cumulative breakdown. It was found out that impurities, defects and

degradation caused by electric field or heat will accelerate the failure (Jonscher and Lacoste 1984). Extensive works have been done to understand the behavior of polymers towards electrical breakdown which has led to considering several factors such as thickness, surrounding medium, pressure and temperature, all along with the complicated morphology and structure of polymers which make the understanding of breakdown process very difficult.

One proposed solution to improve the breakdown strength of polymers consists of adding a reinforcing inclusion as fillers (composites). Despite improvements in mechanical and thermal properties, micro inclusions are believed to decrease the breakdown strength of polymers as they may act as defects (Wang, Iizuka et al. 2011). Consequently, nanofiller inclusions have been introduced recently to overcome the negative effects (Cao, Irwin et al. 2004, Tanaka 2016), thus creating a new area of materials called nanometric dielectrics or nanodielectrics (Lewis 1994). Nanoparticles which may be chemically modified with different approaches in order to have polar or non-polar functional groups on their surface have shown very promising results (Li, Yin et al. 2010). It is well known that they have a great influence on breakdown properties of polymers, especially by the change in morphology of the semicrystalline polymers (Roy, Nelson et al. 2005). They reduce the internal field (Nelson, Fothergill et al. 2002) and alter the space charge distribution within the polymer matrix (Fabiani, Mancinelli et al. 2016). Furthermore, the interface between polymer and nanoparticle plays a crucial role in the dielectric breakdown performance (Lewis 2004, Zazoum, David et al. 2014). The final obtained morphology and the physical and chemical characteristics of the interface are greatly influenced by the dispersion and localization of nanoparticles, and the nature of both phases, which will eventually influence the breakdown process by changing the micro-scale aspects i.e. traps, free volume and carrier mobility (Li, Yang et al. 2016). Therefore, considerable attentions must be paid to tailor the interface with proper physical and chemical methods to obtain improved dielectric breakdown properties (Huang, Ma et al. 2009, Peng, Huang et al. 2010).

Another well-established approach to develop new materials is polymer blending (Robeson 2007). Since usually polymers have low mixing entropy, most polymer pairs tend to make an

immiscible blend (Coleman, Painter et al. 1995). During the mixing process and at rest, the dynamic interplay between rheological phenomena determines the final morphology of the blend. When having different mixing proportion, the minor component tends to distribute all over the major phase as droplets. However, in a narrow range of composition with proper processing, the blend microstructure can turn into co-continuous, distinguished by a mutual interpenetration of the two components. This type of microstructure is well-known for its tunable and substantial combination of functional and structural properties, but is hard to achieve (Pötschke and Paul 2003). It has been well-established that nanoparticles can be adopted to stabilize the morphology of immiscible blends (Filippone, Dintcheva et al. 2010, Kar, Biswas et al. 2015, Pawar and Bose 2015). However, this approach has not been fully employed to discover the potential improvements in electrical breakdown properties of polymers.

In this paper, attempts to evaluate the short-term AC and DC electrical breakdown properties for clay-based nanocomposites of low density polyethylene (LDPE) have been presented, alongside with observation of the morphology of those materials. Also the possibility of using a binary blend to achieve a tailored dispersion of nanoclays to result in an improved AC and DC electrical breakdown was evaluated.

3.2 Experimental

3.2.1 Materials and Processing

Commercially available premixed LDPE/Clay masterbatch (nanoMax®-LDPE) containing 50% organomodified Montmorillonite (O-MMT) was supplied from Nanocor and used as the source of the nanoreinforcement. The masterbatch was further diluted with low-density polyethylene (LDPE), supplied from Marplex in powder form with a density of 0.922 g/cm^3 and MFI of 0.9 g/10 min (190 °C/2.16 kg), to the desired concentrations of clay. Maleic anhydride grafted linear low-density polyethylene (LLDPE-g-MA) was supplied from DuPont (Fusabond M603) and has been used as a compatibilizer. It has a density of 0.940 g/cm^3 and

MFI of 25 g/min, and is being referred to as MA in this manuscript. Two series of nanocomposites were prepared with and without 5 wt% of the compatibilizer, with concentration profile of clay being set as 1, 2.5, 5, 10 and 15%.

The same procedure was used to prepare blends and nanocomposites of LDPE with two grades of polystyrene-b-poly(ethylene-co-butylene)-b-polystyrene (SEBS) thermoplastic elastomer supplied from Kraton: G1652 and FG1901. The former with a MFI of 5 (230 ˚C/2.16 kg) based on ASTM D1238 (as declared by the supplier) is referred to as SEBS in this manuscript. The latter with a MFI of 22, contains 1.4-2 wt% of maleic anhydride (MA) is referred to as SEBS-MA. Both grades contain 30 wt% fractions of polystyrene (PS) block in their structure and have a density of 0.91 g/cm^3.

Melt compounding via extrusion process has been performed using a co-rotating twin screw extruder. All materials were dried prior to extrusion in a vacuum oven at 45 ˚C for at least 36 h and manually pre-mixed. A temperature profile of 145-170 ˚C was set from hopper to die. The pellets obtained were press-molded using an electrically heated hydraulic press into thin plates with various thicknesses regarding the future characterization. Samples were first preheated for 5 minutes and then hot-pressed at 155 ˚C (165 ˚C for blends) for another 5 minutes under the pressure of 10 MPa. Press plates then were water-cooled with a rate of 10 ˚C per minute to the ambient temperature. Table 3-1 represents a summary of the composition of the final blends and nanocomposites. In case of blends the mass fractions of the two phases are set equal.

Table 3-1 Composition and nomenclature of LDPE/SEBS blends and nanocomposites (n=1, 2.5, 5, 10 & 15)

	LDPE (wt%)	Clay (%)	MA (wt%)	SEBS (wt%)	SEBS-MA (wt%)
LDPE/nC	(100 – n)	n	-	-	-
LDPE/MA/nC	(95 – n)	n	5	-	-
LDPE/SEBS	50	-	-	50	-
LDPE/SEBS-MA	50	-	-	-	50
LDPE/SEBS/5C	47.5	5	-	47.5	-
LDPE/SEBS-MA/5C	47.5	5	-	-	47.5

3.2.2 Characterization

The morphology of the as-obtained nanocomposites was characterized by high resolution Scanning Electron Microscopy (SEM) using a Hitachi SU-8230 Field Emission-STEM microscope. Samples were cryogenically cut and sputtered with a 20 nm layer of platinum using a Turbo-Pumped Sputter Coater (Q150T S) prior to the observation. Solvent extraction has been used to investigate the microscopic structure of the blends. Some samples were held in toluene for 24 h while being gently stirred at room temperature and then washed with alcohol before SEM observation.

Transmission Electron Microscopy has been also conducted. With respect to SEM, it employs electron beam instead of light beam. It has been done using a FEI Tecnai G2F20 S/TEM, operated at 200 kV. The device is equipped with a Gatan Ultrascan 4000 4k x 4k CCD Camera System (Model 895). Samples were cryogenically cut to create thin layers that allow electron beam penetration. The point-to-point and line resolutions of the TEM are respectively 0.24 nm and 0.17 nm.

X-ray diffraction has been employed to evaluate the degree of dispersion and intercalation/exfoliation of the nanoclay using PANanalytical X'Pert Pro with Kα radiation (λ = 1.542 Å). Accelerating voltage and electrical current was set to 40 kV and 40 mA respectively. The scanning was conducted from 2° to 10° with a step size of 0.102° and the counting time was 400 ms per step. Bragg's law was used to calculate the intercalate spacing (d_{001}) as:

$$2d \sin\theta = \lambda \qquad (2\text{-}1)$$

Where λ is the wavelength of the X-ray radiation used, d is the distant between the diffraction of lattice plans, and θ is the diffraction angle measured (Pavlidou and Papaspyrides 2008).

The morphological data were further enriched by conducting rheological measurement at 160 ˚C via a strain-controlled rheometer (MCR 501 Anton Paar). First a strain sweep was carried

out to determine the linear viscoelastic range, then small amplitude oscillatory shear (SAOS) tests were performed in the frequency range from 0.01 to 300 rad.s^{-1}. Samples in parallel plate geometry with diameter of 25 mm were used in a 1 mm sample gap.

The AC short-term breakdown test was conducted to measure the dielectric strength of the samples using a BAUR DTA 100 device where the samples are gently held between the electrodes (ball-type, 4 mm diameter) while all immersed in insulating oil (Luminol TR-i, Petro-Canada) to avoid flashover. Method A from ASTM D149 was chosen, according to which the ramp was set to 2 kV/s and continued until failure of the sample. The test was performed at ambient temperature and the insulating oil was dried in vacuum oven for a minimum of 48 h. Twenty specimens were tested for each sample. Each time before changing the sample, the oil was removed and fully replaced, and the electrodes were cleaned. A thickness of 140 μm was used for the breakdown test; while to find out the role of thickness on the breakdown strength variation, the test was also conducted for two other thicknesses (200 μm and 300 μm) for LDPE/Clay nanocomposites. A power law relationship was used to correct the measurement data as a result of the non-uniformity in the thickness of specimens, as discussed in (Helal, Demarquette et al. 2016).

The same approach was used to measure the DC breakdown strength of the samples having 200 μm thickness. Specimens were placed between a spherical electrode on top (30 mm diameter) and a disk-shape electrode on the bottom. The diameter of the lower electrode was 60 with a rounding radius of 7 mm. Electrodes were placed in a container while immersed in mineral oil. The specimens were subjected to a voltage raise of 5 kV/s. Eight specimens were tested for each sample, between which the oil was renewed completely. LabView software was used to computerize the measuring system. Figure 3-1 depicts a schematic representation of the measurement setups used for both high voltage AC and DC breakdown tests. A commercially available software was used to retrieve the data for both AC and DC breakdown strengths based on two-parameter Weibull distribution.

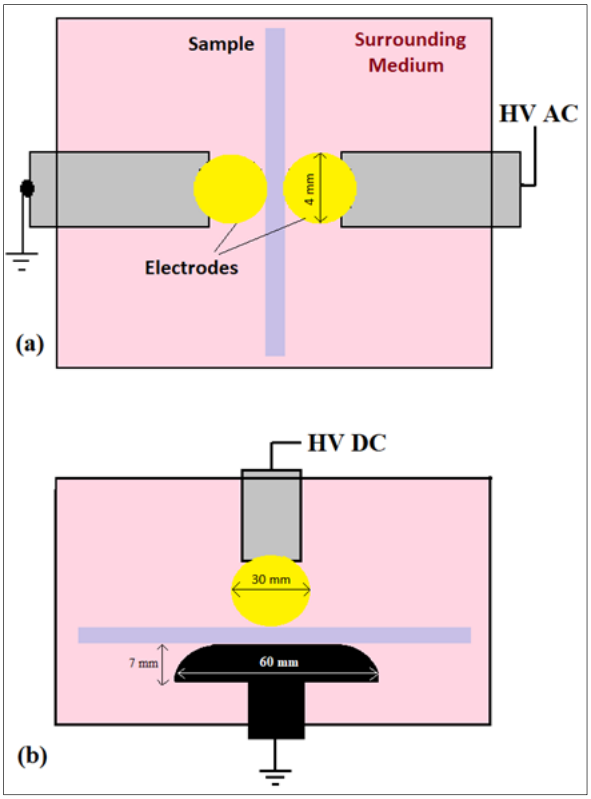

Figure 3-1 Electrical breakdown measurement setup for: a) AC short term, b) DC short term

3.3 Results and Discussion

3.3.1 X-ray diffraction (XRD)

Figure 3-2 shows the X-ray diffraction spectra for the LDPE clay nanocomposites. This technique allows us to determine the interlayer distance of nanoclay by utilizing Brag's law. The identification of the nanocomposite structure can be done via monitoring the intensity, shape and position of the basal reflection peaks. The layers of the silicates usually form stacks with a regular van der Waals gap, called the interlayer or the gallery. A single layer has a thickness around 1 nm but tactoids formed by several layers can reach up to several hundreds of micron when forming stacks (Alexandre and Dubois 2000). According to the Brag's law, a shift of diffraction peak toward lower diffraction angle is a sign of an increase in the interlayer spacing as a result of polymer intercalation. Higher extent of polymer intercalation would

result in a greater shift toward lower value of 2θ, signaling a better dispersion of the clay nanoplatelets (Alexandre and Dubois 2000, Eesaee and Shojaei 2014). This increase in interlayer spacing also decreases the periodicity which reflects a reduction in the intensity of the peak.

The XRD measurements were conducted with two different positions of the samples, having the radiation starting parallel and perpendicular to the surface of the sample. As can be seen in Figure 3-2.a, in parallel emission there is a unanimous peak at 2θ of 6.34 corresponding to an interlayer spacing of around 1.39 nm, and no evident sign of the primary diffraction peak (d_{001}); While the corresponding peak for masterbatch happens at 2θ of 7.26 showing a shift of diffraction peak for nanocomposites to lower degrees originating from the increase in the interlayer spacing during the melt mixing. That means at least one extended polymer chain is intercalated between the stacks of silicate layers. As expected the intensity of the peak increases with the increase in the amount of clay incorporated. For sample containing 5 wt% of MA (LDPE/MA/5C), the diffraction peak occurs at the same place but is broader than the original nanocomposite (LDPE/5C). This broadening of the diffraction peak suggests that the degree of dispersion of the clay within the polymer matrix is further improved, possibly due to the polar interactions between the maleic anhydride groups in the compatibilizer and the hydroxyl groups of clay and the increase in the shear stress because of the low molecular weight of MA. This may end up in formation of covalent bond and facilitate the penetration of polymer chains into the galleries of clay (Dumont, Reyna-Valencia et al. 2007).

When the direction of the radiation is normal to the surface of the sample (Figure 3-2.b), nanocomposites patterns show some fluctuations but no clear peak can be recognized. The same pattern is seen for the masterbatch. This is probably due to the orientation of the clay layers parallel to the surface when molded in hydraulic press under high temperature and high pressure into thin plates. This was possible since the final thickness of the samples were all less than 300 μm, and under pressure the molten polymer had to flow in the directions perpendicular to the applied pressure. Thicker samples have not been prepared, however, it is

expected that the anisotropy of the clay is maximum under the highest applied pressure (Tokarský, Kulhánková et al. 2016).

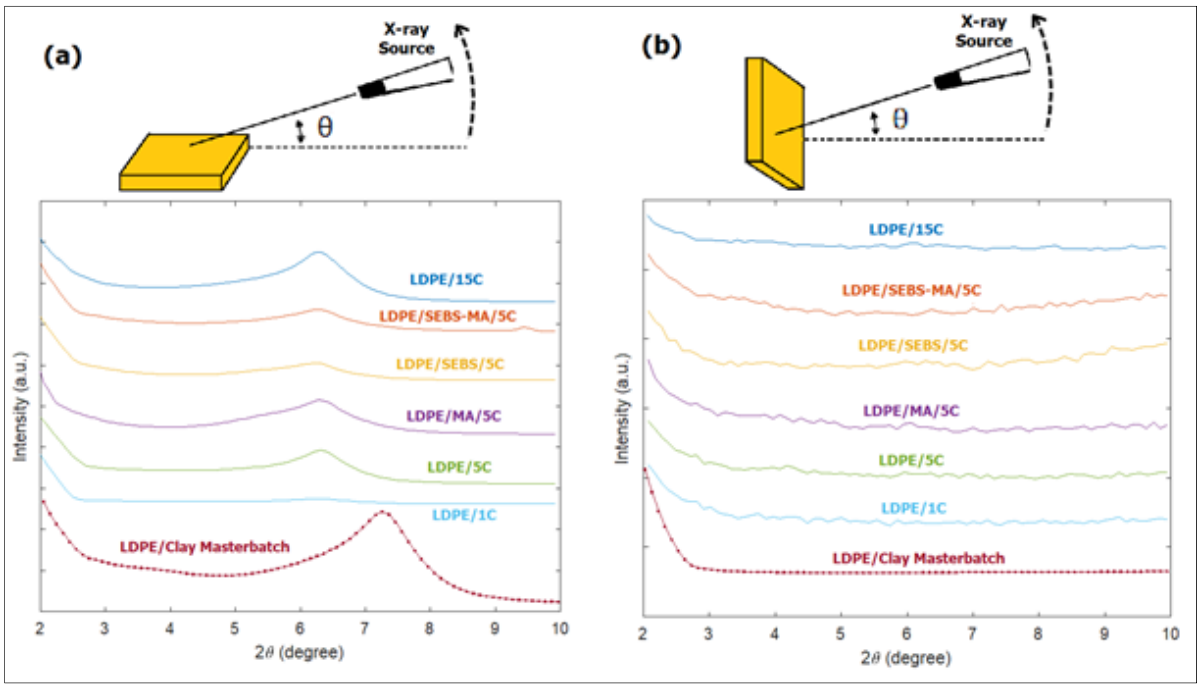

Figure 3-2 X-ray diffraction pattern for LDPE nanocomposites:
(a) Parallel emission and (b) perpendicular emission

However, XRD do not fully reveal the spatial distribution of the layered silicates; besides, some layered silicates do not show observable basal reflections. Therefore, the morphology of the nanocomposite must also be evaluated by other means of spectroscopy.

3.3.2 Scanning (SEM) & Transmission electron microscopy (TEM)

The dispersion of nanoclay was examined using SEM and TEM. Figure 3-3 shows both techniques' micrographs of LDPE nanocomposites reinforced with 5% clay. Stacks of clay tactoids with a high degree of aspect ratio and surface area are visible in both cases. They are uniformly distributed throughout the polyethylene matrix. A noticeable orientation of clay stacks is visible which is in agreement with the XRD results. The distances between clay sheets

are huge and stacks are totally separated from each other. Moreover, there are clear signs of polymer intercalation in some clay stacks as can be seen in TEM micrograph. However, sheets of clay are not fully inlaid within the LDPE matrix and despite the achieved separation, a noticeable amount of gaps is visible from SEM micrograph in the interfacial area. This hints that even surface modification of the clay does not fully repair the poor bond and weak interaction between hydrophilic silicate layers with the hydrophobic polyethylene.

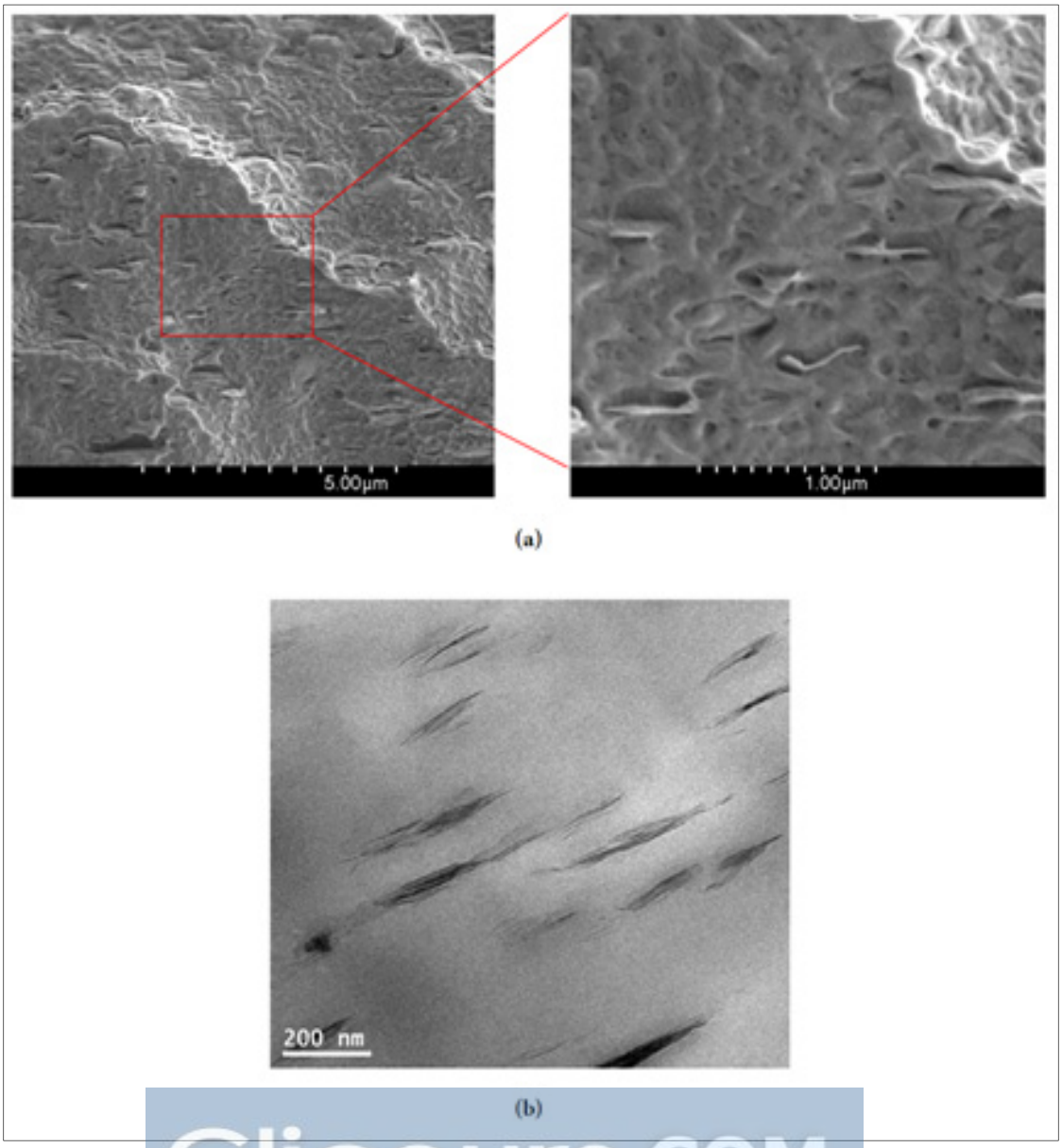

Figure 3-3 SEM (a) and TEM (b) micrographs for LDPE/5C

The SEM micrographs of blends and their nanocomposites are shown in Figure 3-4, alongside with their corresponding images where the SEBS phase is selectively removed using solvent extraction process. The white areas are believed to be the elastomer phase. When SEBS is blended with LDPE (a-d), a random micrometric mixture of the two phases are visible, which is revealed from the solvent extracted images to be a co-continuous structure. When SEBS-MA is used (e-h), the resultant is still a co-continuous structure. However, the elastomer phase is less evident, possibly because of the optical effects of MA grafted to the SEBS molecules.

Due to the complexity of the images, it is hard to point out the possible stacks of clay, but a noticeable change in the structure of both blends is obvious when 5% of clay is incorporated. The nanocomposites maintain the co-continuity but it goes to smaller dimensions. Regarding the elastomer phase, the curves and arcs are much smaller in the presence of nanoclay. Also the black holes in the solvent extracted images, representing the absence of the elastomer phase, have lower diameters. This downsizing effect of clay on the domain size of the constituents of the immiscible blends having cocontinuous structure has been previously reported (As' habi, Jafari et al. 2008, Filippone, Dintcheva et al. 2010). That means the introduction of clay into the blend actually alters the morphology of the blends. Clay may prevent or slowdown the coalescence phenomenon by acting as solid barriers or can act as compatibilizer and interact with the two components simultaneously (Ray, Pouliot et al. 2004, Liu, Wang et al. 2009). Even under weak interaction, clay has been reported to act as coupling agent among the polymer constituents (Si, Araki et al. 2006, Fang, Xu et al. 2007).

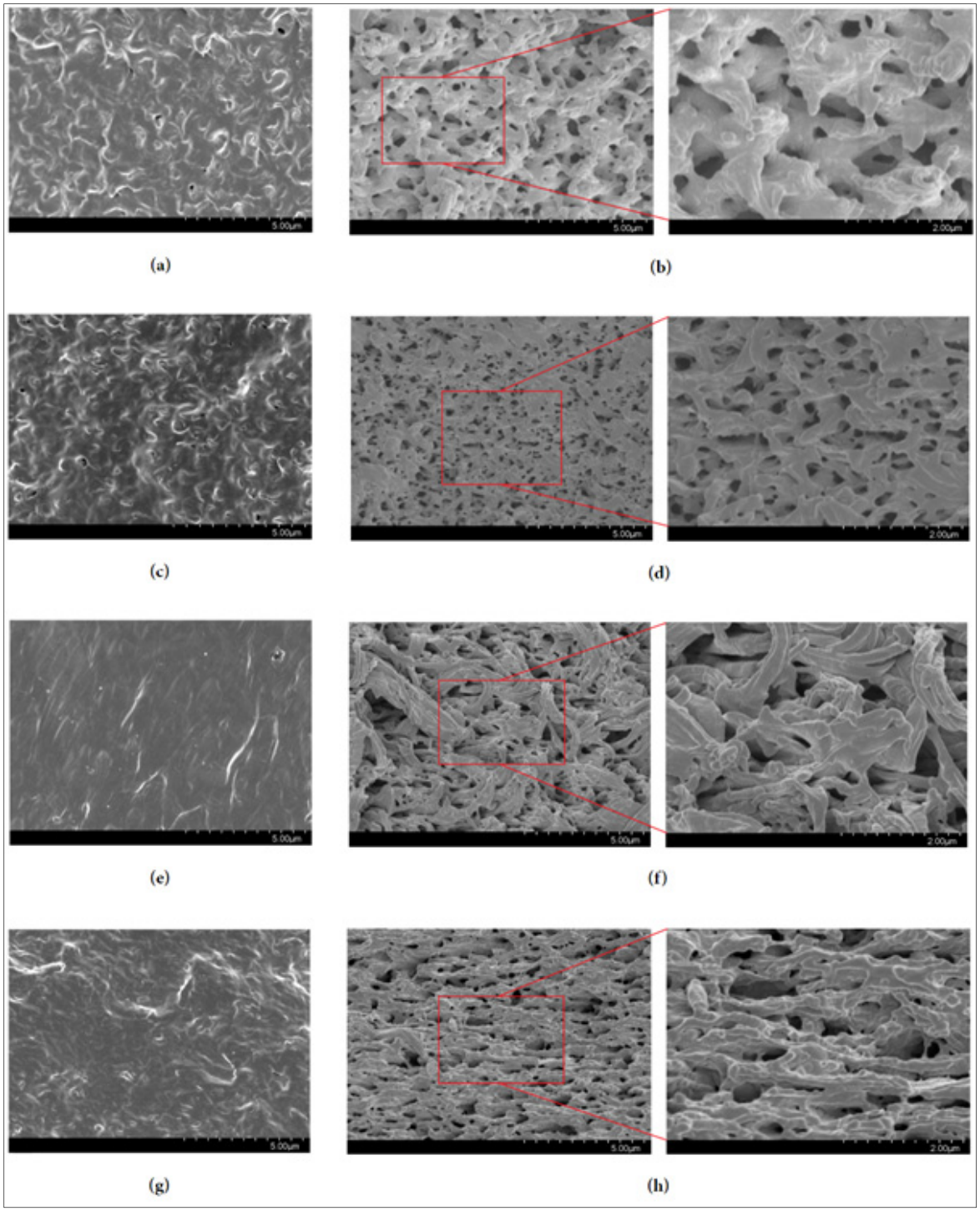

Figure 3-4 SEM micrographs of LDPE blends before and after solvent extraction: (a) and (b) LDPE/SEBS, (c) and (d) LDPE/SEBS//5C, (e) and (f) LDPE/SEBS-MA, and (g) and (h) LDPE/SEBS-MA/5C.

Regarding the SEM images of LDPE/SEBS-MA blend and nanocomposite (Figure 3-4 e&g), the surface texture appears to be more homogenously dispersed and domains are stretched alongside each other, signaling a smooth and strong interaction between the two polymers. This is probably due to the refinement of the SEBS backbone by grafted MA. Lower viscosity ratio of SEBS-MA also would induce a change of hydrodynamic stresses during the mixing, enhance the refinement by improving the phase separation kinetics and decreasing the interfacial tension (Minkova, Yordanov et al. 2003). However, the immiscibility in the blend comes from the polystyrene blocks of the elastomer phase which is highly incompatible with LDPE. Therefore, the refinement of ethylene-butylene midblock of the elastomer cannot dramatically change its mixing behavior. It would, however, make the elastomer phase more attractive towards clay, promote the melt intercalation process and accelerate the clay transportation.

It appears that the localization of clay and its possible selective interaction with the blend matrix constituents controls the morphology of the final nanocomposite. It is well-recognized that the localization of the nanoparticles is mostly determined during the mixing stage and further in the melting process. In low viscosity blends, the thermodynamic preferential attraction between nanoparticles and blend constituents determines the localization of nanoparticles, whereas, for higher viscosity, kinetic parameters such as sequence of feeding and viscosity difference of the components are dominating.

Direct feeding was used to prepare the samples, however, clay was available in the form of masterbatch, meaning it had already been mixed with polyethylene. This order of the component mixing directly influences the clay distribution and preferential localization since polyethylene is the less favorable phase for clay to be distributed in due to the polarity difference and thermodynamic attraction. In a binary system of clay and SEBS matrix, it was shown that clay nanoparticles would locate into polystyrene (PS) cylinders of SEBS and further into poly(ethylene-co-butylene) (PEB) blocks in case of SEBS-MA (Helal, Demarquette et al. 2015). With a narrow range of viscosity difference between the two polymer components, the interfacial energy becomes the main parameter determining the direction of redistribution of

the nanoparticle (Sumita, Sakata et al. 1991, Asai, Sakata et al. 1992, Persson and Bertilsson 1998). Therefore, there is a great chance that during the melt processing clay would be transported from polyethylene phase to the elastomer phase. A similar phenomenon was reported for carbon black nanoparticles and assumed to be the only feasible approach (Zaikin, Karimov et al. 2001, Zaikin, Zharinova et al. 2007). Also in another study Elias et al. (Elias, Fenouillot et al. 2007) reported that the hydrophilic silica would transfer from polypropylene to polystyrene phase during the melt mixing. Later, they reported the same mechanism for silica in polypropylene/Ethylene Vinyl acetate (EVA) blend (Elias, Fenouillot et al. 2008). As a result of this transportation the coalescence mechanism is obstructed and the polymer domains shrink into smaller size.

To evaluate this hypothesis, TEM observation was also conducted on LDPE/SEBS/5C sample, as illustrated in Figure 3-5. As can be seen, the orientation of clay sheets is hugely affected by the co-continuous structure of the blend matrix. Clay stacks and separated layers can be spotted in both phases that confirms the nanofiller's transportation, however, they are mainly located in the interface. This was expected since the mixing time do not exceed a few minutes and is well lower than the Brownian diffusion time required for clay to reach the preferred localization. Also the high aspect ratio of clay reduces the speed of the transportation. For the same reason the chance of clay getting stuck in the interface of the two phases is high, where also happens to be the area with low interfacial energy. Helal et al. (Helal, Amurin et al. 2017) estimated the wetting coefficient of ZnO nanoparticles in PE/SEBS-MA blend and reported that the nanoparticles should be mainly localized in SEBS-MA phase and probably at the interface PE/SEBS-MA. This conclusion can also be applied here since the values of surface tension for ZnO and organomodified clay are close to each other.

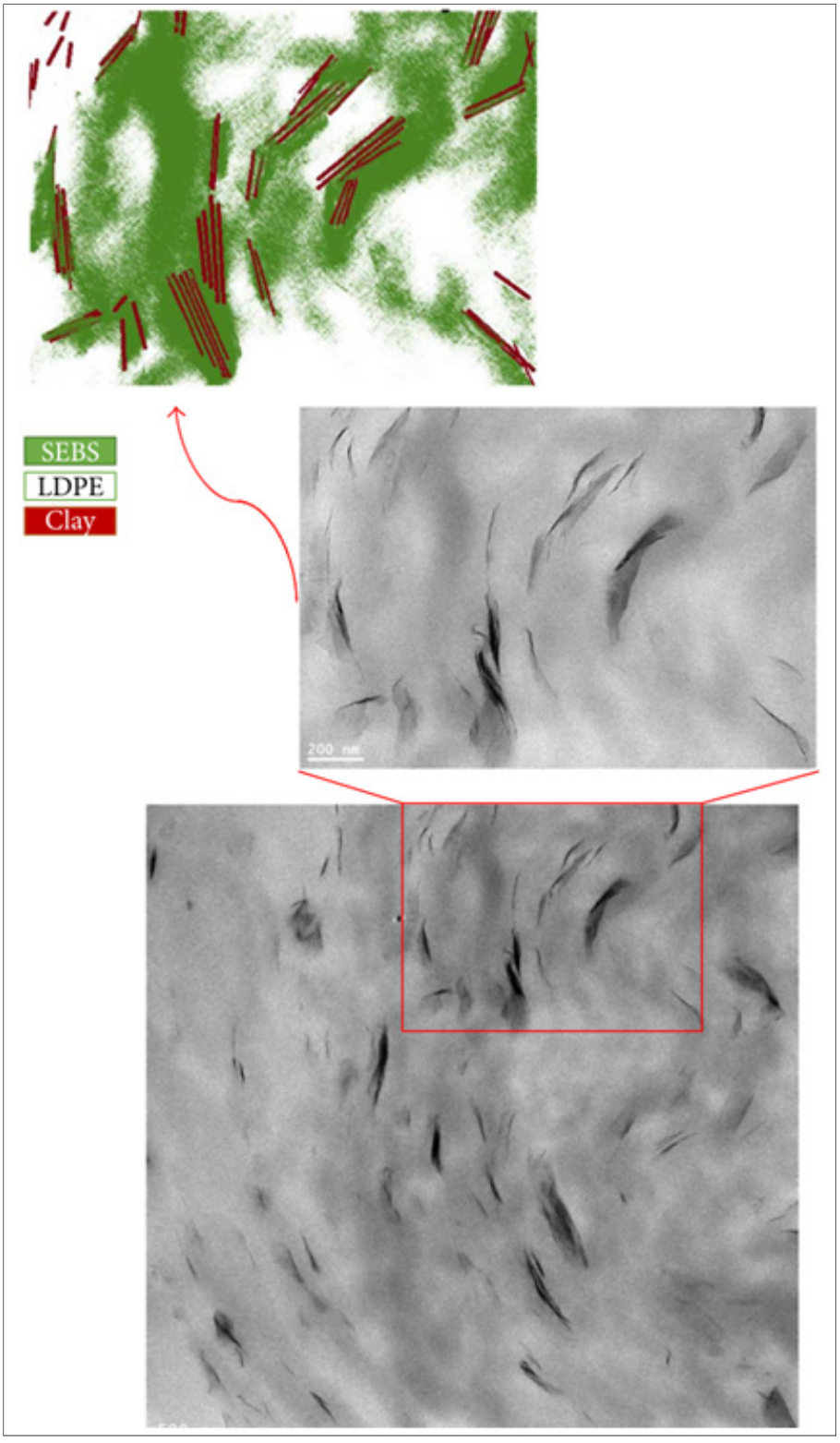

Figure 3-5 TEM micrograph of LDPE/SEBS/5C
(schematic phase representation on top)

3.3.3 Rheological properties

To have more insight of the dispersion of the clay and the morphology of the blends and nanocomposites at larger scale, Small Amplitude Oscillatory Shear (SAOS) test has been conducted. A small amplitude oscillatory strain under the processing temperature will result in a time-dependent linear shear stress. This linear viscoelastic approach of rheology gives us advantages of the sensitivity of rheology to nanostructure to gain understanding of the dispersion and the final morphology obtained in the presence of nanoparticles.

Figure 3-6 shows plots of storage modulus of LDPE and its blends and nanocomposites as a function of angular frequency. For neat LDPE a predictable terminal behavior is seen with a high slop and drop of the modulus at low frequencies. Similar behavior was obtained with the addition of nanoparticle up to 5% of clay where the plots of nanocomposites overlap the LDPE (not shown here) and show a homopolymer-like terminal behavior. This hints a relatively weak interfacial interaction of clay with LDPE, as was seen in SEM micrographs. Therefore, it is believed that within this range the nanoparticles' contribution is limited to the hydrodynamic effect. At 10% loading of clay (LDPE/10C) the curve slightly shifts to higher values. At 15% loading of clay (LDPE/15C) the increase is much larger and a plateau of storage modulus can be seen at low frequencies. At this point the rheological percolation threshold has been reached and nanocomposite exhibits a liquid-solid transition (LST) (Cassagnau 2008, Song and Zheng 2015). The increase of elasticity can be originated from the three-dimensional network formed by the clay-clay and/or clay-LDPE interaction and the resulting limitation in the molecular motion of the polymer which inclines the plot toward a solid-like response (Ren, Silva et al. 2000, Bagheri-Kazemabad, Fox et al. 2012). A similar behavior has been reported for nanoparticles other than clay (Lee, Im et al. 2006, Romeo, Filippone et al. 2008, Sarvestani 2008, Wu, Wu et al. 2008, Gong, Wu et al. 2009). In case of the nanocomposite containing compatibilizer (LDPE/MA/15C) this change of behavior is more pronounced. The low-frequency solid body response of LDPE/MA/15C nanocomposite is stronger than that of LDPE/15C. MA with lower molecular weight can easily enter the clay galleries and form a stronger interaction with the hydroxyl group on the clay layer (Hasegawa and Usuki 2004,

Ton-That, Perrin-Sarazin et al. 2004). This compatibilizing effect of MA increases the degree of interfacial interaction between LDPE/MA matrix and clay tactoids. As a result, due to the enhanced polymer intercalation the effective volume fraction of clay increases and consequently higher degree of clay dispersion is achieved. This is in accordance with the XRD pattern.

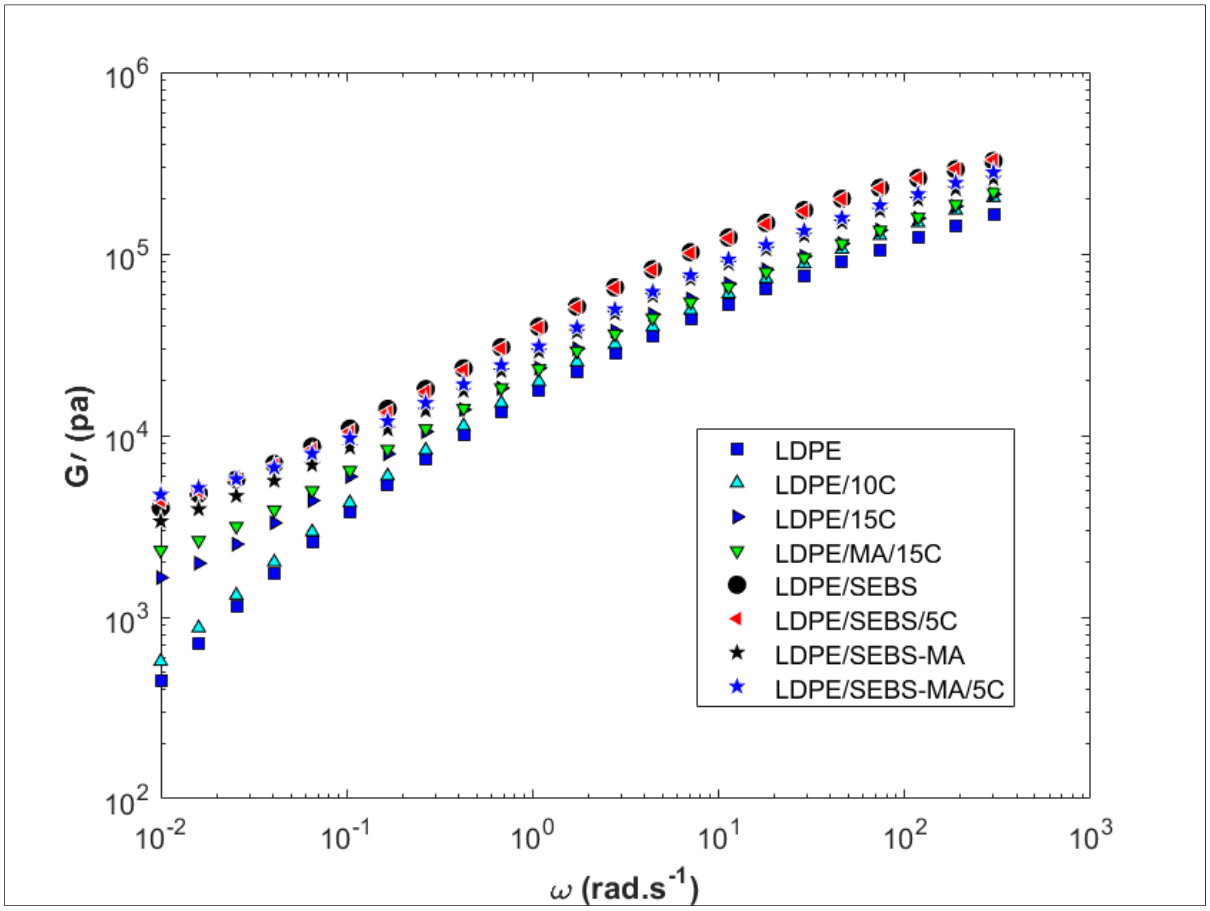

Figure 3-6 SAOS measurements of LDPE, SEBS blends and Clay-reinforced nanocomposites: Storage modulus (G') as function of angular frequency (ω)

A general look at the storage modulus plots for blends and their nanocomposites represents a consistent increase through the whole range and especially in low frequencies. Due to the high level of heterogeneity in block copolymers their rheological behavior is strongly related to the phase-separated morphology and it is brought into the blend. The low frequency increase in the storage modulus is as a result of the characteristic non-terminal behavior of block

copolymers and/or possible presence of droplets that deform and increase the elasticity (Carastan, Demarquette et al. 2008). It has been proposed that the dominant parameter in determining the rheology behavior of co-continuous blends is the components' contribution and it is rarely dependent on the morphology (Veenstra, Verkooijen et al. 2000). In fact, in the case of LDPE/SEBS blend this factor is either so strong that the introducing 5% of clay does not appear to change it or still there is a weak interfacial interaction between clay and the blend matrix similar to the binary nanocomposite. In the matrix of LDPE/SEBS-MA, however, clay noticeably enhances the storage modulus where its slope approaches zero towards low frequencies. Nanofillers dispersed in each phase increase the viscosity of that phase, but more importantly those located in the interface of the two phases change the morphology of the blend by suppressing the coalescence of the blend as was seen by the downsizing effect in SEM micrographs. This will enable the LDPE/SEBS-MA matrix to form a strong network with clay, most likely due to the interaction of functional groups of clay with the maleic anhydride groups grafted on the backbones of SEBS-MA (Helal, Demarquette et al. 2016). Also due to the lower viscosity of SEBS-MA, platelets and/or tactoids of clay are more easily transported, localized and dispersed in the elastomer phase. This improved degree of dispersion of clay helps forming a stronger percolated network structure and showing such a pronounced pseudo solid-like behavior (Khatua, Lee et al. 2004, Chow, Bakar et al. 2005, Tiwari, Hunter et al. 2012).

3.3.4 AC short-term breakdown strength

A two-parameter Weibull distribution was used to retrieve the dielectric breakdown data of blends and nanocomposites via a commercial software. Figure 3-7 exhibits the plots of AC short-term breakdown strength of LDPE/clay nanocomposites with different thicknesses alongside with a column chart to compare the Weibull characteristic breakdown strengths (α), which represent the scale parameter of the Weibull distribution, i.e. the 63.2th percentile. Scale and shape parameters are listed in Table 3-2. From Figure 3-7 (a) it can be found that when having an average thickness of 140 μm, all nanocomposite samples show improved breakdown strength. The characteristic breakdown strength for neat LDPE is 206 kV mm^{-1}, while it goes up upon addition of clay to 227 kV mm^{-1} for 1% incorporation of clay and to 248 kV mm^{-1}

when 2.5% of clay is incorporated. At maximum improvement it reaches 266 kV mm^{-1} for nanocomposite sample containing 5% of clay, showing almost 30% improvement, and then drops to 225 and 223 kV mm^{-1} for LDPE/10C and LDPE/15C samples, respectively.

Overall breakdown strength is enhanced at low nanoclay loadings up to 5% where it reaches the maximum, but decreased beyond a certain value. Consequently, there is an optimum loading of clay beyond which the enhancement is diminished. A similar trend was seen in other works (Li, Yin et al. 2011, Li, Yin et al. 2012). Under AC condition, the direction of the charge carrier transportation keeps changing back and forth which results in local trapping and charge accumulation in the areas close to the electrodes. Therefore, the electric field is enhanced more between the interface of the electrodes and the specimen where breakdown tends to initiate and propagate through the bulk. This suggests that the improvement of AC breakdown strength upon incorporation of clay may be originated from the delaying in the process of charge transfer between electrodes through the material. Layered clay silicates despite having weak interfacial interaction with the polymer matrix would postpone breakdown by creating a tortuous path between and around themselves for charge carriers to reach the opposite electrodes (Fillery, Koerner et al. 2012).

The influence of clay on improving the breakdown strength of polymers has been widely discussed among researchers. Zazoum et al. (Zazoum, David et al. 2014) observed a consistent improvement of dielectric breakdown strength on LLDPE upon addition of clay up to 20% when 5% clay is incorporated. They related the improvement to the impact of the interface between the polymer matrix and the nanoclay on the space charge distribution and charge densities. They also explained the further improvement on sample having compatibilizer to the possible change of microstructure. Thelakkadan et al. (Thelakkadan, Coletti et al. 2011) suggested that clay layers act as scattering sites for the charge carriers. During the scattering, the charges transfer their energy to nanoparticles and lose momentum. However, the nanoparticles are closely packed and do not involve in the breakdown process, therefore it requires additional voltage. This also suggests that the highest improvement happens when nanoclay is in the exfoliated state.

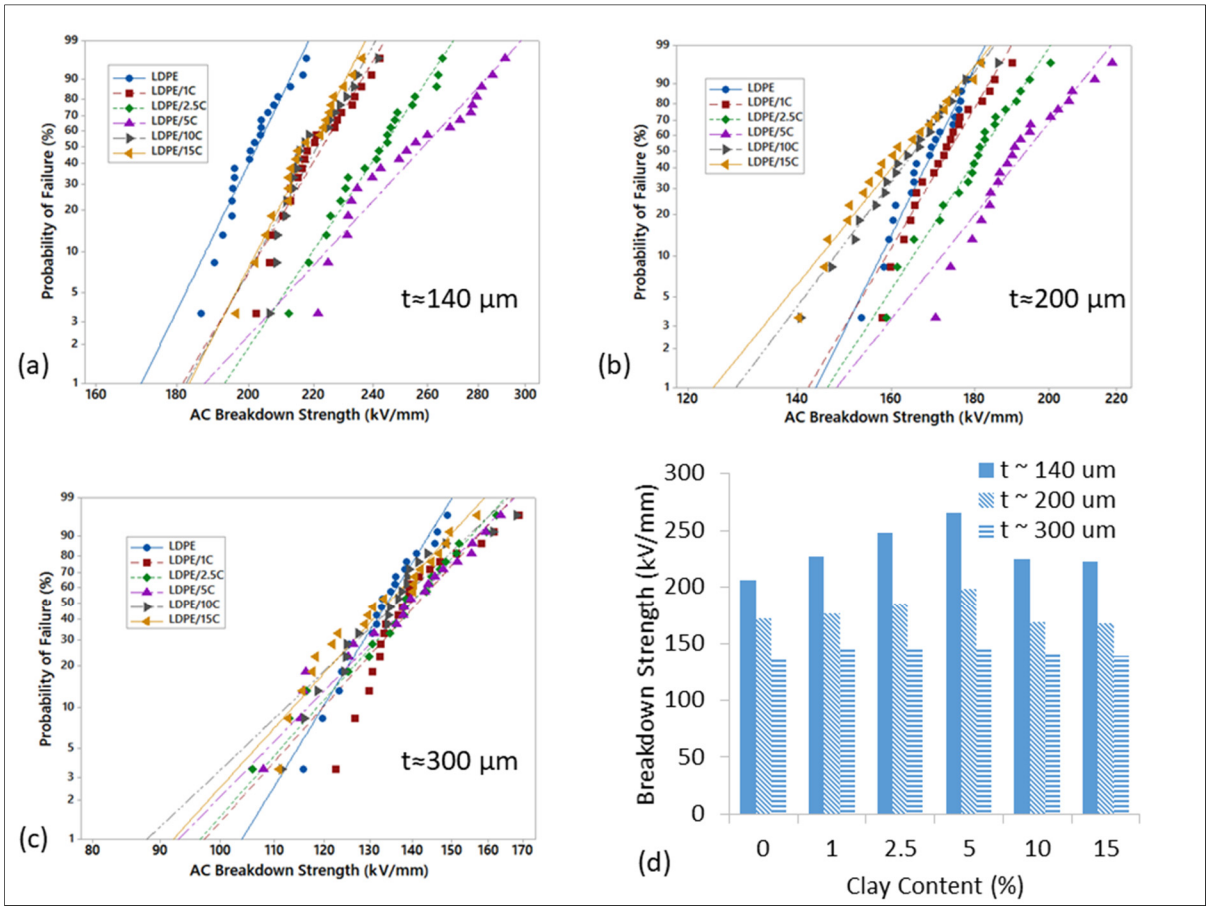

Figure 3-7 Weibull probability plots of LDPE/clay nanocomposites with different thicknesses: (a) 140 µm, (b) 200 µm, and (c) 300 µm. Comparison of the characteristic breakdown strength (d).

Liao et. al (Liao, Bai et al. 2013) investigated the electrical properties of LDPE composites containing various contents of montmorillonite. They found out that the AC breakdown strength increased when 1, 3 and 5% of MMT is incorporated, with the maximum improvement by 11% in case of 1% incorporation of MMT. Shah et al. (Shah, Jain et al. 2009) witnessed a massive 60% and 80% improvement in the dielectric breakdown strength of high density polyethylene (HDPE) upon addition of 5wt% of unmodified and organomodified clay respectively. They assumed that the exfoliated and intercalated clay platelets distribute the electric stress and increase the path length for the breakdown. They concluded that the

modification of clay with quaternary ammonium compound reduces the surface energy of the clay platelets making the intercalation of polymer molecules more feasible.

Moreover, Ghosh et. al (Ghosh, Rahman et al. 2016) reported a remarkable 84% improvement in the dielectric breakdown strength upon incorporation of only 0.2 wt% unmodified nanoclay into a poly(vinylidene fluoride) (PVDF) matrix. They observed a layer-by-layer structure of nanoclay within the PVDF matrix and hypothesized that the formation of the tortuous path between the electrodes blocks the path of the applied electric field and enhances the breakdown strength. This barrier effect has been shown to be maximum when the layers are oriented perpendicular to the field.

Table 3-2 Weibull parameters for AC breakdown test of LDPE/clay nanocomposites.

Sample*	Thickness ~ 140 μm		Thickness ~ 200 μm		Thickness ~ 300 μm	
	α (kV mm^{-1})	β	α	β	α	β
LDPE	206	24.96	172	25.56	137	16.59
LDPE/1C	227	20.73	177	21.26	146	11.33
LDPE/2.5C	248	18.26	185	19.41	144	11.43
LDPE/5C	266	13.20	198	15.75	145	10.40
LDPE/10C	225	22.10	169	16.74	142	9.66
LDPE/15C	223	22.70	167	15.59	139	11.23

* number of specimens is 20 for all samples

Also the orientation of clay layer can add to the magnitude of the improvement. Tomer et al. (Tomer, Polizos et al. 2011) studied the alignment effect of nanoclay on electrical properties of polyethylene. They reported that when 6% nanoclay is randomly distributed, the characteristic DC breakdown strength is not improved and the shape parameter is reduced from 21 to 7 with respect to the original matrix. However, when nanoclay is oriented the breakdown strength increases by 23% and the reduction in shape parameter is negligible. They hypothesized that the randomness acts as defect initiators, promoting electron tree inception; whereas the orientation of filler frustrates the progress of electrical treeing, by offering more

tortuous paths to treeing and possessing larger populations and more structured scattering centers. In their recent work they quantified the effect of orientation and confirmed the barrier effect (Li, Camilli et al. 2017). Bulinski et. al. (Bulinski, Bamji et al. 2010) challenged the type of nanoclay and concluded that polypropylene nanocomposite shows higher breakdown strength when it is reinforced with synthetic clay than with natural clay. They stated that this discrepancy goes to the degree of pureness, and the slightly lower improvement for natural clay is due to the negative effects of the impurities.

Studies on the influence of nanoparticles on the breakdown strength of polymers have not been limited to clay. A huge part of the recent works was dedicated to the polymeric nanocomposites containing silica nanoparticles. The incorporation of nanosilica is widely reported to decrease the AC & DC breakdown strength of polymers (Huang, Liu et al. 2010, Hosier, Praeger et al. 2014, Lau, Vaughan et al. 2014, Hosier, Praeger et al. 2015, Luo, Wang et al. 2016, Ritämaki, Rytöluoto et al. 2016, Krentz, Khani et al. 2017, Lau, Piah et al. 2017). However, there are some reports indicating no change (Tanaka 2005, Iyer, Gorur et al. 2011) or even improvement on the breakdown strength (Roy, Nelson et al. 2007, Takala, Ranta et al. 2010, Hui, Schadler et al. 2013). Readers are referred to a review on the effects of addition of nano-reinforcements on dielectric breakdown properties of polymers that has been published by Li et. al in 2010 (Li, Yin et al. 2010). Later, they published another review (Li, Camilli et al. 2017) with a comprehensive look into breakdown mechanism of nanocomposites.

From Figure 3-7 it is also clear that when the thickness of specimens increases the breakdown strength significantly decreases. For neat LDPE, α drops to 172 kV mm^{-1} and 137 kV mm^{-1} for samples with 200 μm and 300 μm thicknesses respectively. Nanocomposites also show reduced breakdown strength to the point where no significant improvement is detected with the thickest samples. The reduction of breakdown strength with sample thickness is a general trend for solid dielectrics. It is often related to the greater density of defects within the material (Chen, Zhao et al. 2012). Breakdown is believed to initiate from defects where electrons can gain enough energy since the free path length in insulating polymers is short and cannot be easily destroyed by electron avalanche (Theodosiou, Vitellas et al. 2004). These defects

include pre-existing discontinuities and defects generated while under electric field. The number of defects in the pathways of charge carriers is higher in thicker samples which facilitate the percolation path development, thus lowering the breakdown strength (Degraeve, Groeseneken et al. 1998, Kim and Shi 2001, Sune, Jimenez et al. 2001).

When modeling the breakdown mechanism, researchers have incorporated the empirical thickness dependence using a pre-factor term in Lorentz relation firstly introduced by Klein and Gafni (Klein and Gafni 1966). However, very recently J.W. McPherson (McPherson 2016) challenged this long-term belief. He stated that the reduction in breakdown strength of dielectric towards higher thicknesses comes from the reduction in bond strength as a result of higher electric field within the thicker dielectrics. He claimed that bond weakening leads to lower breakdown strength in thicker dielectrics and is independent of actual bond-breakage mechanism.

On higher loading of clay, the reduction in breakdown strength is more pronounced. This is because with increasing amount of clay, chance of particle agglomeration increases which adds to the defect density. Electric field is enhanced around these agglomerates and eventually advances the breakdown (Nelson and Fothergill 2004, Vaughan, Swingler et al. 2006, Lau, Vaughan et al. 2012). In samples with thickness of 200 μm (Figure 3-7, b) this effect dominates the mechanism, neutralizes the improvement of clay and takes α below the neat LDPE. Here the saturation effect happens at 5% of clay, above which the breakdown strength is heavily diminished. With 300 μm of thickness (Figure 3-7, c), the general defect density is large enough to solely dominate the breakdown mechanism and is independent of agglomeration effect of clay.

According to Table 3-3, Weibull shape parameter (β) is maximum for neat LDPE for all series but significantly decreases upon incorporation of clay. This is most likely originated from an evolution of the sensitivity of the measurement to defects which speeds up the breakdown and increases the unreliability. This scattering probability is mostly determined by the presence of clay tactoids boundaries, as was evidence in SEM images, and the possible agglomerates.

Figure 3-8 exhibits the Weibull probability plots for AC breakdown strength of a series of LDPE/Clay nanocomposites containing 5 wt% MA as compatibilizer (a), and blends of LDPE and two types of SEBS along with their corresponding nanocomposites containing 5% of clay (b). Comparing to the original LDPE/Clay nanocomposites, here more or less a similar trend in increasing the breakdown strength can be seen for samples containing MA. Saturation happens at 5% of clay and then reduces but still remains above the neat LDPE. However, the improvement is not significant as to compare when MA is not incorporated. This means the addition of MA compatibilizer was unnecessary and does not affect the breakdown strength enhancement, yet diminishes it to some degree.

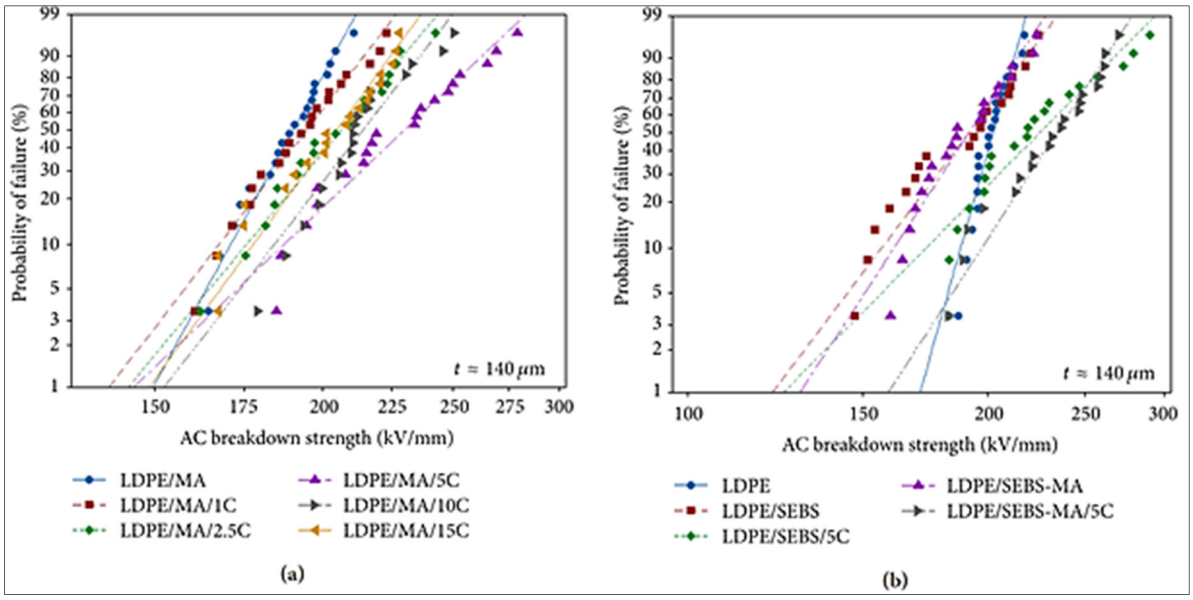

Figure 3-8 Weibull probability plots of LDPE/MA/clay nanocomposites (a) and LDPE/SEBS blends and nanocomposites (b).

Regarding the AC breakdown strength of blends of LDPE with SEBS elastomers (Figure 3-8, b), a noticeable reduction is seen comparing to the neat LDPE. α is down to 199 kV mm^{-1} for LDPE/SEBS and to 198 kV mm^{-1} for LDPE/SEBS-MA, while β is significantly reduced. This can be explained by the dilution effect, as neat SEBS polymer generally possesses lower breakdown value than the neat LDPE and according to the rule of mixture for plastics,

LDPE/SEBS blend is expected to have lower breakdown strength (Crawford 1998). The lower breakdown value for SEBS elastomer probably comes from its lower Young's modulus (Kollosche and Kofod 2010), where electromechanical tensile strength generated orthogonal to the field during breakdown mode would induce more voids and crack propagation in a similar manner to that caused by mechanical stress (Jones, Llewellyn et al. 2005). Upon addition of 5% clay, the characteristic breakdown strengths of blends significantly increase, similar to the result of original LDPE/clay nanocomposite.

3.3.5 DC short-term breakdown strength

Figure 3-9 compares the DC breakdown strength of blends and nanocomposites of LDPE. Table 3-3 lists the statistical variables of the mentioned plots. One can see that the DC breakdown strength of neat LDPE is as high as 470 kV/mm. From Figure 3-9.a, it goes down upon addition of clay for all the formulations and sinks to around 294 kV/mm at highest amount of nanofiller. The DC breakdown strength decreases with increased loading of clay. The only comparable result is seen for 2.5% loading of clay which shows a characteristic DC breakdown strength of 439 kV/mm. Blends of LDPE with both types of SEBS also show a noticeable 18% reduction in DC breakdown strength with having α around 386 kV/mm. Further reductions are seen for the corresponding nanocomposites containing 5% of clay.

Unlike the AC breakdown strength, the DC breakdown trend is completely different. It is strongly sensitive to the type of matrix and the amount of nanofiller and in all cases the DC breakdown strength is lower than that of neat LDPE. This behavior is not strange and has been reported before (Ma, Hugener et al. 2005, Yin, Dong et al. 2007, Huang, Ma et al. 2009, Lau, Vaughan et al. 2012). The reduction in DC breakdown strength could be originated from several parameters and it is beyond the agglomeration effect of nanofiller which was the primary reason for reduction in AC breakdown strength. Nevertheless, the particle agglomeration still remains as a simple explanation and its effect might be more pronounced on DC breakdown strength due to the higher required voltage for breakdown.

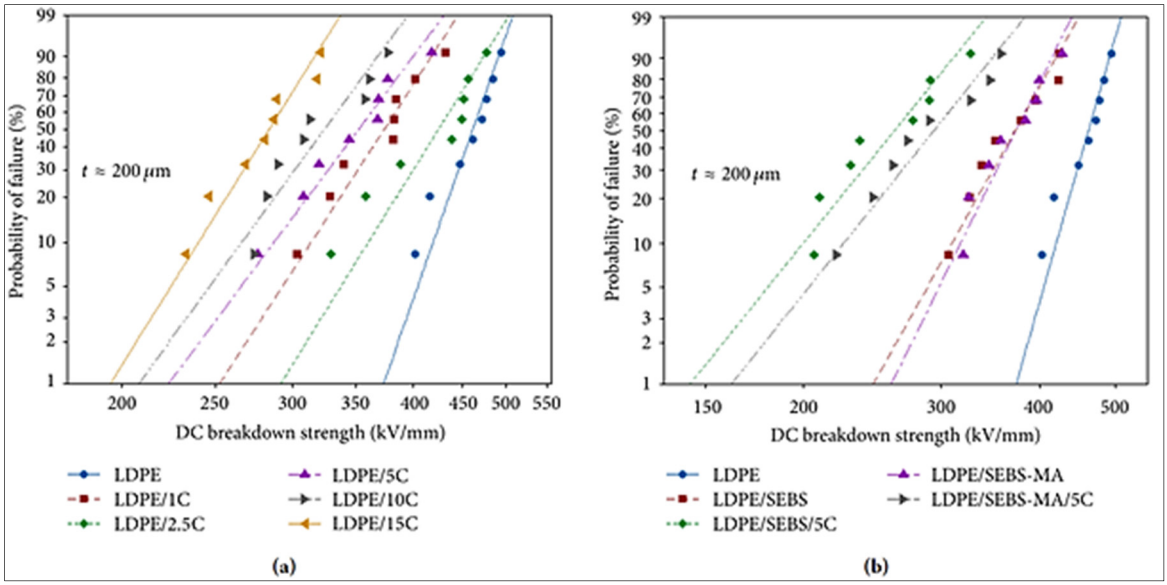

Figure 3-9 Weibull plots of LDPE nanocomposites reinforced with clay (a) and blends of LDPE and two types of SEBS along with their corresponding nanocomposites containing 5% of clay.

The increased charge trapping as a result of the introduction of clay can also contribute to the reduction of DC breakdown strength in nanocomposites. Charges can become stationary in trap sites around the nanoparticle, also known as space charge effect. This will increase the field inside the material and advance the breakdown. Space charge is not an issue for AC systems where the oscillating polarity reversal does not allow sufficient time for charge to be trapped. The poor dispersion of clay tactoids also adds to the magnitude of charge trapping and the breakdown strength goes to lower amount with increasing in clay loading. Thermal breakdown is another possible process of DC breakdown for LDPE (Nagao, Kimura et al. 1990), which under DC supply can be affected largely by the electrical conductivity. As the voltage goes up much more before breakdown comparing to AC test, it is possible that thermal instability of the material advances the breakdown.

Table 3-3 Weibull parameters for DC breakdown test of LDPE/clay blends and nanocomposites.

Sample	No. of Specimens	α (kV mm^{-1})	β	95% Confidence Intervals	
				Lower	Upper
LDPE	8	470	19.87	453	478
LDPE/1C	8	387	10.77	361	414
LDPE/2.5C	8	439	11.23	412	469
LDPE/5C	8	366	9.33	338	396
LDPE/10C	8	337	9.54	312	364
LDPE/15C	8	294	11.16	275	314
LDPE/SEBS	8	386	10.14	359	415
LSPE/SEBS/5C	8	276	7.02	248	306
LDPE/SEBS-MA	8	385	11.55	361	410
LDPE/SEBS-MA/5C	8	309	7.09	279	343

3.4 Conclusions

In this study dielectric breakdown properties of clay-based LDPE nanocomposites have been investigated as one of the most important parameters to evaluate the potentials to replace the current HV cable insulating materials. Clay layers have been shown to be widely dispersed and distributed in LDPE matrix, especially when a compatibilizer is utilized. As a result, a remarkable improvement on the AC breakdown strength of the nanocomposites has been achieved. This was maximized when 5 % of clay was incorporated, while the degree of improvements in lower amount of clay are still significant. It suggests that organo-modified clay has the potentials to make electrical properties of LDPE matrix comparable to currently used XLPE-type cable insulation materials considering its easy access and cheap price.

The use of immiscible blends of LDPE with two types of SEBS copolymer also showed interesting results upon addition of clay. It was witnessed that clay can alter the morphology of the blend when it is firstly mixed with the polyethylene through the migration process into the elastomer phase, and results in higher AC breakdown strength comparing to the unfilled

blends. Considering the proven mechanical flexibility of SEBS copolymer, this type of blends has the potentials to be used as insulating materials in HV applications.

Acknowledgements

The Authors acknowledge the sincere cooperation of the staff of the Laboratory of Innovation Technologies (LIT) at University of Bologna, especially Dr. Fabrizio Palmieri.

CHAPTER 4

ARTICLE 2: CHARGE TRANSPORT AND ACCUMULATION IN CLAY-CONTAINING LDPE NANOCOMPOSITES

M. Eesaee[1], E. David[1], N.R. Demarquette[1], Davide Fabiani[2], Fabrizio Palmieri[2]

[1] Mechanical Engineering Department, École de Technologie Supérieure, Montréal, QC, Canada
[2] Department of Electrical, Electronic, and Information Engineering, University of Bologna, Bologna, Italy

This article has been published in:
IEEE Transactions on Dielectrics and Electrical Insulation
Volume: 26 , Issue: 1, Pages: 292 – 299, February 2019,
DOI: 10.1109/TDEI.2018.007541

Abstract

This paper discusses the charge transport and accumulation in clay-containing LDPE nanocomposites. LDPE is shown to host charges of both polarities in the form of homo and heterocharge when subjected to high electric fields. Addition of nanoclays has been shown to always increase the high field DC conductivity of the nanocomposites by creating a transport network for charge carriers. This is shown to actually work in favor of the ability of the material to prevent the accumulation of space charge by slowly, but persistently, allowing space charges to flow across the insulation wall. However, in severe conditions of a combined high electric field and high temperature, the current flow exceeds a threshold where massive injected charges negatively impact the charge profile and the electric field distribution is heavily distorted.

Keywords: Conductivity measurement, Space charge, PEA, Electric field distortion.

4.1 Introduction

Underground and submarine cables are important components in the power grid for the transmission and distribution of electricity and it is of vital importance that they should function reliably for many years. To reach this goal and further improvements in transmission capacity, efforts must take place to improve the insulation layer as the heart of the HV cable. By this date, a huge portion of HV cables installed around the world comprise paper-oil insulation. However, in recent decades polymeric extruded insulation cables have been gained attentions in this regard. In particular, the cross-linked polyethylene insulation cables or XLPE has become the primary cable insulation material for both high voltage AC and DC applications because of its mechanical flexibility, thermal endurance and excellent dielectric properties (Lawson 2013, Chen, Hao et al. 2015, Wang, Li et al. 2016).

Despite all the advantages, XLPE cables can suffer from several problems such as thermal degradation and the lack of recyclability (Liu, Liu et al. 2017, Ouyang, Li et al. 2017, Wu, Wang et al. 2017). Those employed for high voltage direct-current (HVDC) applications have also been shown to have the tendency to accumulate space charge, which can lead to failure, especially when encountering polarity reversal operations (Hanley, Burford et al. 2003, Wang, Luo et al. 2017). Interests have been expressed as to improve the performance of HV cables as the use of XLPE cables grew. Nanometric dielectrics, or nanodielectrics, consisting mainly of a polymeric matrix and a nanometric reinforcement have been the subject of many researches in recent decades since the introduction by Lewis (Lewis 1994). A great choice of nanoreinforcement is layered silicate fillers, for which many nanocomposites have been produced and analyzed. The incorporation of small percentage of nanoclay has shown to improve the thermal and mechanical properties of polymers. They are also reported to have superior electrical breakdown strength (Eesaee, David et al. 2018), improved partial discharge and volume resistivity to erosion (Kozako, Fuse et al. 2004, Tanaka 2010) but always higher dielectric losses at power frequency (David, Fréchette et al. 2013) comparing to unfilled polymer.

In addition, mitigation of space charge accumulation can potentially be reached with such nanocomposites which is of vital importance since less accumulated space charge in the insulation material allows for higher applied electric field at the same cable geometry and as a result the weight and cost of power equipment will be decreased. This can be possible due the barrier effect of the clay platelets, ioning trapping of the inorganic filler and also a slight increase of the DC conductivity allowing space charges to slowly flow across the insulation wall instead of accumulating inside the insulation bulk. Thus, understanding the space charge behavior of clay-containing polymers is of necessary for designing new materials for HV applications.

This manuscript is a continuation to the authors' previous work where it was shown that the addition of clay nanofiller significantly improves the AC electrical breakdown strength of LDPE and its blend with SEBS (Styrene-Ethylene-Butylene-Styrene block copolymer), while always results in inferior, but comparable, DC electrical breakdown properties (Eesaee, David et al. 2018). This investigation resumes in this report by evaluating the charge transport and accumulation within the same materials to have a general view of their potential for applications as insulating walls in HV cables or for other applications for which surface or internal charging is an issue such as spacecraft dielectrics (Hands and Ryden 2017).

4.2 Experimental

4.2.1 Materials and Processing

A premixed LDPE/Clay commercially available masterbatch was diluted with pure LDPE in powder form to achieve clay-containing LDPE nanocomposites with desired concentrations of nanofiller (1%, 2.5%, 5%, 10% and 15%) in a co-rotating twin screw extruder. The masterbatch contains nominal 50 wt % of montmorillonite clay which has been treated with compatibilizing agents to enhance their dispersion within the polymers. The obtained pellets were then press-molded into thin plates with thickness around 280 μm. Morphology of the as-obtained nanocomposites were investigated in the authors' previous work where it was shown in SEM

images that stacks of nanoclay are uniformly distributed throughout the polyethylene matrix. Further observation through TEM images revealed clear signs of polymer intercalation where numerous individual high aspect ratio clay platelets were spotted separated from each other and partial exfoliation is achieved (Figure 4-1). The apparent orientation of the nanoparticle was related to the high pressure and high temperature condition of the molding process of pellets into thin plates. The readers are referred to the authors' previous work for detailed information about the materials, nomenclature and experimental procedure (Eesaee, David et al. 2018).

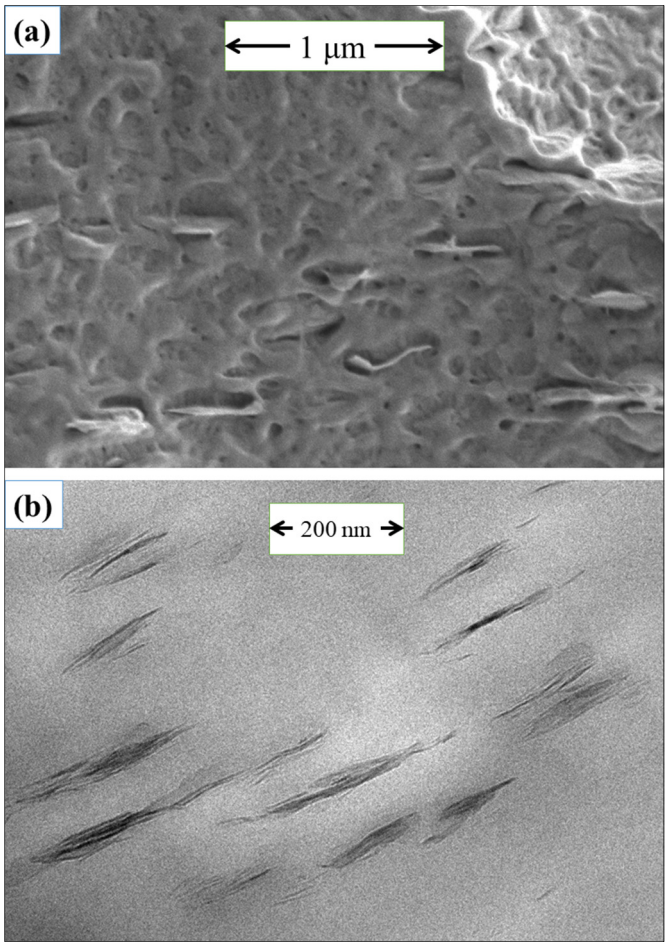

Figure 4-1 Micrographs of LDPE/5C:
a) SEM and b) TEM

4.2.2 Characterization

Conduction current measurements were conducted using a three electrodes system under a field of 50 kV/mm at 30 ˚C. Supplementary measurements have been conducted on neat LDPE and LDPE/2.5C nanocomposite (containing 2.5% nanoclay) under different fields (30, 40 & 50 kV/mm) and different temperatures (30, 50, 70 & 90 ˚C) to evaluate the effect of temperature and field variations. Samples were sputtered by gold prior to testing. Figure 4-2 shows the detailed experimental setup used to measure the conductivity of the samples. The system is consisted of main and guard electrodes on one side, and a counter electrode on the other side. The whole system was placed in an oven, where the temperature was stabilized before starting the test. The measurement lasted until the steady state conduction was achieved which took an average time of 24 hours for each sample. An average of the last 100 points after stabilization was considered as the conduction current. Charging and discharging current was continuously monitored using a digital electrometer (Keithley 6514) and the system was computerized using a Labview application.

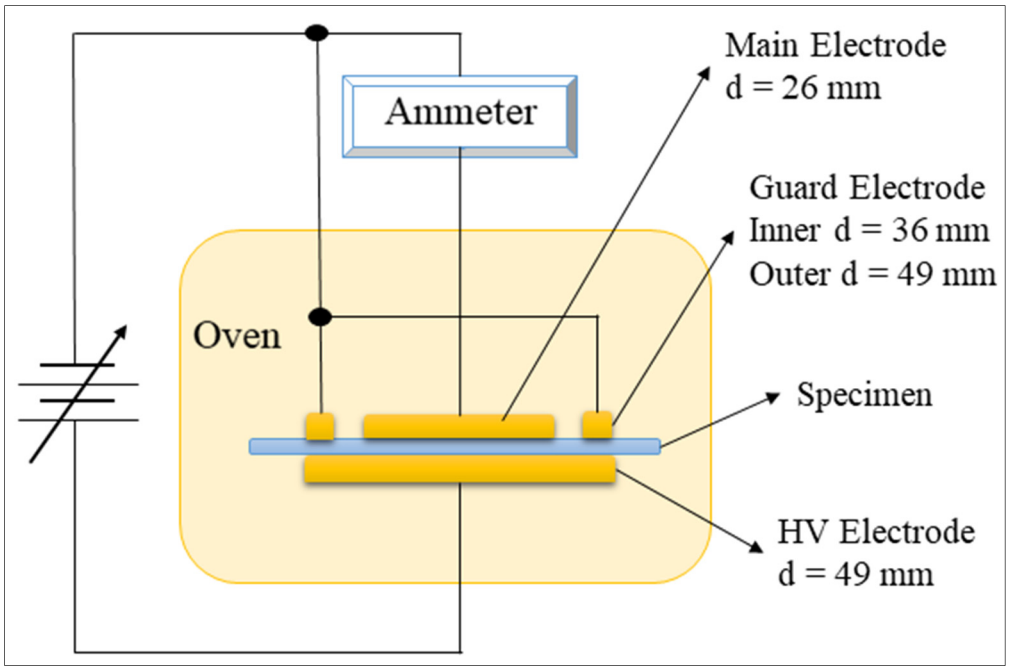

Figure 4-2 Experimental setup for the conduction current measurement

Pulsed Electroacoustic technique (PEA) has been used to measure the space charge profile under the application of DC electric fields. In this method the interaction of a pulsive electric field and space charges inside the sample creates acoustic waves that propagate through the sample to be detected by the transducer. More information about this technique can be found elsewhere (Maeno, Futami et al. 1988, Jiang, Peng et al. 2017). In order to attenuate sonic impedance mismatch, a semiconductive layer was placed between the specimen and HV electrode. While samples were experiencing the DC field for a duration of 10000 s in the polarization stage, a HV pulse with an amplitude of 500 V and duration of 10 ns was applied to collect the charge profile information within the specimen. At the end of the polarization phase, the HV source was short-circuited to record the depolarization profile for a duration of 3000 s. The space charge measurements have been conducted on different samples at ambient (25 ˚C) and higher (60 ˚C) temperature under different electric fields. Figure 4-3 illustrates a schematic representation of the PEA setup used in this study.

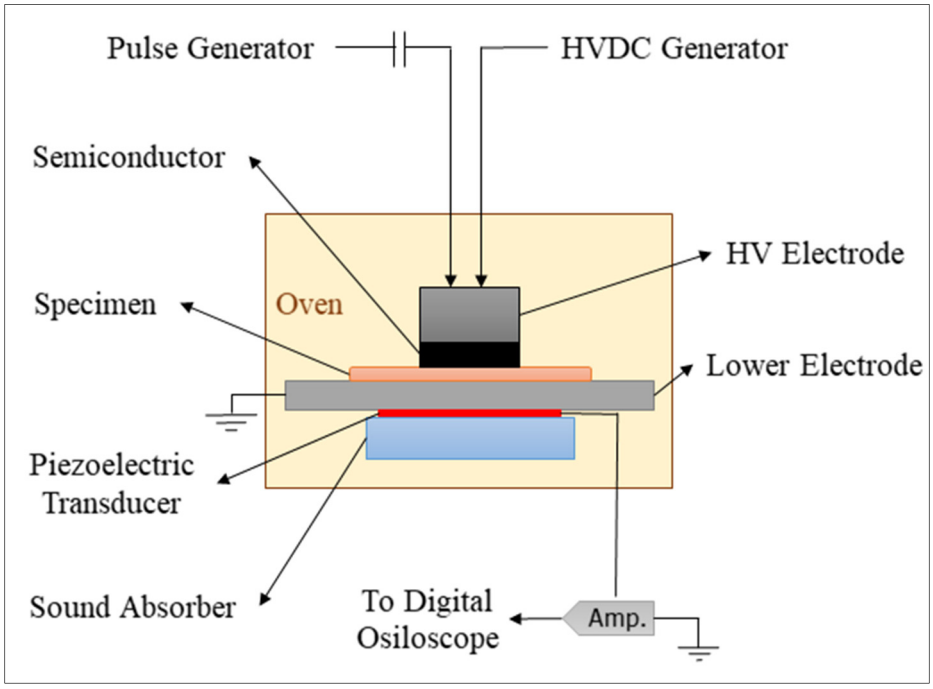

Figure 4-3 Schematic representation of the PEA setup

4.3 Results and Discussion

4.3.1 Electrical DC conductivity

High-field DC conductivity measurements are important to gain understanding of conduction mechanisms of insulating materials especially for their usage in HVDC extruded cable systems. Polarization (charging) currents of neat LDPE and its clay-containing nanocomposites over time at 30 ˚C and under 50 kV/mm electric field are depicted in Figure 4-4.a. The calculated corresponding DC conductivities from the measured conductive current after achieving the steady state are shown in Figure 3b. For neat LDPE, the polarization current immediately decreases by three decades which corresponds to the fast polarization. It then gradually decreases over time, corresponding to slow polarization, and after around 24 h the steady state is achieved and the current is believed to be fully conductive. The calculated conductivity for LDPE at 50 kV/mm is around 1 x 10^{-15} S/m which is close to the values reported in the literature (Murata, Sekiguchi et al. 2005, Andersson, Hynynen et al. 2017). Upon addition of clay, there is a significant increase in the level of high-field conductive current and hence the high-field DC conductivity. There is more than 2 decades increase in conductive current when only 1% of clay is incorporated, and it continues to increase towards higher percentages of clay. From 5 to 10% of clay loading, there is an increase of almost three decades of current and the DC conductivity reaches to 1.9 x 10^{-12} S/m when 15% of clay is incorporated.

The presence of a maximum value in the time dependence of the current for the LDPE/1C nanocomposite is in good agreement with the space-charge limited current theory and also in agreement with the numerical solution of the transport equations when trapping and detrapping of charge carriers are taken into account and when Schottky conditions are used at the electrodes (Le Roy, Segur et al. 2003). It also appears that under high electrical field, a sharp increase of the conductivity, similar to a percolation threshold, is already achieved at a concentration of 1 wt% (which was not observed at lower field). Very low percolation thresholds are typical of high aspect ratio inclusions. They are indeed commonly observed in

the case of CNT-based composites (De Lima, Amurin et al. 2016) and can also be predicted by Monte Carlo simulation of composites filled with circular nano-disks (Oskouyi and Mertiny 2011).

On the other hand, reductions in electrical conductivity of nanocomposites have been reported several times for nanocomposites containing metal-oxide nanoparticles (Fleming, Pawlowski et al. 2005, Fleming, Ammala et al. 2008, Murakami, Nemoto et al. 2008). The main explanation given is that during the cooling stage, the polymer molecules are encouraged to regain the natural polycrystalline morphology where hydrocarbon chains form planar crystalline lamellae 10-20 nm thick and ~100 nm wide growing out from nucleation points to form spherulites. Growing crystalline lamella will reject the particles, impurities and entangled polymer chain structures to form inter-lamella amorphous phase. In case of nanometric particles, such as metal-oxide, some particles might be left in the inter-crystalline amorphous phase as crystallization proceeds that will strongly influence the hole/electron tunneling between lamella across the amorphous phase. Due to the difference in the band gap of the most metal-oxide nanoparticles with polyethylene, additional potential barriers are involved which results in increased mean tunneling barrier and lowered local hole inter-lamella transition rate (Lewis 2014). Consequently, the overall macroscopic mobility and conductivity is lowered. The number of affected transition depends on the average diameter and concentration of the nanoparticle.

In case of layered silicate, such as montmorillonite clay, and due to the high aspect ratio and the tendency to form stacks and agglomerates, they are not expected to be included in the inter-lamella regions. Instead, they are most likely accommodated in the inter-spherulites region and therefore, will not engage directly in a hole or electron tunneling process between crystallites at the nanometric level. The increase in the conductivity of nanocomposites can be more simply related to the formation of high field conductive paths and the increase of mobile charge carriers including free ions introduced by clay nanoparticles due to mobile ion scavenger capability of nesosilicates dispersed within the polymer matrix. It should be noted that the

connectivity criterion changes from low field to high field since hopping between inclusions is strongly field-dependent.

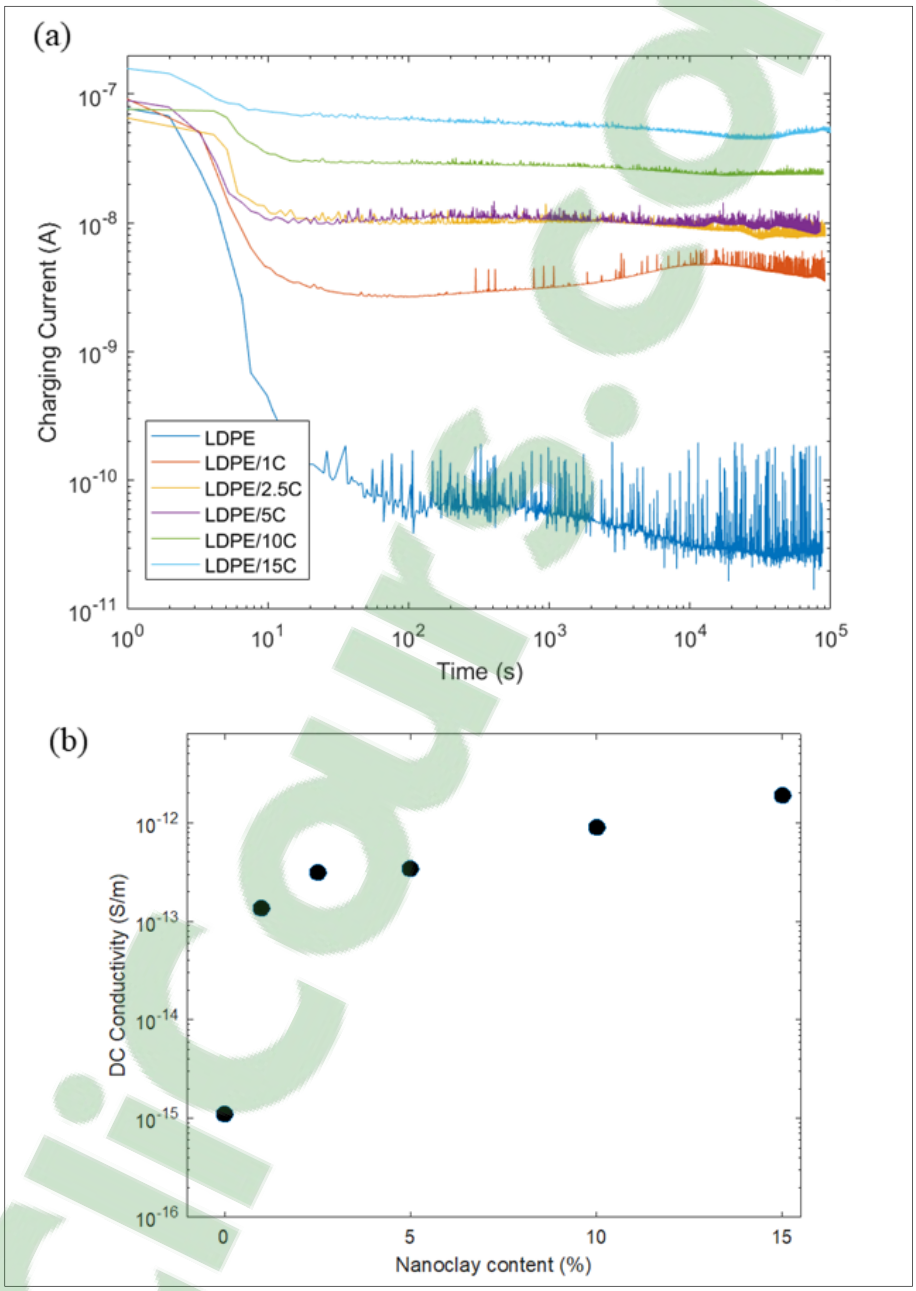

Figure 4-4 a) Charging currents of LDPE and its nanocomposites at 30 ˚C and under applied DC electric field of 50 kV/mm; b) calculated DC conductivities from steady state part of the charge currents

Since the crystallites do not support ionic transport, the remaining ionic path is in the amorphous phase where the majority of clay nanoparticles are located. The structural symmetry due to the intercalated structure and the huge aspect ratio of clay nanoplatelets even more facilitate the conduction path and make it possible to obtain a massive increase in the conductivity even at low concentration of nanoclay. It should also be noted that even if ionic conductivity is involved in the early conduction process, the long term steady-state current is essentially due to electronic conductivity that takes over after the ionic species reach an equilibrium state resulting in electrode polarization.

DC conductivity in polymeric material is temperature and electric field dependent and this dependency is often analyzed using the empirical equation below (Murata, Sekiguchi et al. 2005):

$$\sigma = \sigma_0 \exp(\alpha T) \exp(\beta E) \tag{3-1}$$

Where α and β are the temperature and electric field coefficients respectively. The dependency to electric field is shown in Figure 4-5.a where the DC conductivities for neat LDPE and LDPE/2.5C nanocomposite are illustrated at 30˚C and under different fields: 30, 40 and 50 kV/mm. The DC conductivity for LDPE remains almost the same while it monotonously increases for the nanocomposite. According to equation 3-1, the estimated electric field coefficients for LDPE/2.5C is almost ten times higher than that of neat LDPE ($\beta_{2.5}$C=0.132 mm/kV, β_{LDPE}=0.014 mm/kV). The DC conductivity can also be modelled by a power law relationship towards electric field (Alison and Dissado 1996, McAllister, Crichton et al. 1996, Zhang, Li et al. 2016):

$$\sigma = \sigma_0 \exp(\alpha T) E^{\beta} \tag{3-2}$$

The experimental results fit as well equation 3-2 with the same field coefficient ratio ($\beta_{2.5}$C=5.49, β_{LDPE}=0.55). It appears that electric field variation directly influences the conductivity of nanocomposite and a stronger applied field enhances the mobility of charge carriers to drift/migrate to the opposite electrode rather than accumulate at the interface region.

The dependency to temperature is shown in Figure 4-5.b where the DC conductivities of neat LDPE and LDPE/2.5C nanocomposite are illustrated under 50 kV/mm of electric field at different temperatures: 30, 50, 70 and 90 ˚C. Applying equation 3-1 fits well to the experimental results if the low temperature DC conductivity of the nanocomposite is ignored. The temperature coefficients have almost the similar values ($\alpha_{2.5C}$=0.083 K^{-1}, α_{LDPE}=0.074 K^{-1}) indicating that temperature variation effect is mostly controlled by the matrix not by the nanofillers. Generally, it is believed that the conductivity of polymers is thermally activated and Arrhenius-type model can describe this physical phenomenon:

$$\sigma(T) = \sigma_0 \exp(-E_a/kT) \tag{3-3}$$

where σ_0 represents the pre-exponential factor, E_a represents the activation energy and k represents the Boltzmann constant. The estimated activation energy for LDPE/2.5C is slightly higher (0.84 eV) than that of neat LDPE (0.7 eV). However, four points of data is certainly not enough to accurately estimate the activation energy. It was reported in the literature that above 45 ˚C the activation energy of LDPE changes from 1 eV to 0.6 eV (Boudou, Griseri et al. 2004). This may also explain the low temperature deviation noted for LDPE/2.5C.

The increased DC conductivity at higher temperatures following an exponential relation can readily be explained referring to bulk limited conduction mechanisms for which the material is represented by a series of potential wells with given depth and separation. The conduction process then relies on thermally assisted hopping between localized states, which leads, after some approximations, to the exponential expression given in equation 3-2. Much more detailed (and more sound) models have also been reported using an effective mobility given by an equation similar to 3-3 and taking also into account bipolar trapping and recombination of carriers as well as Schottky injection at the electrode/dielectric interface (Le Roy, Segur et al. 2003). The transport equations can then be numerically solved yield the current density as a function of time. It generally leads, as expected, to an increase of the number of effective

charge carriers as well as their mobility resulting in a higher conductivity as the temperature increases.

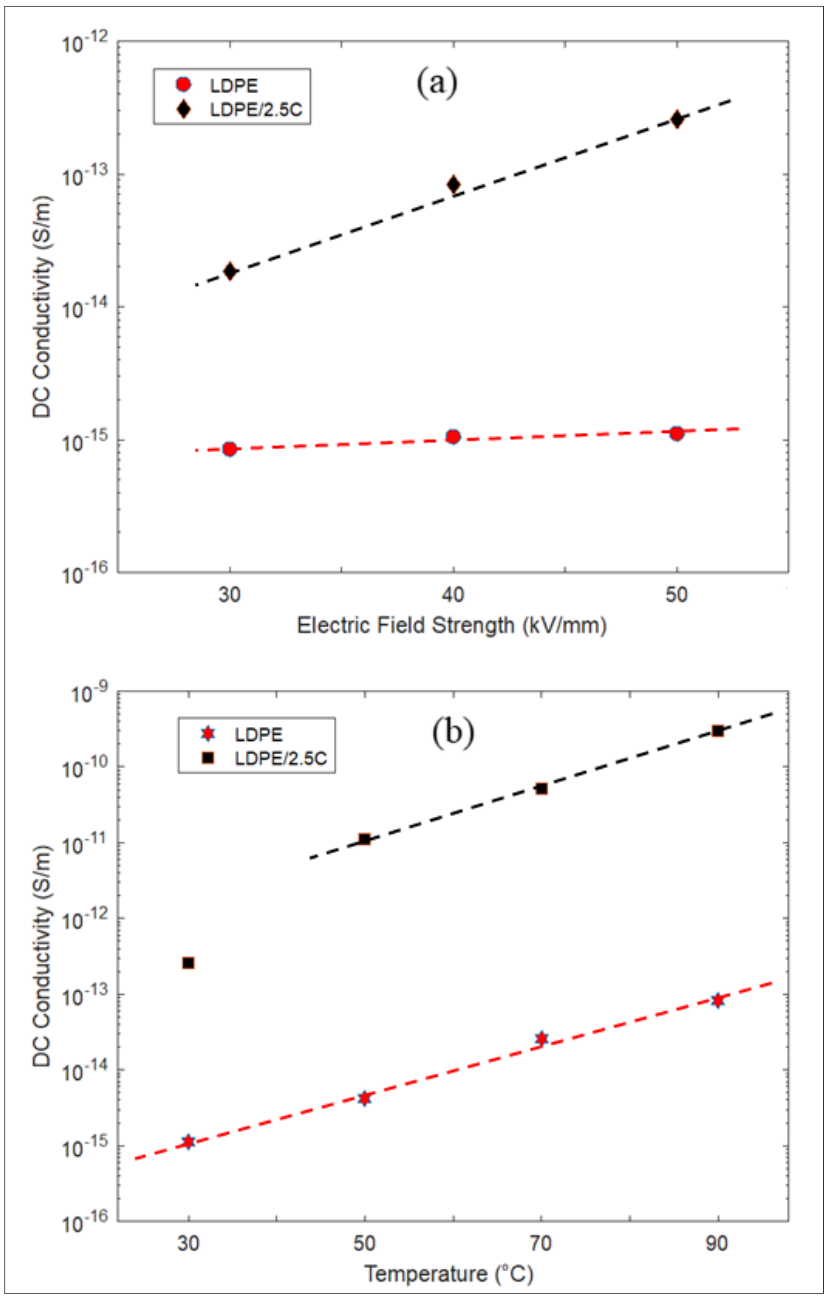

Figure 4-5 Effect of field variation (a) and Temperature (b) on charging currents of LDPE and LDPE/2.5C at 30 ˚C

It must be noted that to reach the highest voltage levels and transmission capacity of HVDC power cables the insulating materials must display low DC conductivity, controlled space charge accumulation together with high electrical breakdown strength. The low DC conductivity is favorable but is not the ultimate goal. The major cause of failure in HVDC systems is the accumulated space charge and its distribution is a function of the gradient of the DC conductivity in the insulation layer. The tendency to space charge accumulation is being investigated in the following section.

4.3.2 Space Charge Measurement

Figure 4-6 illustrates the time-dependent charge distribution profiles of LDPE and LDPE/5C under different poling fields from 10 kV/mm to 70 kV/mm at 30 ˚C. At the lowest applied electric field (10 kV/mm) no accumulated space charge is detected in the bulk of LDPE or LDPE/5C nanocomposite.

For neat LDPE at 30 kV/mm, a packet of positive charge is injected by the HV electrode which gradually penetrates and disperses in the polymer bulk while a thin layer of negative homocharge on LV electrode builds up. For nanocomposite, however, the increase in the electric field does not appear to have more than a slight effect on the charge distribution: a very small heterocharge buildup close to the electrodes can be observed at the beginning of depolarization step.

When the electric field goes up to 50 kV/mm, the positive charge packet leaving the HV electrode is much bigger in LDPE than at 30 kV/mm. The vast amount of injected positive charge overwhelms negative charge injected from LV electrode, thus spreading in all the insulation bulk. Positive charge is accumulated mostly as homocharge close to the anode.

When the electric field is at the highest level (70 kV/mm), a big amount of negative charge injected from the LV electrode triggers several positive charge packets which transit in the insulation bulk repeatedly during polarization step in a background of bulk negative charge.

The nanocomposite sample shows the same pattern under 50 kV/mm of electric field, but with a slightly more enhanced negative charge layer in the middle.

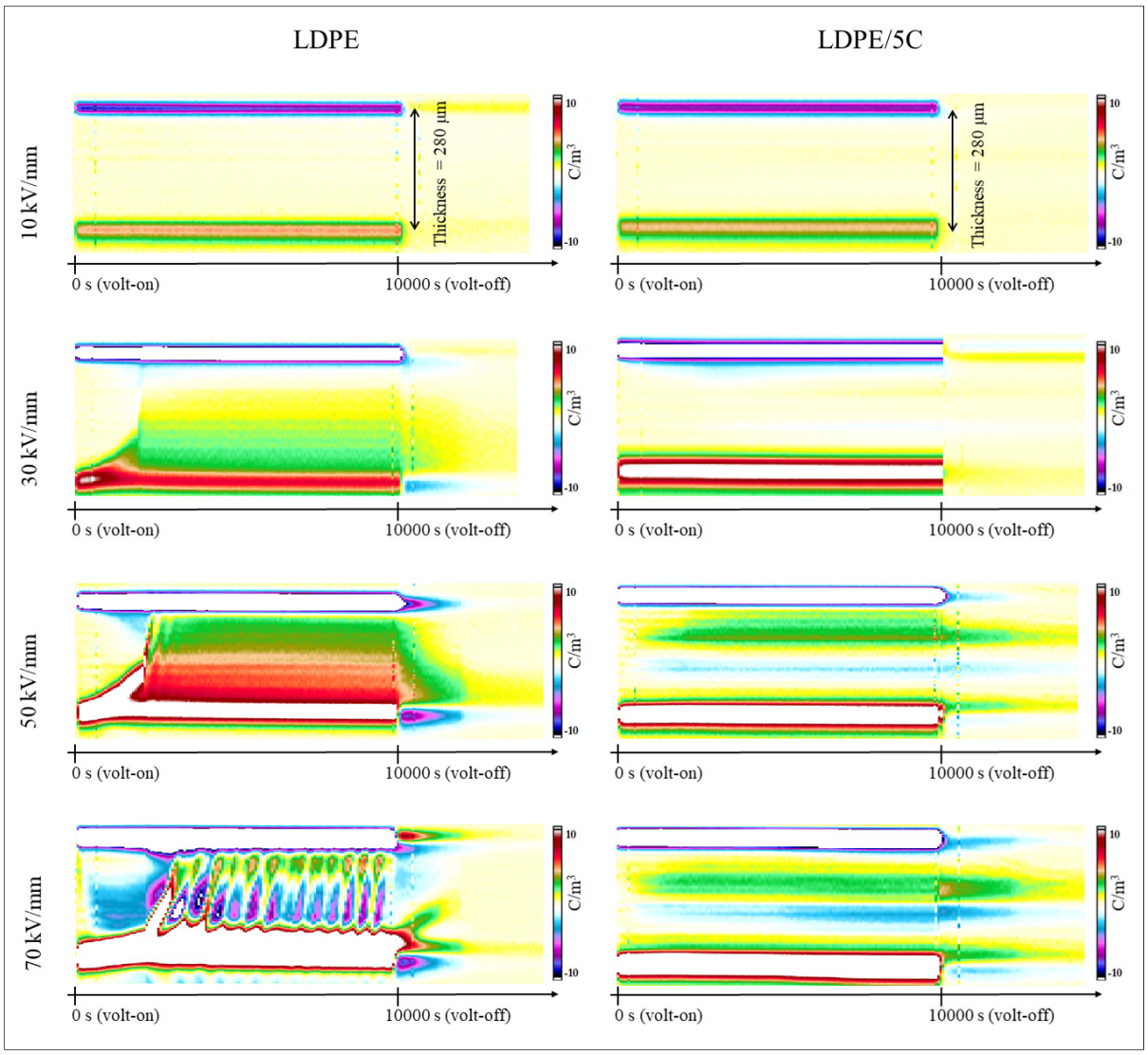

Figure 4-6 Space charge patterns for LDPE and LDPE/5C nanocomposites at 20 ˚C under different applied electric fields

Although polyethylene family and its cross linked analogue (XLPE) are known for low carrier mobility and high trap concentration (Yuanxiang, Jiankang et al. 2014), they greatly tend to accumulate large amount of space charge under high DC voltage (Zhang, Lewiner et al. 1996). Main mechanisms are the charge injection from electrodes to create homocharge, and charge

generation as a result of the ionization of impurities and/or trapped charge at the electrodes to create heterocharge (Takada, Hayase et al. 2008, Fabiani, Montanari et al. 2009).

Figure 4-7 plots the maximum field during the polarization for LDPE and LDPE/5C at four different applied electric fields corresponding to the space charge patterns illustrated in the Figure 4-6. At 10 kV/mm, the maximum field patterns almost overlap each other, very close to the absolute applied field hinting a probable ohmic behavior. For other higher applied electric fields, ohmic behavior does not hold anymore and the maximum fields are always above the applied electric fields. The deviation is bigger for neat LDPE in comparison to LDPE/5C nanocomposite and its intensity increases for stronger applied electric fields at each step. The heterocharge layers at each electrode are responsible for this significant increase. The maximum electric field for LDPE at 70 kV/mm heavily fluctuates and shows a peak every time a charge packet from HV electrode reaches the LV electrode. It occurs, on average, every 700 seconds which can be translated into a charge packet speed of about 4×10^{-7} m/s considering the thickness of the LDPE sample (280 μm).

Attention must be paid when interpreting the space charge accumulation graphs, since at each point the net charge is being displayed. The PEA signal cannot distinguish between the exact amount of positive and negative charge. An area with low charge level could also be due to overlapping of charges having opposite polarity. Therefore, low amount of detected charge in the graphs does not necessary mean that there is low electrical conduction across the thickness of the insulator. In fact, according to the DC conductivity results it was observed that for nanocomposite, even for the lowest loading of nanofiller, the conduction current level is significantly higher than that of neat LDPE.

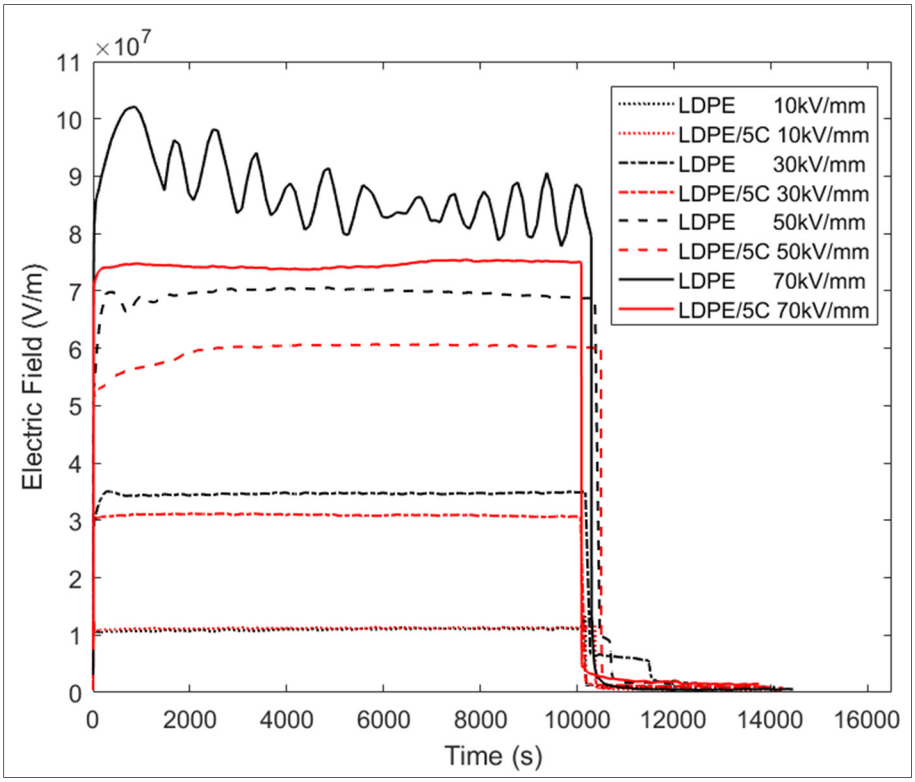

Figure 4-7 Maximum recorded electric field during the polarization period corresponding to the space charge patterns of Figure 3-5

It appears that the increase in the DC conductivity of nanocomposites allows space charge to flow across the insulation wall instead of accumulating inside the insulation bulk. In fact, clay seems to be effective in reducing the space charge not entirely by preventing it from happening but with creating a smooth passage network for charge carriers to be transported away. However, it must be noted that shallow traps are mostly responsible for conduction process, while the incorporation of nanoclay certainly introduces a great portion of deep traps, especially on the surface of nanoparticle (Montanari, Fabiani et al. 2004). The growth of interfaces of nanoparticles due to the intercalation of LDPE chains increases the density of defects on the surface of nanoparticles resulting in increased number of localized states within the band gap of the material. This will narrow the band gap and hinder the charge transport. As a result, the trap density and trap depth distribution is modified. Overall the presence of nanoclay facilitates the conduction process by introducing more charge carriers to be transported through shallow traps, while suppresses the space charge accumulation by

introducing deep traps. This mechanism is particularly efficient at the electrode/insulation interface, because it prevents the injection of excess charge from the electrode at high fields. In other words, most of the charge carriers crossing insulation through shallow traps are extracted at the electrode while some of the electrode-injected charges are immobilized in deep traps near electrodes. This explains the locations of accumulated charges which are near the electrodes in case of nanocomposites, but mostly appears in the bulk of the unfilled LDPE.

Space charge patterns for LDPE and its corresponding nanocomposites at elevated temperature (60 ˚C) under 50 kV/mm of electric fields are illustrated in Figure 4-8. For neat LDPE a huge amount of negative charge gradually appears in the whole insulation bulk, and no positive charge packet was detected. Surprisingly, despite the massive negative charge injected from LV electrode, it shows relatively lower amount of accumulated charge than the low temperature pattern at the same poling field where injected positive charge dominated. The domination of negative charge at elevated temperature in LDPE has been recently reported (Wang, Wu et al. 2017).

Space charge patterns are improved upon incorporation of nanoclay at any concentration: negative heterocharge gradually builds up near HV electrode while thin layers of positive charge appear in the center. Negative heterocharge build-up instead of dispersing in the whole specimen is another sign of increased charge mobility (conductivity) where negative charges manage to travel across the thickness to reach HV electrode. The thermal energy provided accelerates the detrapping process, combined with the electric field effect induced by the trapped charge itself that allows a part of trapped charges to become mobile and reach the opposite electrode.

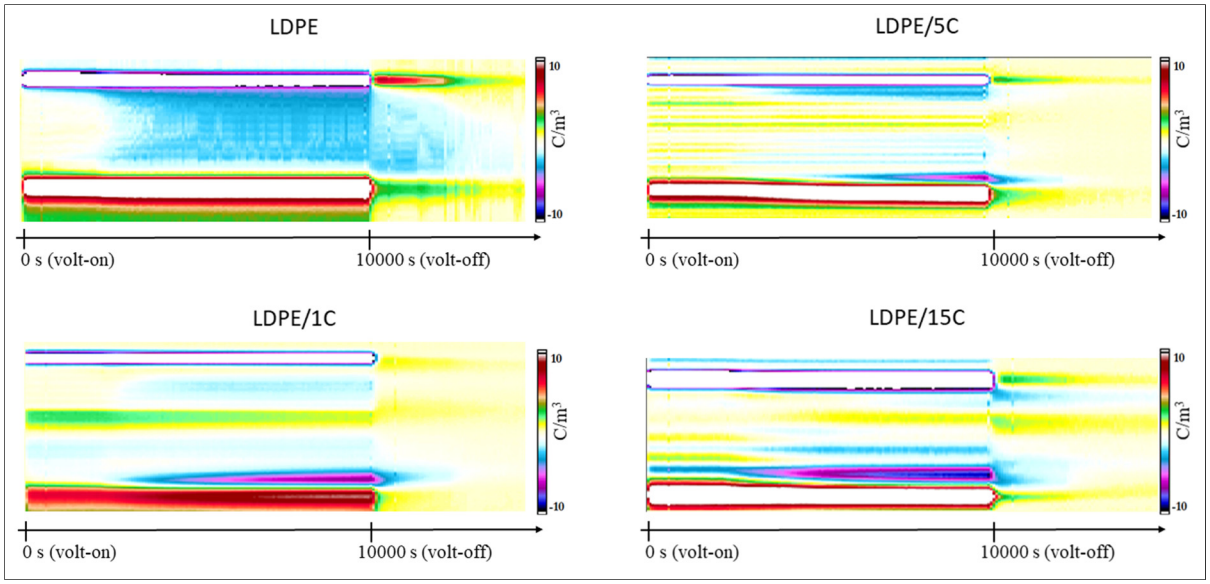

Figure 4-8 Space charge patterns for LDPE and its clay-containing nanocomposites at 60 ˚C and 50 kV/mm of applied electric field.

Space charge patterns for LDPE and LDPE/5C at elevated temperature (60 ˚C) under 70 kV/mm of applied electric fields are illustrated in Figure 4-9. For LDPE thin layers of heterocharge are close to both electrodes while negative charges are spread across the thickness of the specimen. The nanocomposite sample (LDPE/5C), however, exhibits the most distorted space charge behavior of all where heterocharge layers being immediately built up close to both electrodes. The corresponding charge profile for LDPE/5C is illustrated in Figure 4-10 for further analysis. Charge profile within the specimen is hugely affected by these heterocharge layers and never reaches the steady state. While the maximum electric field for LDPE never exceeds 81 kV/mm, for LDPE/5C it constantly increases and reaches 180 kV/mm at the end of the polarization (not shown here).

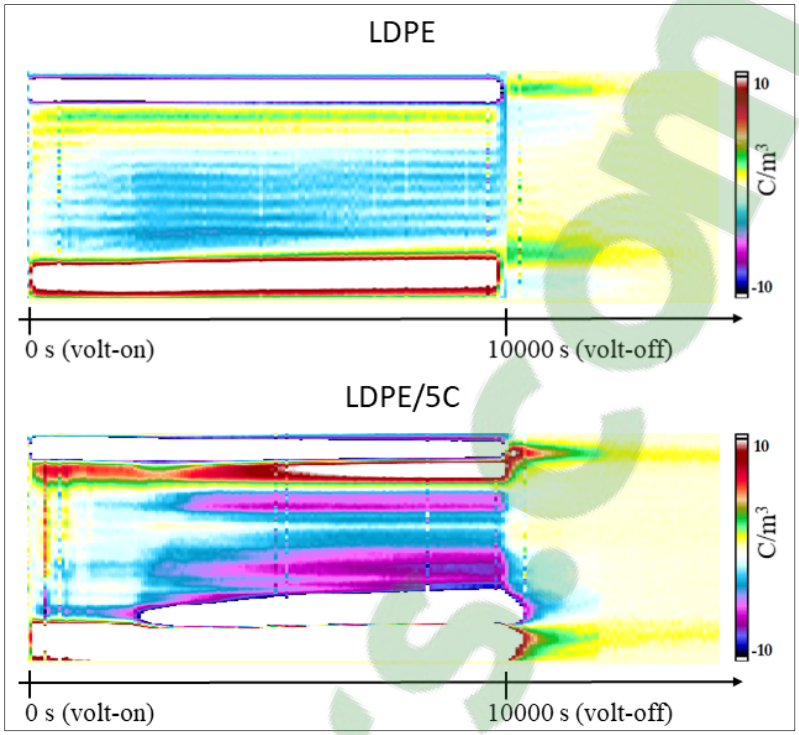

Figure 4-9 Space charge patterns for LDPE and LDPE/5C at 60 ˚C under 70 kV/mm of applied electric fields

When combined by high poling field, elevated temperature completely reverses the charge profile trend for neat LDPE and its clay-containing nanocomposite. First for neat LDPE, charge packet travelling across the sample were not observed anymore unlike what was measure at room temperature, as illustrated in Figure 4-6. It seems that the increase of conductivity is high enough to allow dispersion of the charge packets and injected charges to be drifted away but not high enough for charge carrier to be massively tapped within the insulation bulk. For LDPE/5C, under these temperature and field conditions, the conductivity was found to reach 10^{-10} S/m, which is mainly due to electronic conductivity as explained previously. Due to this relatively high value (for a material that is mainly non-conductive) significant heterocharge accumulation occurs close to both electrodes as depicted in Figure 4-9 and Figure 4-10. This fact can be explained again considering the deep traps introduced by nanoclays which prevent injection but also extraction of charges. Since the activation energies for both processes can be different, at high fields / temperatures extraction barrier can prevail, determining a significant delay for charge extraction which leads to a huge heretocharge accumulation.

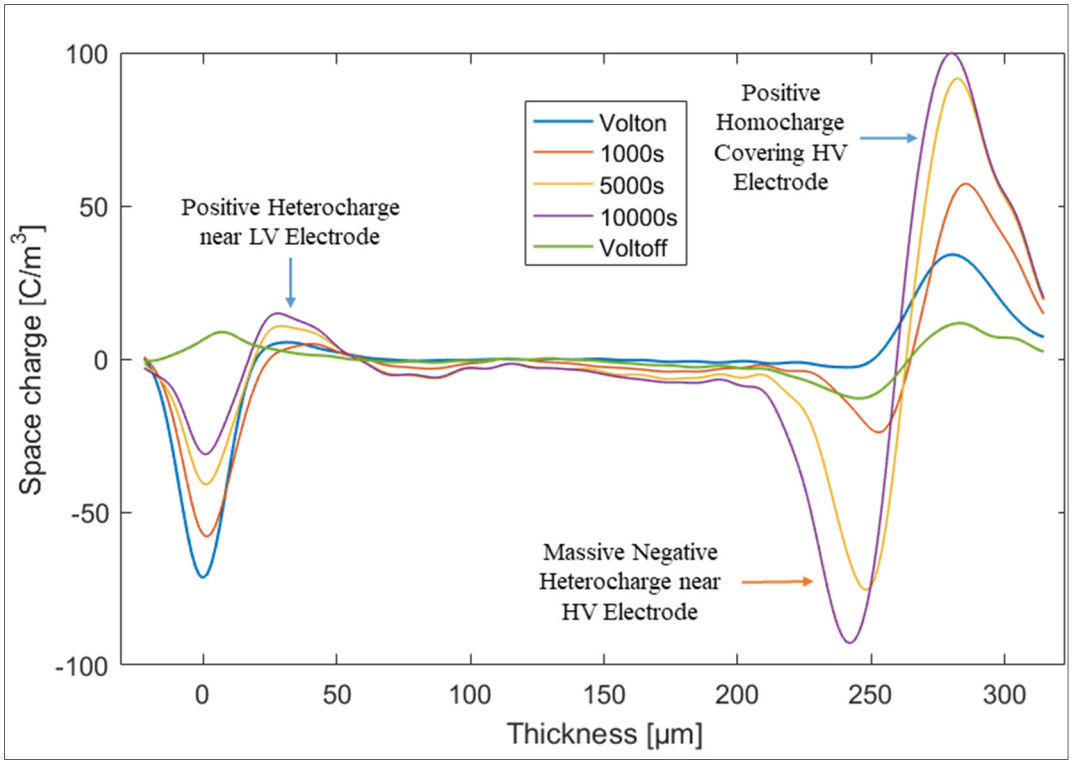

Figure 4-10 Space charge profile for LDPE/5C at 60 ˚C
under 70 kV/mm applied electric field.

4.4 Conclusion

Charge transport and accumulation under high electric fields were studied for neat LDPE and its clay-containing nanocomposites. The incorporation of nanoclay in LDPE was shown to significantly increase the DC conductivity. This increase was shown to be directly related to the temperature, electric field and the loading of nanofiller. The increased conductivity of the nanocomposite with regard to the neat LDPE together with the trapping effect of clay nanoparticles was found to lead to an improvement in the mitigation process of space charge at high fields and room temperature where extremely low accumulation of space charge was detected for nanocomposites comparing to the base polymer. However, at elevated temperature the conductivity of the nanocomposites reaches a point (~10^{-10} S/m) where it doesn't provide anymore benefit allowing to leak out the space charge but rather enhance the space charge accumulation resulting in heavy charge build up close to the electrodes.

Acknowledgements

The main sponsor of this project is the Natural Sciences and Engineering Research Council of Canada (NSERC). The Authors acknowledge the sincere cooperation of the staff of the Laboratory of Innovation Technologies (LIT) at University of Bologna.

CHAPTER 5

ARTICLE 3: DIELECTRIC RELAXATION DYNAMICS OF CLAY-CONTAINING LDPE BLENDS AND NANOCOMPOSITES

M. Eesaee, E. David, N.R. Demarquette

Mechanical Engineering Department, École de Technologie Supérieure,
Montréal, QC, Canada

This article has been submitted to:
Journal of Polymer Science
On February 2019

Abstract

Series of clay-containing nanocomposites have been prepared from a commercially available premixed masterbatch and investigated using broad-band dielectric spectroscopy from 10^{-1} to 10^{6} Hz at different temperatures. Different matrix materials have been used: neat LDPE with and without compatibilizer, and co-continuous blends of LDPE with two grades of Styrene-Ethylene-Butylene-Styrene block (SEBS) copolymers. Two major relaxation modes were detected in the dielectric losses of all the nanocomposites associated with the Maxwell-Wagner-Sillars interfacial polarization and the dipolar relaxation. The experimental data were analyzed with the sum of Havriliak–Negami function and a power-law term to take into account the contribution of charge carriers. The characteristic relaxation rates, activation energies, and dielectric strength and shape parameters of LDPE/clay nanocomposites were discussed. The addition of compatibilizer was shown to slightly increase the dielectric loss of the nanocomposites while slowing the dynamics especially for the MWS relaxation due to an

improved dispersion. When combined with high loading of nanofiller (15%), the compatibilizer addition led to low frequency dispersion in the form of significant increase of dielectric loss at low frequencies. A new relaxation process was observed for the nanocomposites with the blend matrix. Several speculations were discussed as the origin of this phenomenon, all of which was related to the elastomer phase.

Keywords: Polymer Nanocomposites, Nanoclay, Broadband Dielectric Spectroscopy, Polymer Blend.

5.1 Introduction

In recent decades, huge progress has been made in the field of advanced dielectric and electrical insulating materials using nanotechnology. Indeed, polymer-based nanocomposites are material of interest for potential applications that can be satisfied through active designs by adding a small amount of nanofiller, mostly inorganic, into conventional polymers. They are mostly characterized by their internally formed interface between nanofillers and the polymeric matrix which, when properly controlled, can lead to significant improved performance compared with neat polymers (Paul and Robeson 2008). Among all, polymer/layered silicate (clay) nanocomposites have attracted a great deal of interest, industrially and academically, over the past two decades. A small fraction of clay contains a sufficiently large number of silicate layers and they can easily be intercalated/exfoliated with various polymers. Clay is cheap, has relatively high aspect ratio and is capable of being organically modified to enhance the compatibility when embedded in non-polar polymers such as polyethylene (Pavlidou and Papaspyrides 2008, Alateyah, Dhakal et al. 2013).

Despite all these efforts, not much work has been conducted regarding the dielectric behavior of clay-containing polymer nanocomposites, given the fact that this subclass of nanodielectrics is believed to have great potentials for various electrical applications (Fréchette, Reed et al. 2006, Kindersberger, Tanaka et al. 2011). For insulation purpose, polyethylene is a material of choice and especially for cable insulation. Indeed, polyethylene shows high dielectric

breakdown strength, very low dielectric loss, and the ability to be easily processed and recycled (when uncrosslinked) (Tanaka, Montanari et al. 2004, Huang, Jiang et al. 2007, Fim, Basso et al. 2013). The main challenge in fabricating clay-containing polyethylene is the incompatibility between non-polar/hydrophobic polymer matrix and the hydrophilic nanofiller (Kiliaris and Papaspyrides 2010). To achieve an exfoliated state of the clay tactoïds, that is the dispersion of individual clay platelets into the polyolefin matrix, often the nanoclay is undergone a surface treatment using organic modifier in order to have an extended basal spacing and increased hydrophilicity (Wang, Choi et al. 2001, Gilman, Awad et al. 2002, Ray and Okamoto 2003, Shin, Simon et al. 2003, Hakim, Nekoomanesh et al. 2018), and/or an external material is used as a compatibilizer to link the nanofiller and the matrix (Reichert, Nitz et al. 2000, Garcıa-López, Picazo et al. 2003, Sánchez-Valdes, López-Quintanilla et al. 2006, Durmuş, Woo et al. 2007, Xu, Nakajima et al. 2009).

Taking a step forward, the ideas of incorporating a secondary polymer as compatibilizer to facilitate the interaction/dispersion of nanofiller in the base polymer (Pluta, Jeszka et al. 2007, Tomer, Polizos et al. 2011, Zazoum, David et al. 2013), or forming a polymer blend matrix as a nanostructured template to effectively host the nanofiller (Sengwa, Sankhla et al. 2010, Hamzah, Jaafar et al. 2014, Deshmukh, Ahamed et al. 2015, Du, Xu et al. 2016, Helal, Demarquette et al. 2016) have been examined recently especially in the context of HV applications. Blends of thermoplastic elastomers with polyolefins have also been investigated recently. In particular, polystyrene-b-poly(ethylene-co-butylene)-b-polystyrene (SEBS) and polystyrene-b-poly(ethylene-co-butylene)-b-polystyrene grafted maleic anhydride (SEBS-MA) thermoplastic elastomers have been shown to have enhanced electrical properties in the form nanocomposite when used solely as the base polymer (Helal, Demarquette et al. 2015, Helal, David et al. 2017) or in conjunction with another polymer forming a blend (Helal, Pottier et al. 2018). Because of the combination of the soft elastomer phase and a hard polystyrene phase, their spatial organization can modify the morphology of the blend and selectively accommodate the chosen nanofiller. In fact, in the authors' previous work (Eesaee, David et al. 2018), it was shown that the greater affinity of clay nanoparticles to the block copolymer resulted in a partial migration of nanofiller out of polyolefin phase to the interface and the

elastomer phase, obstructing the coalescence phenomena and shrinking the polymer domains into smaller size. This enabled the blend matrix to form a strong network with clay and improved the electrical breakdown properties.

Here, further investigation is reported on the evaluation of the dielectric relaxation phenomena of the same sets of materials. Frequency-domain broadband dielectric spectroscopy (BDS) was used as the main technique to explore the dielectric properties. It allows the study of relaxation mechanisms, through the motion of dipoles under the action of an electric field, as well as the monitoring of charge carrier fluctuations and the direct conductivity (Schönhals and Kremer 2003). For nanocomposites, the investigation of the broadband dielectric response can also provide valuable information regarding polymer/nanoparticle interactions, material's morphology and distribution of nanoreinforcement.

5.2 Experimental

5.2.1 Materials and Processing

A commercially available premixed LDPE/Clay masterbatch was used as the source of nanofiller (Nanocore, nanoMax®-LDPE). The masterbatch contains 50 wt% of organo-modified montmorillonite. Low-density polyethylene (LDPE) was used to dilute the masterbatch to prepare granules of nanocomposites with different concentration of clay. LDPE in powder form was supplied from Marplex with a density of 0.922 g/cm^3 and MFI of 0.9 g/10 min (190 °C/2.16 kg). Maleic anhydride grafted linear low-density polyethylene (LLDPE-g-MA) was supplied from DuPont (Fusabond M603) with a density of 0.940 g/cm^3 and MFI of 25 g/min (190 °C/2.16 kg). It has been used as a compatibilizer and is being referred to as "MA" in this manuscript.

A co-rotating twin screw extruder was used to prepare two series of nanocomposites, with and without 5wt% of compatibilizer (MA), by means of melt compounding with concentration profile of clay being set as 1, 2.5, 5, 10 and 15% where LDPE powder and masterbatch granules were directly fed. The same procedure was used to prepare blends and nanocomposites of

LDPE with two grades of polystyrene-b-poly(ethylene-co-butylene)-b-polystyrene (SEBS) thermoplastic elastomer supplied from Kraton: G1652 and FG1901. The former with a MFI of 5 (230 ˚C/2.16 kg) based on ASTM D1238 (as declared by the supplier) is referred to as SEBS in this manuscript. The latter with a MFI of 22, contains 1.4-2 wt% of maleic anhydride (MA) is referred to as SEBS-MA. Both grades contain 30 wt% fractions of polystyrene (PS) block in their structure and have a density of 0.91 g/cm^3.

All materials were dried in a vacuum oven at 50 ˚C for at least 36 h and manually pre-mixed prior to extrusion. Temperature profile of extruder was set to 145-170˚C from hopper to die. The pellets obtained were then press-molded using an electrically heated hydraulic press into thin plates with thickness around 300 μm. The pellets were first preheated for 5 minutes and then hot-pressed at 155 ˚C (165 ˚C for blends) for another 5 minutes under the pressure of 10 MPa following a water-cooling period with a rate of 10 ˚C per minute to the ambient temperature. Nanocomposites are named as LDPE/nC, with "n" referring the nominal percentage of incorporated clay. In case of blends the mass fractions of the two phases are set equal, 47.5 wt% for each phase when 5% of clay has been used (i.e. LDPE/SEBS/5C).

5.2.2 Measurements and Characterizations

Thermogravimetric analysis have been conducted on some samples using a PYRIS Diamond TG-DTA. Samples were heated from 50 ˚C to 600 ˚C with a heating rate of 15 ˚C/min under nitrogen atmosphere to investigate the thermal degradation of blends and nanocomposites and reveal the real weight percentage of nanofiller.

Dielectric relaxation spectroscopy experiments have been conducted on all the available samples using a Novocontrol broadband dielectric spectrometer in the frequency range of 10^{-1} to 10^6 Hz. Samples with the average thickness of 300 μm were sandwiched between two solid brass electrodes in a parallel-plate geometry (40 mm of diameter) while placed in a temperature-controlled chamber with a stability of 0.5 ˚C. The applied excitation voltage was set to 1 V_{rms}. A wide range of temperature was chosen to produce isothermal series of complex

dielectric permittivity from 20 ˚C to 90 ˚C. All samples were dried at 50 ˚C in a vacuum oven for at least 24 hrs.

5.2.3 Fitting Procedure

Among all the well-known and widely applied relaxation functions (Debye (Debye 1912), Cole–Cole (Cole and Cole 1941), Davidson–Cole (Davidson and Cole 1951), and Havriliak–Negami (Havriliak and Negami 1967)), the Havriliak-Negami (HN) function is the most effective due to its ability to model a broad and asymmetric distribution of relaxation times. Complex dielectric permittivity can be well described by a combination of the HN function and a conductivity term, as shown below:

$$\hat{\epsilon}(\omega) = \epsilon'(\omega) - i\epsilon''(\omega) = -i\left(\frac{\sigma_0}{\epsilon_0 \omega}\right)^N + \sum_{k=1}^{M}\left[\frac{\Delta\epsilon_k}{(1+(i\omega\tau_k)^{\alpha_k})^{\beta_k}} + \epsilon_{\infty k}\right] \qquad (4\text{-}1)$$

Where ω is angular frequency; $\hat{\epsilon}$ is the complex dielectric permittivity; ϵ' is the real part of the complex dielectric permittivity, also known as the dielectric constant, which represents the stored energy; ϵ'' is the imaginary part, or dielectric loss, related to the dissipated energy; N is the exponential factor which always lies between 0 and 1; τ_k specifies the relaxation time corresponding to relaxation process k; $\epsilon_{\infty k}$ is the value of ϵ' at infinite frequencies; Δϵ gives the difference in ϵ' at very low and infinite frequencies, and is also proportional to the area below the ϵ'' relaxation peak; β_k and α_k are the asymmetry and the width parameters, respectively ($\alpha_k \beta_k$ gives the slope of the high frequency side of the relaxation in ϵ'').

Fitting was done using a commercially available software by means of nonlinear computation procedures. The measured experimental dielectric spectra, both real and imaginary parts, were considered for fitting. At each step fitting continued until being stable. The stability was determined by the mean square deviation (MSD) which was calculated by the software at any time during the fitting process. Reaching a MSD value lower than 10^{-4} was set as the minimum limit below which the fit is considered stable. Nonetheless, at least 3 iterations were done at each step.

The relaxation time corresponding to the peak maximum frequency at each temperature was determined from the HN fit using the equation below:

$$\tau_{max} = \tau_{HN} * \left[\frac{\sin\left(\frac{\pi\alpha\beta}{2(\beta+1)}\right)}{\sin\left(\frac{\pi\alpha}{2(\beta+1)}\right)}\right]^{\frac{1}{\alpha}} \quad (4\text{-}2)$$

Where τ_{max} is the relaxation time of the peak maximum frequency; τ_{HN} is the calculated relaxation time from Equation 4-1. And, α and β are the width and asymmetry parameters obtained from Equation 4-1.

The temperature dependence of the relaxation rate (reciprocal of relaxation time) can be well described when plotted against the inverse temperature by Arrhenius equation:

$$f(T) = f_0 \exp\left(\frac{-E_A}{k_B T}\right) \quad (4\text{-}3)$$

Where f_0 is the pre-exponential factor; k_B is the Boltzmann constant and E_a is the corresponding activation energy of the relaxation process.

5.3 Results and Discussion

5.3.1 Thermal Properties

TGA measurements have been conducted on neat LDPE, its blend (LDPE/SEBS), nanocomposites (LDPE/1C, LDPE/5C, LDPE/15C & LDPE/SEBS/5C) and the source masterbatch. Figure 5-1 illustrates some of the TGA curves (the rest of the curves are omitted due to the similarity in the trend). Full thermal degradation parameters are listed in Table 5-1. As can be seen, the initial degradation temperature of nanocomposites is much higher than that of neat LDPE and the blend. This trend continues to the end of the measurement indicating that the addition of clay adds to the thermal stability of the base polymer. This improvement in thermal stability is due to the intercalated/exfoliated structure of clay within the polymer

which enhances the barrier properties against gas diffusion and prolongs the decomposition of the material. The decomposition temperature at 10 wt% and 50 wt% of the nanocomposite sample containing 5 wt% of the compatibilizer (LDPE/MA/5C) is further increased comparing the binary nanocomposite. The possible explanation is the role of MA to improve the degree of dispersion of the clay in the LDPE matrix as it was witnessed by its broadened XRD pattern (Eesaee, David et al. 2018).

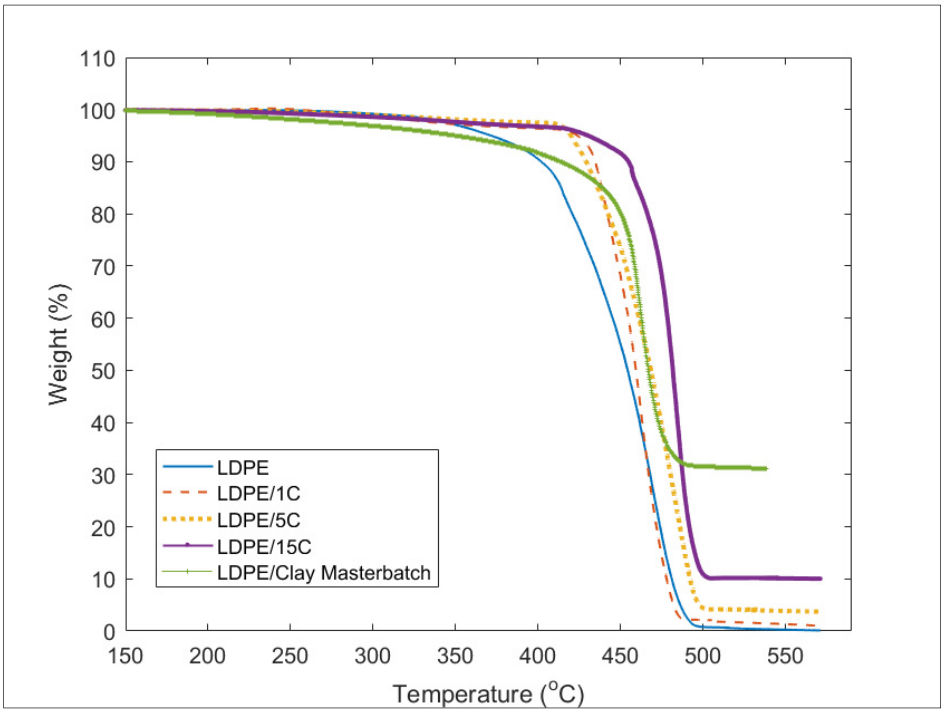

Figure 5-1 TGA decomposition curves of neat LDPE, its nanocomposites and the source masterbatch in nitrogen atmosphere

The source LDPE/Clay masterbatch supposedly contains 50 wt% nanoclay, however, its actual ash content is as low as 31 wt%. The other 19 wt% is believed to be the organic modifier. The inorganic residues for nanocomposites are lower than the assigned loading numbers. There is also a slight increase in the ash content of the blend comparing to the neat LDPE, which is probably due to SEBS having more impurities.

Table 5-1 TGA data of LDPE and its blend, nanocomposites and source masterbatch

Sample	$T_{10wt\%}$(˚C)	$T_{50wt\%}$(˚C)	Inorganic Residue (wt%)
LDPE	401.9	454.3	0.06
LDPE/1C	434.6	459.3	0.79
LDPE/5C	429.1	468.4	3.55
LDPE/15C	454.8	481.7	9.93
LDPE/MA/5C	448.9	480.1	3.87
LDPE/SEBS	403.6	451.5	0.26
LDPE/SEBS/5C	432.8	469.1	3.86
LDPE-Clay Masterbatch	413.9	466.9	31.19

5.3.2 Low-field Dielectric Measurement

The isothermal curves of the real and the imaginary part of the complex dielectric permittivity of LDPE are plotted versus frequency for temperature ranging from 20 to 90 ˚C in Figure 5-2. Non polar, low loss-materials like PE are characterized by nearly frequency-independent losses over several orders of magnitude, typically between sub-audio and microwaves frequencies, where the dielectric losses reach very low values, in the vicinity of 10^{-4}, and does not vary by more than one or two orders of magnitude for the whole measurable frequency range. A very good text describing such behavior can be found in (Jonscher 1996). Figure 5-2 illustrates, for the temperature range from 20 to 90 ˚C, the typical spectrum of the real and imaginary parts of the relative permittivity of LDPE. The dielectric losses stay very low for the whole frequency range, often lower than the sensitivity of the measurement equipment which led to negative values for the intermediate frequency range (not plotted in the log-log graph). The real part of the dielectric constant is frequency independent and its value decreases with temperature as

predicted by the Clausius-Mossotti equation. No relaxation process is observable in either parts.

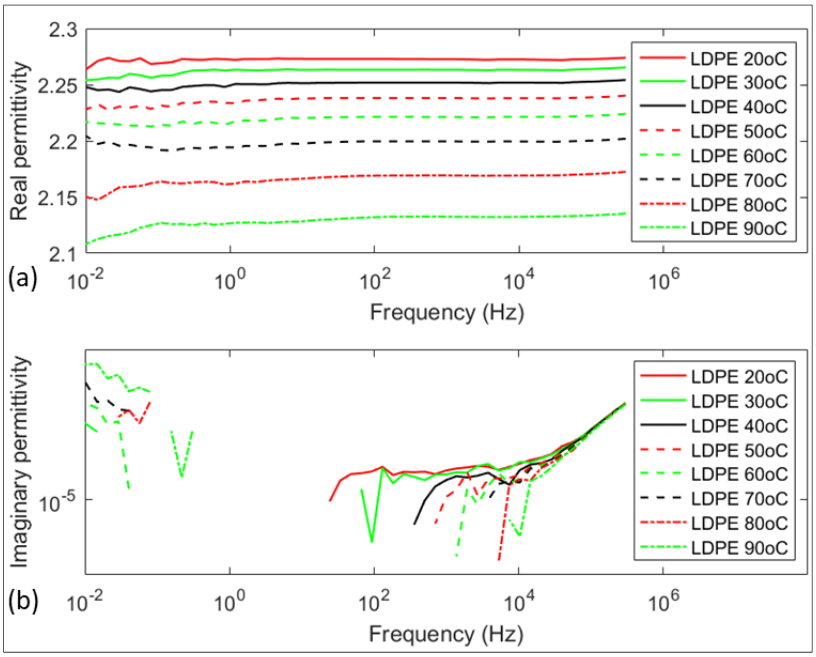

Figure 5-2 Plots of real (a) and imaginary (b) parts of the permittivity for the neat LDPE versus frequency at different temperatures

In order to clearly observe the effect of temperature on the relaxation processes of nanocomposites, isothermal plots of dielectric loss for LDPE/nC samples are depicted in Figure 5-3. The dielectric behavior of the neat polymer is strongly affected by the presence of nanofillers. One can notice a broad interfacial relaxation peak at low frequencies moving towards higher frequencies as the temperature goes up from 20 to 90 ˚C showing a thermally activated behavior. This is expected since the ionic conductivity along clay platelets increases with temperature, therefore results in decreasing the relaxation times (Fréchette, Larocque et al. 2008). The dielectric loss levels are approximately 2-3 orders of magnitude higher compared to those of neat LDPE at each temperature. A double peaks structure gradually develops in the nanocomposites representing two relaxation modes arising from the addition of clay nanofiller into the base polymer. This double peak structure has been previously reported for polymer/clay nanocomposites (Tomer, Polizos et al. 2011, David and Fréchette 2013, Zazoum, David et al. 2013).

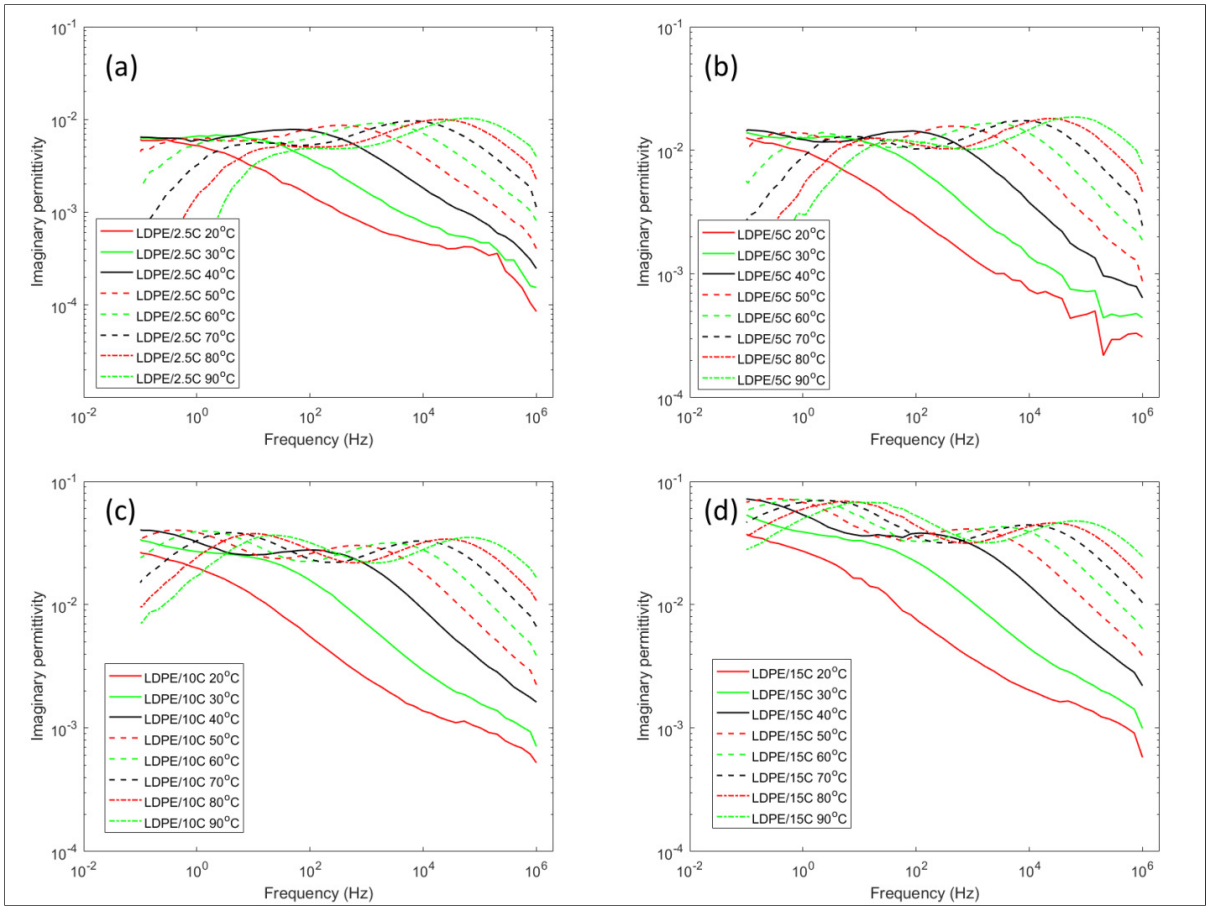

Figure 5-3 Dielectric loss (ϵ") of nanocomposites as a function of frequency in different temperatures for different clay loadings: a) 2.5%, b) 5%, c) 10%, and d) 15%

The first relaxation is detected at low frequency which is most likely due to the enhanced trapping of charge carriers in the interface areas between nanofiller and the base polymer known as Maxwell-Wagner-Sillars (MWS) polarization. The driving force of this charge blockage is the conductivity difference of the two phases [40]. Mobile charges migrate under the influence of the electric field and accumulate at the interface of the nanofiller and polymer matrix and form large electric dipoles which attempt to follow the orientation of the applied field. In low frequencies, they have enough time to align themselves parallel to the field direction. When the frequency increases the time delay in the orientation results in the occurrence of a dielectric relaxation process. The second relaxation is detected at higher frequency which is most probably due to the orientation (dipolar) polarization associated with the polar domains of the organic intercalant present in the masterbatch that was used for surface

treatment of clay layer. The weight ratio of the organic modifier to clay is calculated to be around 0.6:1 according to the TGA results in the previous section. The relaxation time for MWS polarization, on average, is around 10^4 times slower than the dipolar polarization. This indicates that the movement of trapped charge carriers in the clay phase towards the polymer/clay interface takes much longer time than the orientation of the polar domains. No clear DC conductivity term is observable when fitting the data for this particular series of nanocomposites which is probably due to the restriction on charge diffusion/fluctuation that is brought by the polyethylene-clay nanostructured network.

To further analyze the dielectric response, the experimental data were fitted into the Havriliak-Negami (HN) function to obtain the best-fit dielectric parameters for the observed relaxation processes. This was combined, when necessary, with a power law term to evaluate the contribution of charge fluctuations. Only the experimental data at 45 ˚C and higher were considered for quantitative assessment as the two relaxation peaks are clearly discernible in this temperature window. The relaxation times corresponding to the peak maximum frequency at each temperature were calculated from HN fit using Equation 4-1. Figure 5-4 illustrates the characteristic relaxation rates (f_{max}) of the two relaxation processes for different variation of clay nanocomposites versus inverse temperature. At increasing clay concentration, the relaxation rates decrease for MWS process. This is a common behavior for nanocomposites having non-conductive matrices where the volume fraction of the filler induces a slight increase of the relaxation time (Schönhals and Kremer 2003, David and Fréchette 2013). Another explanation is the possible formation of bigger agglomerates with lower effective conductivity. On the other hand, the relaxation rates for dipolar polarization slightly increase with increasing the clay concentration. The resulting activation energies from fitting to the Arrhenius model (Equation 4-3) are displayed on the plot. It is evident that both processes follow the Arrhenius' equation. These activation energies reflect the electrostatic interaction of charge carriers within the system. The activation energies for fast polarization is higher than the ones for slow polarization and this discrepancy is more pronounced for higher loadings of clay (with the exception of LDPE/5C). This is expected as the charge carriers motion experiences lower electrostatic barriers within the polar groups of intercalant than when

diffusing between neighboring interfaces. Obeying Arrhenius plot confirms that none of the two relaxations represent the α-relaxation, the relaxation related to the molecular dynamics controlling the glass/rubber transition of the amorphous part of the polymer i.e. the segmental dynamics (Donth 1992), as it would instead follow the Vogel-Fulcher-Tammann (VFT) equation (Sengers, Van den Berg et al. 2005).

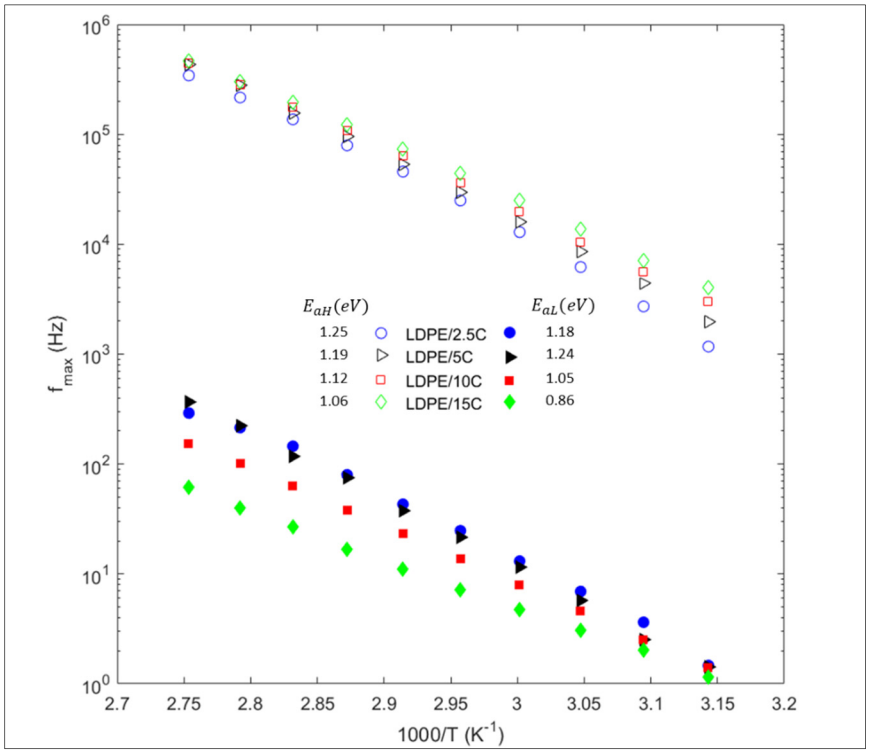

Figure 5-4 Arrhenius plot for the relaxation rate of the low frequency (filled) and high frequency (unfilled) relaxation processes with their corresponding activation energies calculated from Arrhenius equation.

The dielectric strength of the two relaxations, $\Delta\varepsilon_L$ and $\Delta\varepsilon_H$, are plotted against the reciprocal of temperature in Figure 5-5. The level of the dielectric relaxation strengths is proportional to the amount of nanoclay which further confirms that both relaxations are at the origin of the addition of nanofiller. The dielectric relaxation strengths are almost independent of temperature at any concentration of nanofiller which indicates that similar amount of dipoles are contributing to both relaxation processes, according to the Debye-Fröhlich-Kirkwood theory (Schönhals and Kremer 2003). Increasing trend of dielectric strength with increasing

temperature is mostly reported for secondary relaxations in polymeric systems where the enhanced mobility of the molecular dipoles is mainly ascribed to a higher mobility of the polymer matrix or to an increase of the density of dipoles.

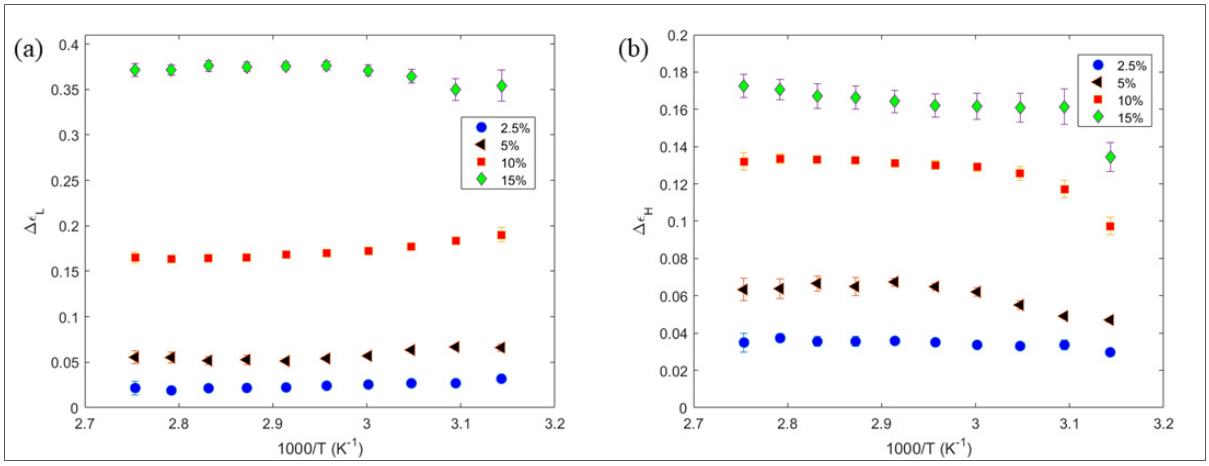

Figure 5-5 Δε of the (a) MWS and (b) dipolar relaxations of LDPE/nC as a function of reciprocal temperature.

The shape parameters of the two relaxations are depicted in Figure 5-6. The width parameter (α) represents the broadness of the relaxation curve. Higher α means the relaxation peak is narrower. For the low frequency relaxation, α_L was found to decrease when the nanofiller loading was increased. This implies that the distribution of the MWS relaxation times increases by increasing clay content. For the high frequency relaxation, the width parameter (α_H) are very close and similar in different temperatures indicating a symmetrical broadening comparable to Debye peak and a good dispersion level of organic modifier (and hence of clay sheets and tactoids also). The asymmetry parameter for the fast polarization (β_H) is very close to unity indicating that this relaxation process can be relatively well described by a Cole-Cole distribution. However, at highest loading of nanofiller (15%) there is a deviation from Cole-Cole distribution (β_H~0.8) which might be explained by the change in the mobility of charges related to the structural change of polymer-clay interface. The asymmetry parameter for the fast polarization (β_L) is far lower than unity for 2.5 and 5% of clay loadings. This asymmetry in the slow relaxation process (MWS) reflects a temperature-induced change in the trapping

mechanism of the space-charge and can also be attributed to local heterogeneities i.e. the existence of regions with exfoliated clay platelets.

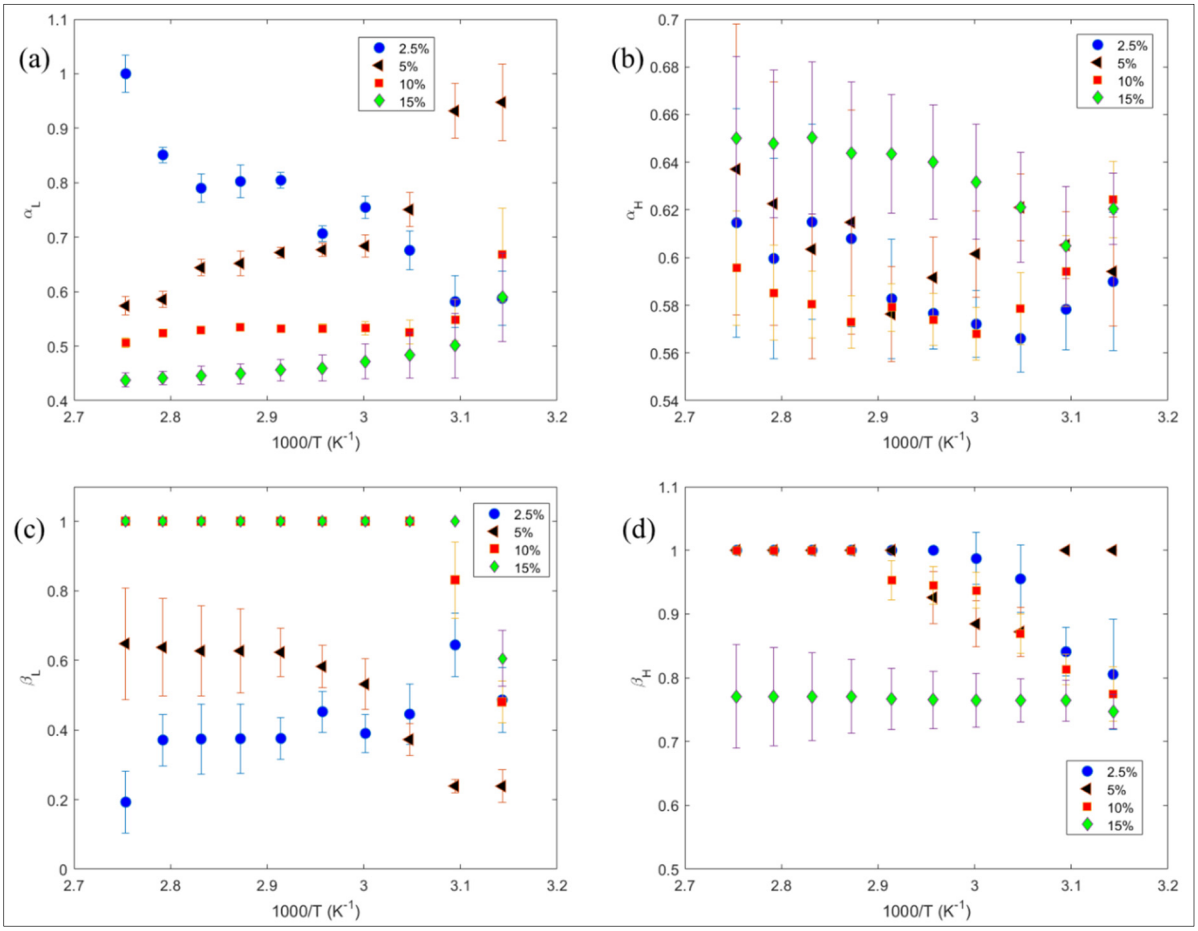

Figure 5-6 Shape parameters of the MWS (a&b) and dipolar (c&d) relaxations of LDPE/nC as a function of reciprocal temperature.

Series of LDPE/clay nanocomposites samples containing 5 wt% of compatibilizer (MA) exhibit the same double peak structure in dielectric spectra as depicted in Figure 5-7. The dynamics are very similar to the binary nanocomposites (LDPE/nC) and omitted for the sake of brevity. The level of dielectric loss is slightly higher comparing to the binary nanocomposite. However, no separate dielectric relaxation can be spotted for MA compatibilizer. A similar behavior has been reported in the literature (Khalf and Ward 2010, David, Fréchette et al. 2013, Zazoum, David et al. 2013, Zazoum, David et al. 2014).

The MWS relaxation is more intense for LDPE/MA/nC nanocomposites comparing to the binary nanocomposites and is slightly shifted to the lower frequencies indicating slower dynamics. This is expected as the MA would be close/attached to the nanofiller due to thermodynamic effects and can be related to the enhancement role of MA on the dispersion of nanofiller within the polymer matrix. The role of compatibilizer is to improve the level of dispersion of clay with the help of the polar interactions between the maleic anhydride groups in the compatibilizer and the hydroxyl groups of clay as was confirmed by the broader diffraction peak in XRD patterns (Eesaee, David et al. 2018). A similar trend has been reported previously (David, Zazoum et al. 2015). This improvement of the dispersion level increases the interfaces of nanofiller with the polymer matrix resulting in more interfacial chain cooperativity and hence longer relaxation times. The increase of dielectric loss in low frequency might also arise from the random orientation of stacks of clay platelets that were intercalated with the help of MA (David, Fréchette et al. 2013). The interfacial relaxation peaks being narrower comparing to the binary nanocomposites suggests a somewhat narrow distribution of nanofiller.

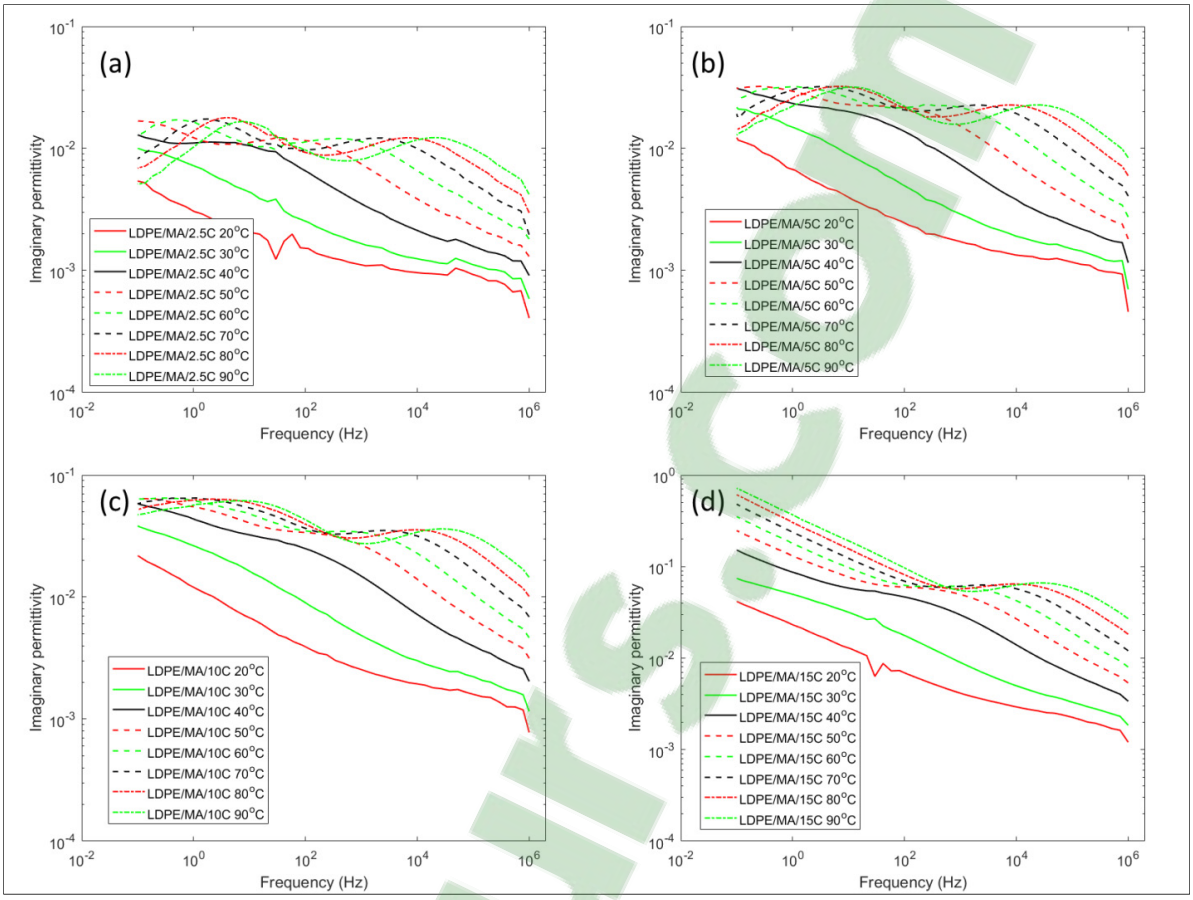

Figure 5-7 Dielectric loss (ϵ") of nanocomposites containing 5% MA as a function of frequency in different temperatures for different clay loadings: a) 2.5%, b) 5%, c) 10%, and d) 15%

At highest loading of nanofiller (15%) there is a consistent increase in the level of dielectric loss towards low frequencies which completely overshadows the MWS relaxation. This is accompanied with an increase in the real part of the permittivity (not shown here). This increase of both real and imaginary parts of the permittivity is known as low frequency dispersion. The optimum fit parameters for LDPE/MA/15C are listed in Table 5-2, and an example of fitting to Equation 4-1 is illustrated in Figure 5-8. The MWS relaxation process was detected only in the temperatures above 60 ˚C. In addition to the relaxations processes, the charge fluctuation term is also detected. This high level of charge carriers' contribution is a direct result of the combination of high nanofiller loading and the presence of MA compatibilizer enhancing the filler dispersion and allowing the creation of a percolating network. A similar effect has been

observed in ZnO loaded SEBS and SEBS-MA (Helal, David et al. 2017) for which a significant contribution from the charge carrier was observed when the dispersion was enhanced. The DC conductivity exponent (the slope of the plot of imaginary permittivity versus frequency curve in log-scale) never exceeds 0.34 which is far from the ideal electronic conductivity (~1), indicating that the contribution of charge blockage at the interface of the specimen and metal electrodes (electrode polarization) is more than charge leakage through the specimen. Low field conduction is a common phenomenon in nanocomposites where nanofillers are believed to be the source of ionic carriers increasing the conductivity (Tanaka 2005). The DC conductivity might also arise from impurities introduced by MA or nanofiller (i.e. the by-products of organic modification reactions). Addition of compatibilizer was certainly accompanied with some additional impurities as was observed in the TGA results.

Table 5-2 Optimum fit parameters for LDPE/MA/15C

	DC Conductivity		Low frequency relaxation				High frequency relaxation			
T (˚C)	σ_0 (S/m)	N	α_L	β_L	$\Delta\epsilon_L$	$\tau_L\ (s)$	α_H	β_H	$\Delta\epsilon_H$	$\tau_H\ (s)$
45	8×10^{-15}	0.251	-	-	-	-	0.67	0.73	0.096	5.1×10^{-4}
50	2.7×10^{-14}	0.267	-	-	-	-	0.68	0.66	0.12	2.7×10^{-4}
55	6.7×10^{-14}	0.278	-	-	-	-	0.67	0.67	0.139	1.5×10^{-4}
60	1.4×10^{-13}	0.287	-	-	-	-	0.63	0.72	0.154	8.2×10^{-5}
65	2.9×10^{-13}	0.302	0.66	1	0.011	0.05	0.6	0.8	0.178	6.5×10^{-5}
70	5.5×10^{-13}	0.323	0.54	1	0.062	0.042	0.6	0.79	0.198	3.8×10^{-5}
75	8.8×10^{-13}	0.336	0.53	1	0.107	0.038	0.6	0.8	0.211	2.3×10^{-5}
80	1.3×10^{-12}	0.339	0.5	1	0.142	0.037	0.61	0.8	0.216	1.4×10^{-5}
85	1.7×10^{-12}	0.337	0.55	1	0.139	0.027	0.62	0.8	0.22	8.7×10^{-6}
90	2.1×10^{-12}	0.334	0.58	1	0.143	0.022	0.63	0.81	0.224	5.4×10^{-6}

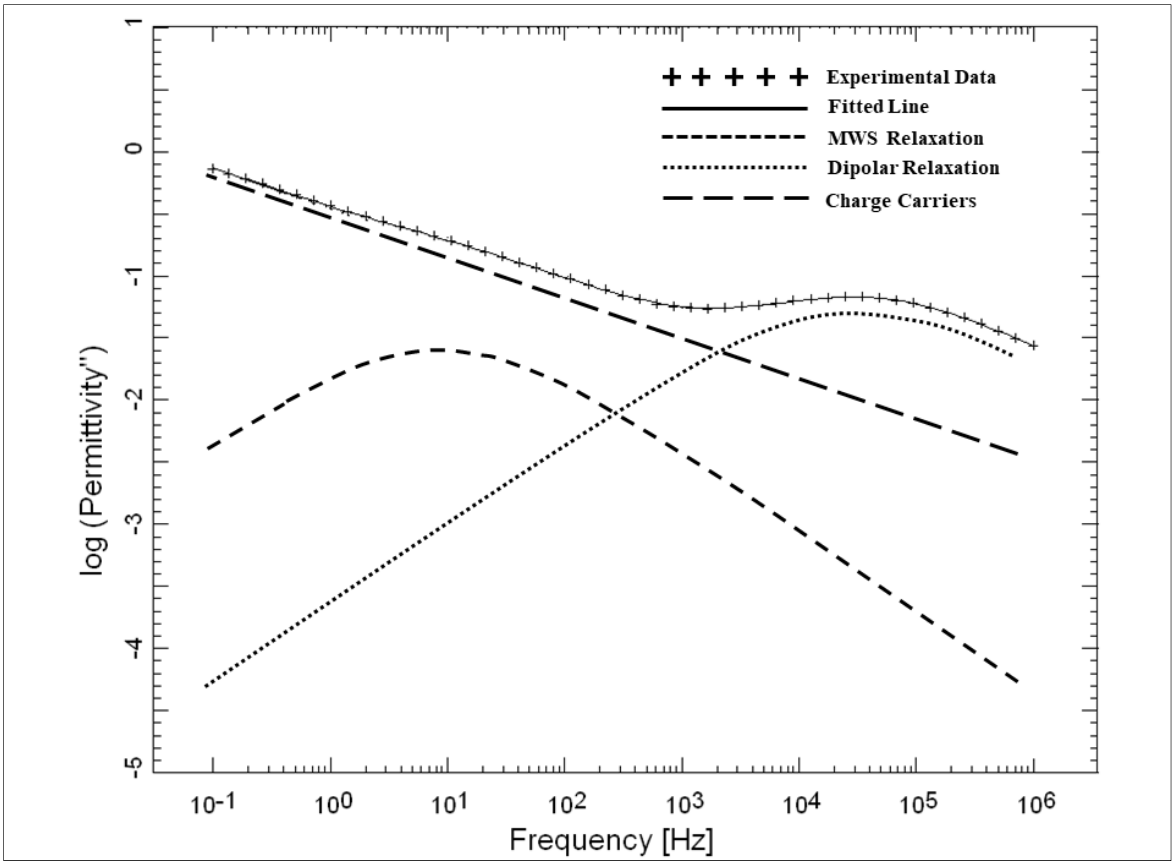

Figure 5-8 An example of fitting corresponding to LDPE/MA/15C at 90 ˚C

The dielectric loss spectra of unfilled blends are reported in Figure 5-9 (a&b). Since neither SEBS nor the maleate compatibilizer are strongly polar, they are not expected to significantly increase the dielectric losses when blended with LDPE. Indeed, the dielectric loss spectra showed in Figure 5-9 (a&b) were found to remain low, in the 10^{-4} vicinity and close to the limit of the measuring device, with no specific relaxation process observable in the chosen frequency/temperature windows. No contribution from the segmental relaxation associated with the glass transitions of the constituents of the thermoplastic copolymer phase was expected as it is too slow for the polystyrene (PS) and too fast for the rubbery midblock (PEB) to occur within the frequency and temperature windows of this work. The level of dielectric loss for LDPE/SEBS-MA blend, however, is slightly higher than that of LDPE/SEBS which is most likely due to the presence of MA polar groups. Addition of 5% clay into the blend of LDPE with SEBS and SEBS-MA (Figure 5-9 c&d) resulted in a similar double peak structure

than the one that was observed previously. Comparing to the corresponding binary nanocomposite (LDPE/5C), both relaxations start to appear in lower frequencies. It is obvious that this change is as a result of the interaction of clay nanofiller with the cocontinuous structure of the blend matrix and the intrinsic dielectric behavior of the thermoplastic copolymer. In fact, the double peaks structure has also been observed for clay/rubbers nanocomposites (Hernández, Carretero-González et al. 2009, Vo, Anastasiadis et al. 2011). LDPE/SEBS/5C shows no trend of frequency dispersion at any studied temperature, however, LDPE/SEBS-MA/5C becomes slightly conductive only at 90 ˚C with a conductivity lower than 10^{-17} S/m and an exponent of 0.48. This can be attributed to the interaction of MA with functional groups on the surface of clay particles leading to improved dispersion and slightly higher conductivity (Helal, Pottier et al. 2018).

The MWS process occurring in lower frequencies can be explained by the selective localization of nanofiller. In our previous work it was shown that during the mixing stage, clay has tendency to leave the polyethylene and migrate into the thermoplastic phase where it has more affinity towards the aromatic rings of the PS block and to the mobility of chains in the rubbery PEB phase (Eesaee, David et al. 2018). Although a number of nanoparticles get stuck in the interface of the two polymer phases, this migration results in intercalation of the elastomer chains in clay galleries and helps creating a more exfoliated structure by disrupting the regular stacked layer structure of nanofiller. This improvement in the degree of clay exfoliation, similar to the effect of MA compatibilizer, results in a larger number of interfaces and less efficient restriction of chains motions which will eventually increase the cooperativity of interfacial chains resulting in increased relaxation times (Wu, Tang et al. 2013).

The high frequency peak being broader and more intensified might be as a result of the overlapping of one or several relaxation processes with the dipolar relaxation. In addition to the above mentioned modes and charge fluctuation term a new relaxation peak was observed for both sets of blend nanocomposites in the vicinity of the high frequency relaxation (Figure 5-9 e&f). A common hypothesis to explain the origin of this new relaxation mode is the presence of an adsorbed water layer at the interface of nanofiller and the polymeric matrix.

Water would constitute a conductive layer leading to an interfacial relaxation observable usually in the intermediate frequencies which can also influence the dipolar relaxation dynamics (Glaskova and Aniskevich 2009, Couderc, David et al. 2013, Lau, Vaughan et al. 2014). The water effect, however, was shown to be negligible for several reasons: the organomodified clay is believed to have a high hydrophobicity level (Darie, Pâslaru et al. 2014), the polymeric constituents of the blend matrix are apolar, and there are reports that no significant impact of water was observed on dielectric properties of nanocomposites containing modified clay based separately on polyethylene (David, Zazoum et al. 2015) and SEBS (Helal, David et al. 2017).

Panaitescu et al. (Panaitescu, Vuluga et al. 2013) witnessed a similar relaxation process when only 10% of SEBS was added to their clay-containing polypropylene nanocomposite. They related this new relaxation process to the local motions inside EB blocks due to the possible presence of polar groups as a result of oxidative degradation. Dielectric spectroscopy of neat SEBS done by Chen et al. (Chen and Zhao 2011) also revealed a similar relaxation process located between α-relaxations of PS and EB phases. They speculated that the origin of this process might be either due to the molecular motions in the interface regions of PS/EB of high thicknesses or the interfacial polarization relaxation in the interface of hard and soft domains. Another speculation is the local segmental relaxation of rubber chains with reduced mobility located at clay interface with the polymeric matrix (Hernández, Carretero-González et al. 2009, Qu, Deng et al. 2011, Lin, Liu et al. 2015). The contributions of the each proposed modes are unclear and further investigations are required.

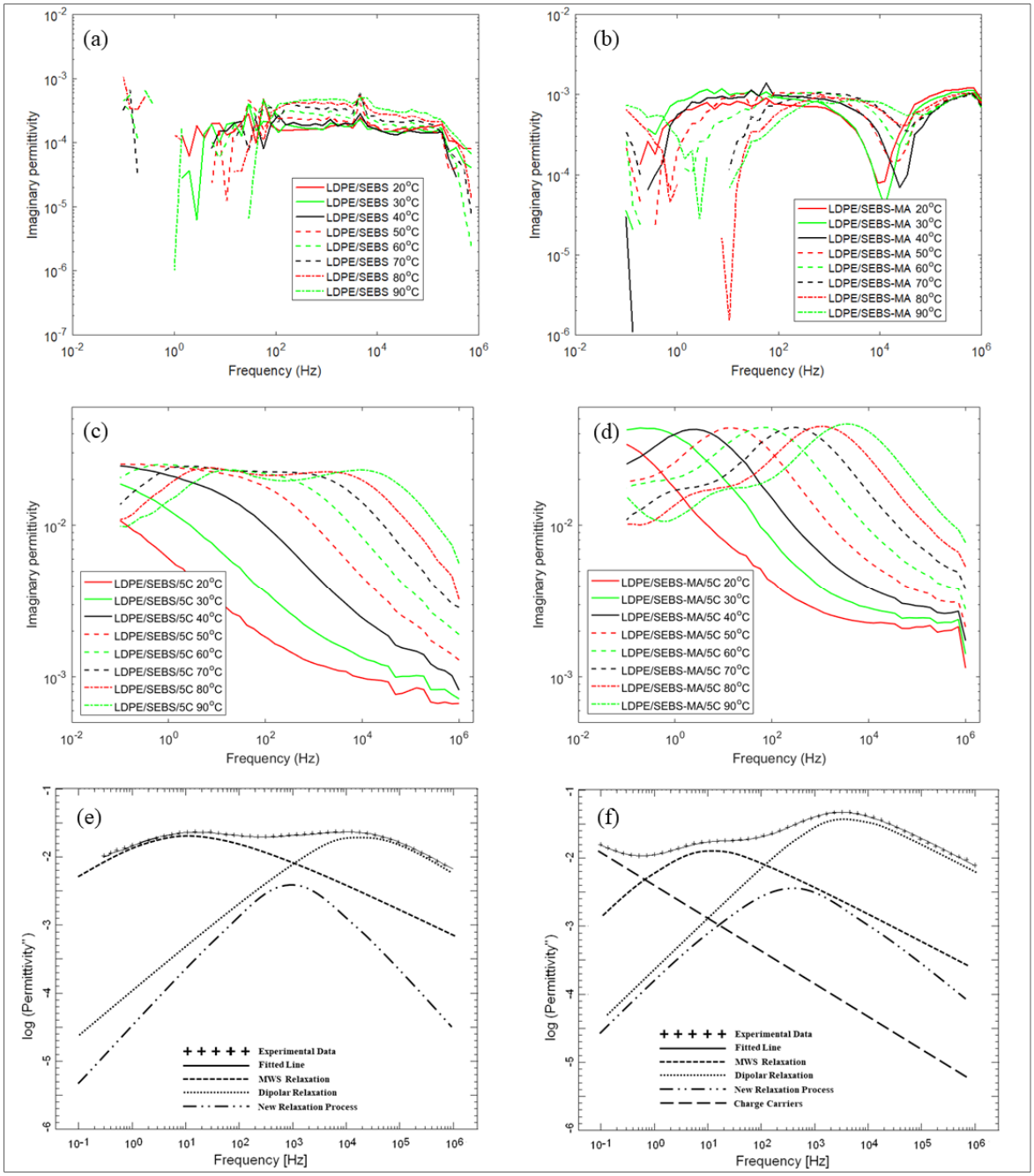

Figure 5-9 Dielectric loss (ϵ") as a function of frequency and temperature: a)LDPE/SEBS, b)LDPE/SEBS-MA, c)LDPE/SEBS/5C, d)LDPE/SEBS-MA/5C. Fitting at 90 ˚C for e)LDPE/SEBS/5C and f) LDPE/SEBS-MA/5C.

The dipolar relaxation for LDPE/SEBS-MA/5C is noticeably more intense than LDPE/SEBS/5C. This is expected due to the great compatibility of MA to the nanofiller

resulting in more pronounced intercalation of the elastomer chains in clay galleries as was confirmed by the stretched and smaller phase domain in the SEM micrographs and also the broad X-ray diffraction peak (Eesaee, David et al. 2018). More intercalation/exfoliation also means that more organic intercalants are exposed to the blend matrix and contribute to the dipolar relaxation. Another explanation can be the possible relaxation process assigned to localized fluctuations of the polar maleic anhydride groups (Böhning, Goering et al. 2005).

Concluding Remarks

Low field dielectric properties of nanocomposites comprising of neat LDPE or its cocontinuous blends with SEBS family as the matrix and clay nanoparticles as the reinforcement were studied in this work in a wide range of frequency and temperature. A commercially available masterbatch was used as the source of nanofiller, which was roughly comprised of 50wt% LDPE, 31% montmorillonite clay and 19% organic modifier. The masterbatch was diluted to form desired concentrations of nanofiller. The dielectric spectra were fitted with at least two terms of Havriliak-Negami function and, when needed, a charge fluctuation term to cover the low frequency dispersion (DC conductivity + electrode polarization).

All the nanocomposites showed two dielectric relaxation processes, that were absent in neat LDPE, representing the charge trapping in the polarized domains (MWS) and the dipolar orientation. The dielectric behavior was shown to be thermally activated as the dielectric losses were unanimously moving to higher frequencies with the increase in temperature. The addition of 5 wt% MA compatibilizer slightly increased the dielectric loss while increasing the relaxation times due to the obtained further improvement in the dispersion of nanofiller. Low frequency dispersion phenomenon was observed only in the nanocomposite containing the highest loading of clay accompanied by compatibilizer. This was explained to be related to increased charge carriers' fluctuations, either being immobilized in the interface of the specimen and metal electrode (electrode polarization) or leakage current through the specimen (DC conductivity) coming from the creation of a percolating network. The double peaks structure was also witnessed for the nanocomposites with the blend matrix. However, a new

relaxation process was detected close to the dipolar relaxation. Comparing to the binary nanocomposites, the existence of this new process was believed to be related to the SEBS phase. Several speculations were presented to explain this phenomenon; however, the authors did not achieve a decisive explanation.

CHAPTER 6

ARTICLE 4: EFFECT OF BLENDING AND NANOCLAY ON DIELECTRIC PROPERTIES OF POLYPROPYLENE

M. Eesaee, E. David, N.R. Demarquette

Mechanical Engineering Department, École de Technologie Supérieure,
Montréal, QC, Canada

This article has been submitted to:
IEEE Transaction on Dielectrics and Electrical Insulation
On January 2019

Abstract

This paper investigates the effects of organomodified montmorillonite (clay) and styrene-(ethylene-co-butylene)-styrene triblock copolymer (SEBS) on the morphological and electrical properties of polypropylene (PP). Several PP-clay as well as PP/SEBS blend clay composites were obtained. The nanofillers were found to be well-embedded into the polymeric matrix with a high degree of dispersion. The microstructure of the blend matrix revealed a co-continuous structure for the equal proportion of the two polymers. This was shown to control the localization of nanofiller by triggering them to migrate into the SEBS phase, mostly getting stuck at the interface and creating a strong network which eventually resulted in more exfoliation of clay platelets and comparable/superior electrical properties comparing to binary nanocomposites. The incorporation of clay resulted in a solid-like rheological behavior which was more enhanced in blend nanocomposites due to the nature of clock copolymer and the stronger network of nanofiller. The dielectric spectra of the nanocomposites were analyzed with the sum of Havriliak–Negami function and a power-law term revealing two major

relaxation processes aroused by the presence of clay: The Maxwell-Wagner-Sillars interfacial polarization at low frequency and the dipolar relaxation at high frequency. A new relaxation process was observed for the nanocomposites with the blend matrix. Several possibilities are presented as the origin of this phenomenon. Both blending and nanofiller inclusion resulted in less accumulated space charge. A significant improvement in the AC breakdown strength of PP was witnessed upon addition of clay. This was associated to the barrier effect of clay, creating tortuous path for charge carriers which prolongs the breakdown time. Despite the less inherent breakdown strength of SEBS, the blend nanocomposites showed even more enhanced breakdown properties confirming the further improvement of nanofiller network structure.

Keywords: Polypropylene, clay-polymer nanocomposites, HV insulating material

6.1 Introduction

Nowadays extruded cables employing a solid dielectric as insulation wall are dominating the underground high voltage (HV) transmission and medium voltage distribution network. The most common dielectric material in this regards is polyethylene (PE). PE is cheap, can easily be processed and has a high chemical resistance and a very low electrical loss. However, PE family has low thermal stability and operating temperature. Therefore, LDPE is normally crosslinked into crosslinked polyethylene (XLPE) which exhibits higher thermo-mechanical stability and can withstand temperatures up to 90 ˚C (Vahedy 2006). On the other hand, the crosslinking process makes XLPE a thermoset material which cannot be easily recycled raising concerns to its long term sustainability. The development of ecofriendly insulation materials for HV cables is now of significant importance.

Polypropylene (PP) has the advantage of offering a much higher thermal stability and mechanical integrity at elevated temperatures than PE while maintaining almost all the other advantages without the need to crosslink, and therefore can meet the increasing demands of environmental protection and sustainable development. Its main drawback is being too stiff

and brittle at room temperature for incorporation into a cable system (Kurahashi, Matsuda et al. 2006).

To overcome this limitation and improve the mechanical properties of PP, researchers have developed novel materials via blending PP with other thermoplastic polymers (Graziano, Jaffer et al. 2018), copolymerization with other olefins (Nitta, Shin et al. 2005) and incorporation of inorganic nanofillers (Manias, Touny et al. 2001) while addressing the environmental issues. Due to their unique microstructure, polymer nanocomposites developed for electrical applications (nanodielectrics) are shown to have improved electrical properties including enhanced dielectric breakdown strength and space charge suppression (Tanaka, Montanari et al. 2004). However, their efficiency directly depends on the quality of the nanofiller dispersion and the quality of its interface with the polymer matrix. Studies revealed a strong impact of the level of filler dispersion and interfacial adhesion to the matrix on the toughness characteristics of PP composites (Tjong, Bao et al. 2005). For this reason, the inorganic nanofillers usually undergo a modification step in order to have more compatibility towards the host polymer (Delbem, Valera et al. 2010). In this work a natural clay, montmorillonite, was used as the nanoreinforcement available in a premixed masterbatch. It has been treated with compatibilizing agents to minimize the surface attraction force, enabling the particles to disperse to nanoscale size. Clay is cheap, available in low cost and high amount, has a high aspect ratio and is regarded as a promising reinforcement to be involved in nanocomposites for electrical applications (Kindersberger, Tanaka et al. 2011).

Further modification on PP's mechanical properties can be achieved through blending with another thermoplastic polymer. In particular, polystyrene-b-poly(ethylene-co-butylene)-b-polystyrene (SEBS) is an interesting candidate. As a thermoplastic elastomer (TPE), SEBS offers a combination of elastic property of elastomers and process-ability of thermoplastic polymers. SEBS has shown to have excellent electrical properties when used as the base polymer (Helal, David et al. 2017) or in a blend (Helal, Demarquette et al. 2015). SEBS is expected to drastically improve the toughness of PP (Panaitescu, Vuluga et al. 2013). Besides, the unique structure of SEBS and the incompatibility between SEBS and PP make it possible

to create a nanostructured template to host the nanofiller and facilitate the dispersion/interaction of nanofiller in the blend matrix (Helal, Demarquette et al. 2016). The combination of a soft elastomer phase and a hard polystyrene phase can navigate the nanoclay and selectively accommodate to create a strong network which would eventually improve the electrical properties of the blend.

Although clay-filled PP nanocomposites have been studied extensively in the literature, little work has been done on their performance on electrical insulating parts. The current study aims to evaluate the dielectric properties of PP based nanocomposites and examine their potentials for insulation applications, in particular replacing XLPE. First, the morphology of the nanocomposites was examined by means of X-ray diffractometer, electron microscopy and rheometry. Then the dielectric properties were discussed including the low-field dielectric response, dc conductivity, space charge accumulation and short-term AC breakdown strength.

6.2 Experimental

6.2.1 Materials and Processing

A commercially available premixed PP/Clay masterbatch was used as the source of nanofiller (Nanocore, nanoMax®-PP). The masterbatch contains 50 wt% of organomodified montmorillonite. An electrical grade of polypropylene (Pro-Fax EP315J) was used to dilute the masterbatch into desired concentrations of nanoclay. PP was supplied from LyondellBasell in powder form with a density of 0.902 g/cm3 and MFI of 2.6 g/10 min (230 °C/2.16 kg).

A co-rotating twin screw extruder was used to prepare two series of nanocomposites by means of melt compounding with concentration profile of clay being set as 1, 2.5, 5, 10 and 15% where PP powder and masterbatch granules were directly fed. The same procedure was used to prepare blend nanocomposites of PP with polystyrene-b-poly(ethylene-co-butylene)-b-polystyrene (SEBS) thermoplastic elastomer supplied from Kraton (FG1901) having a MFI of 22 (230°C/2.16 kg) and a density of 0.91 g/cm^3. SEBS contains 30 wt% fractions of

polystyrene (PS) block in its structure. This grade of SEBS also contains 1.4-2 wt% of maleic anhydride attached to the rubbery block.

All the ingredients were dried in a vacuum oven at 60 ˚C for 48h prior to use. They were manually pre-mixed before being fed to the extruder. The temperature profile of extruder was set to 190-230 ˚C from hopper to die. The outcome of the extruder was cooled and grinded into small pellets. The obtained pellets were used to make thin plates (200 μm thickness) in an electrically heated hydraulic press. After 5 minutes of preheat, the pellets were hot-pressed for another 5 minutes at 210 ˚C and then water-cooled to ambient temperature with a cooling rate of 10 ˚C per minute. Nanocomposites are named as PP-n, with "n" referring the nominal percentage of incorporated clay. In case of blends the mass fractions of the two phases are set equal for each phase while incorporating 1 or 5% of clay (PP-SEBS-1, PP-SEBS-5).

6.2.2 Measurements and Characterization

High resolution Scanning Electron Microscopy (SEM) was used to characterize the morphology of the as-obtained nanocomposites using a Hitachi SU-8230 Field Emission-STEM microscope. Prior to the observation, samples were cryogenically cut and then sputtered with a layer of platinum (20 nm) using a Turbo-Pumped Sputter Coater (Q150T S). Solvent extraction has been used to investigate the microscopic structure of the blend nanocomposite. Blend sample was held in Toluene for 24 h at room temperature while being gently stirred and then washed with alcohol before SEM observation.

The degree of dispersion and intercalation of the nanoclay was evaluated through X-ray diffraction using PAN-analytical X'Pert Pro with Kα radiation (λ = 1.542 Å) having an accelerating voltage and electrical current of 40 kV and 40 mA respectively. The scanning was conducted from 2° to 10° with a step size of 0.102°. The counting time was set to 400 ms per step. The intercalate spacing (d_{001}) was measured, if needed, by Bragg's law ($2d \sin\theta=\lambda$), where λ is the wavelength of the X-ray radiation used, d is the distant between the diffraction of lattice plans, and θ is the diffraction angle measured

Rheological measurements were conducted at 210 ˚C via a strain-controlled rheometer (MCR 501 Anton Paar). The linear viscoelastic range was first determined by carrying out a strain sweep, then small amplitude oscillatory shear (SAOS) tests were performed in the frequency range from 0.01 to 300 rad.s^{-1}. Samples having 25 mm diameter were used in parallel plate geometry with 1 mm sample gap.

A novocontrol broadband dielectric spectrometer was used to record the dielectric spectra of available samples in the frequency range of 10^{-1} to 10^{6} Hz. Samples with the average thickness of 300 μm were sandwiched between two gold-plated electrodes in a parallel-plate geometry (40 mm of diameter) while all placed in a temperature-controlled chamber with a stability of 0.5 ˚C. The applied excitation voltage was set to 1 V_{rms}. A wide range of temperature was chosen to produce isothermal series of complex dielectric permittivity from 10 ˚C to 90 ˚C. All samples were dried at 50 ˚C in a vacuum oven for at least 24 hrs. Some data were fitted into Havriliak-Negami (HN) function to further analyze the observed relaxation processes. When necessary, a power law term was used to take into account the contribution of charge fluctuations.

The space charge profile has been determined using pulsed electroacoustic technique (PEA) where the acoustic waves created as a result of the interaction of a pulsive electric field and space charge inside the material is detected by a transducer. A HV pulse with an amplitude of 500 V and duration of 10 ns was applied to collect the charge profile information while the specimens were experiencing the DC field for a duration of 10000s after which the HV source was disconnected to record the depolarization profile for another 2000s. A semiconductive layer was placed between the HV electrode and the specimen to attenuate the sonic impedance mismatch. The measurements were done at 30 ˚C.

The AC short-term breakdown strength of the samples were measured using a BAUR DTA 100 device at ambient temperature. Samples were gently held between two ball-type electrodes (4 mm diameter) in a surrounding medium of insulating oil (Luminol TR-i, Petro-Canada) to

avoid flashover. The measurement was carried out according to method A from ASTM D149. The ramp was set to 2 kV/s and continued until the breakdown occurred. The insulating oil was dried in vacuum oven for a minimum of 48 h at 60 ˚C. Ten specimens were tested for each sample. Each time before changing the sample, the insulating oil was removed and fully replaced, and the electrodes were cleaned. A thickness of 160 μm was used for the breakdown test. The non-uniformity in the thickness of specimens were corrected using a power law relationship as discussed in (Helal, David et al. 2017).

6.3 Results and Discussion

6.3.1 X-ray Diffraction

The X-ray diffraction spectra for nanocomposites are displayed in Figure 1. The intensity, shape, and position of the basal reflection peaks helps identifying the microstructure of nanocomposite and the degree of intercalation/exfoliation of nanoclay. A single silicate layer has a thickness of around 1 nm, but they tend to form stacks of tactoids where the layers have a Van der Waals gap known as the interlayer of the gallery. The thickness of stacks of tactoids might reach up to several hundreds of microns. Polymer intercalation within the interlayer of nanoclay usually results in increased interlayer spacing and projects as a shift of the diffraction peak towards lower angles, according to Brag's law.

As seen in Figure 6-1, the XRD patterns of binary PP-clay nanocomposites show similar distinct peaks indicating an intercalation of clay layers in PP. The interlayer spacing (d_{001}) of nanoclay can be calculated from the primary diffraction peak using Bragg's law. The masterbatch indicates a (d_{001}) peak around $2\theta=3.2^{\circ}$ corresponding to an interlayer spacing of 2.7 nm. It can also be seen that nanocomposite peaks are on the right side of the corresponding peak in the masterbatch indicating that the dilution with pure PP led to a decrease in the basal spacing. The interlayer spacing for nanocomposites are around 2.15 nm and 1.96 nm for PP-5 and PP-1 respectively. While it shows that there is no sign of exfoliation, it also indicates collapsing of the silicate layers during compounding (Aloisi, Elisei et al. 2010). Another

explanation could be that the layered silicate particles are dispersed in thin stacks consisting only of few layers, forming edge-to-edge structure and the distance between the plates decreases causing a reduction in peak height. For nanocomposites with blend matrix, however, there is no sign of diffraction peaks which is a strong indication of layered silicates being separated to a point to form an exfoliated state where the interlayer spacing cannot be defined and individual layers are far from each other. It appears that the dispersion of clay is strongly affected by the evolution of the co-continuous structure of the blend matrix during the mixing stage. The affection of clay towards the elastomer phase and possible migration between the two phases helped clay platelets to get separated.

It must be noted that XRD cannot solely define the microstructure of the layered silicates and other means of spectroscopy are necessary to fully evaluate the dispersion/distribution of nanoclay.

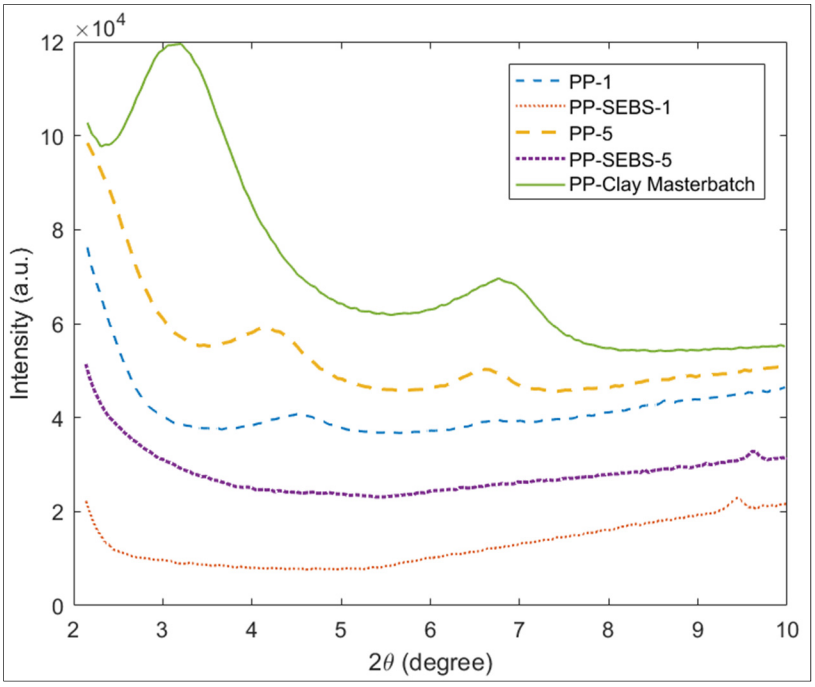

Figure 6-1 X-ray diffraction patterns for polypropylene/clay nanocomposites

6.3.2 Scanning Electron Microscopy (SEM)

The dispersion of nanoclay in PP was examined using SEM. The SEM micrographs of PP-clay nanocomposites are shown in Figure 6-2. It is hard to spot delaminated platelets but stacks and aggregates of clay are easily seen (shown by arrows). The stacks are fairly separated and almost uniformly distributed within the PP matrix. However, a small gap can be seen in the interfacial area around some of the stacks indicating a somewhat poor bond between clay layers with the hydrophobic PP matrix most indicating that the surface modification did not fully modify the hydrophilicity of clay.

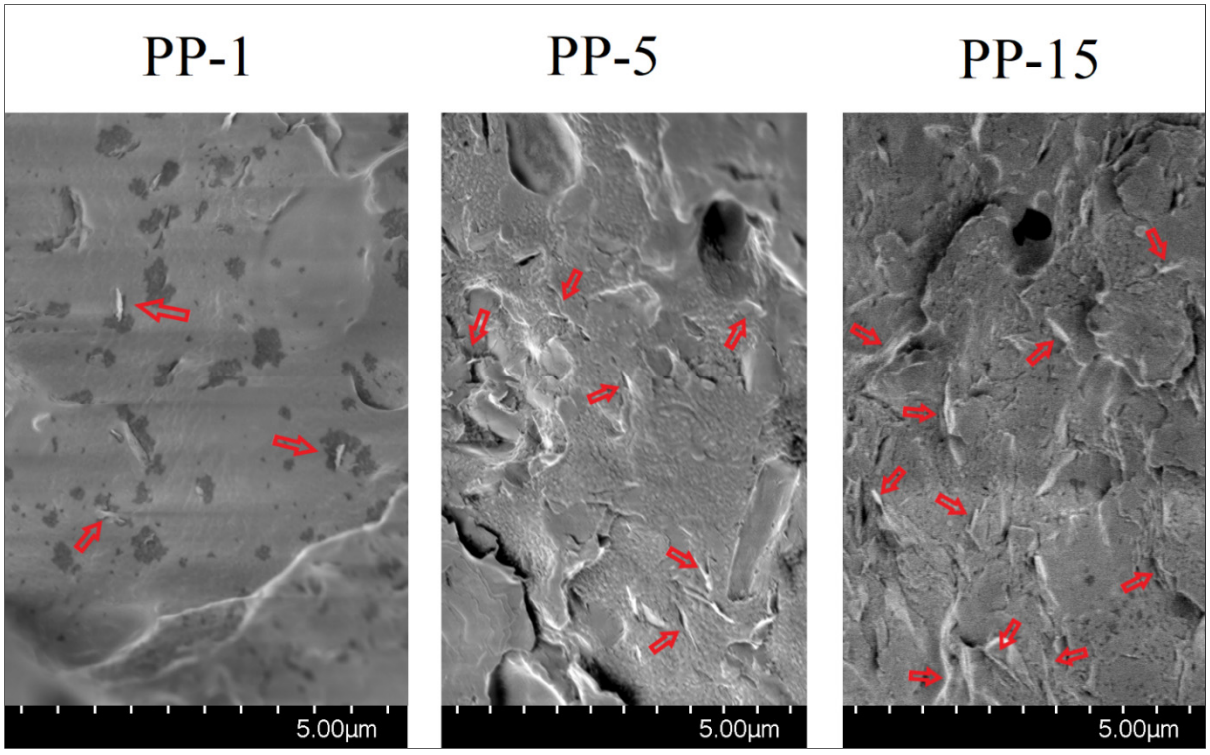

Figure 6-2 Scanning electron microscopy micrographs of PP-clay nanocomposites in different concentrations

The SEM micrographs of the blend nanocomposite containing 5% of nanoclay are depicted in Figure 6-3. Due to the immiscibility, similar viscosity and equal ratio of the two phases a co-continuous structure is expected. This random micrometric mixture is visible in the SEM

micrograph and is being shown by red dotted area. The co-continuity is confirmed when the elastomer phase is selectively removed via solvent extraction. Despite the presence of nanofiller, they are hard to spot due to the complexity of the images. They are, however, expected to be located in both phases and mostly in the interface of the two phases. The thermodynamic attraction of the elastomer phase to nanoclay results in a migration of nanofiller from the PP phase and during this process a huge amount of clay stacks and platelets would be stuck in the interface due to the short mixing time and high aspect ratio of the nanoclay (Figure 6-4). This transportation process of nanoclay has been thoroughly discussed in the authors' previous work in a similar formulation with having LDPE instead of PP [Chapter 2].

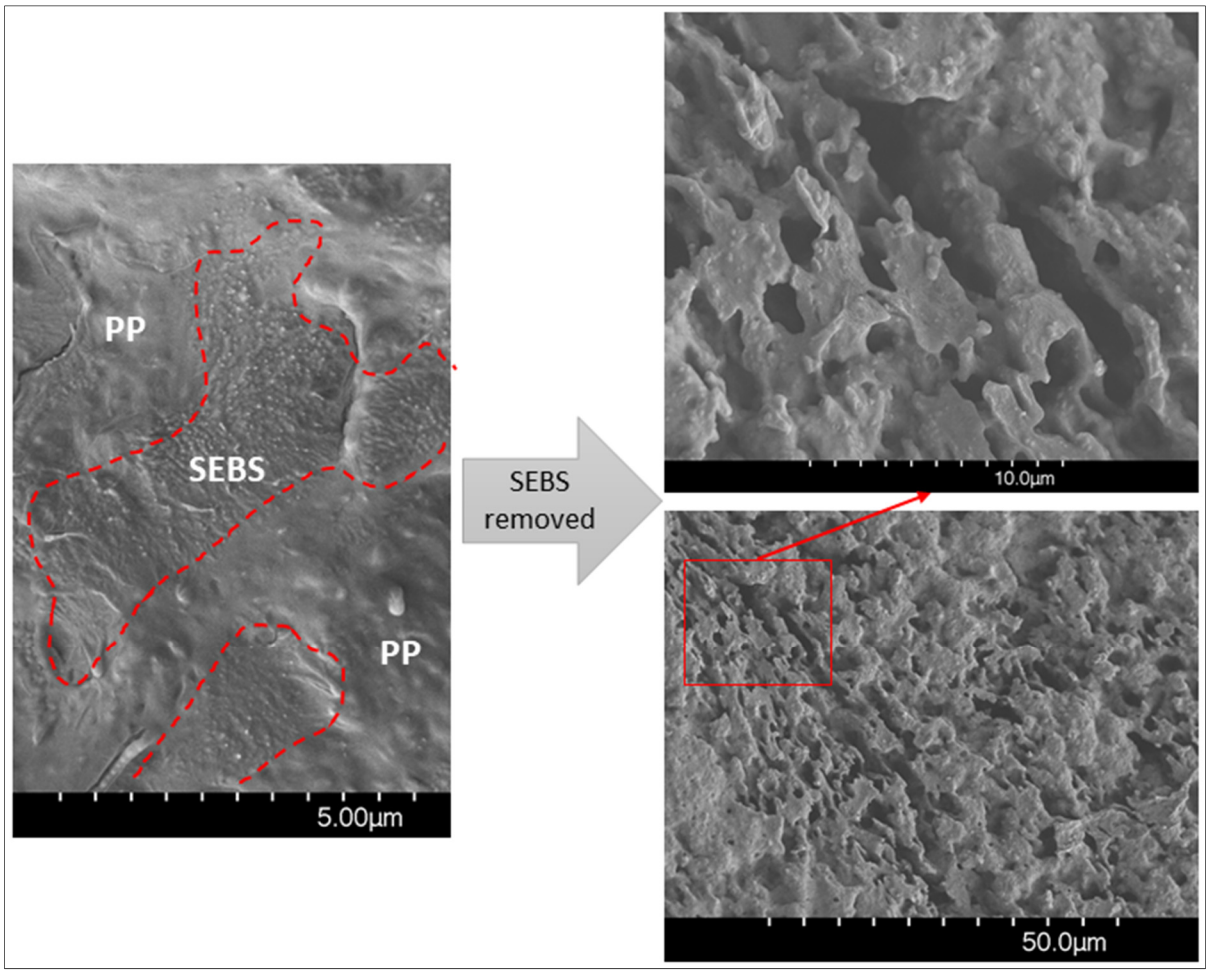

Figure 6-3 SEM micrographs of PP/SEBS-5 before (left) and after (right) solvent extraction

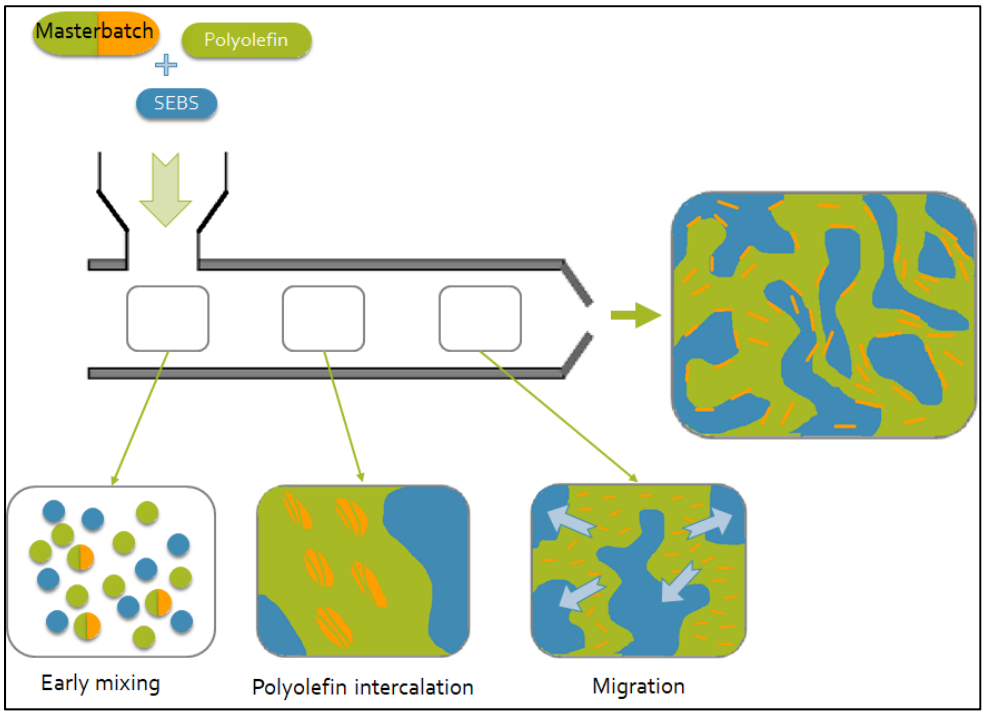

Figure 6-4 Schematic representation of morphology development during melt-mixing

6.3.3 Rheological Properties

Small Amplitude Oscillatory Shear (SAOS) test has been carried out to deepen the understanding of the morphology and the dispersion of the clay. The storage modulus (the real part of the complex modulus) and the magnitude of the complex viscosity of the nanocomposites as a function of frequency are shown in Figure 6-5. PP shows an expected semi-terminal behavior with a high slope and drop of the modulus at low frequencies. Upon addition of 1% clay the curves slightly deviate from the homopolymer and shift to higher values in low frequencies. The same trend is visible for higher loadings of clay with more deviation to the point where a plateau of storage modulus can be seen at low frequencies. At 5% concentration of nanoclay the rheological percolation threshold is already reached and nanocomposite shows a liquid-solid transition (LST). The increase in the level of storage modulus and viscosity towards lower frequencies is probably due to the creation of a network

of nanofiller with themselves and/or polymer matrix to restrict the molecular motion of PP matrix.

A strong pseudo solid-like behavior can be seen for nanocomposites with blend matrix. There is a consistent and huge increase in the level of storage modulus and complex viscosity when compared with PP. This is due to the phase separated morphology and high level of heterogeneity of block copolymer that is involved into the blend matrix. The change in the loading of nanofiller from 1 to 5% has little impact on both curves implying that the block copolymer's contribution is stronger that the impact of morphology. This is a common behavior in co-continuous blends (Veenstra, Verkooijen et al. 2000). Nonetheless, nanoclay enhance the rheological properties mostly due to the presence of clay in the interface of the two phases that would suppress the coalescence of the blend resulting in a stronger network of nanofiller with the matrix.

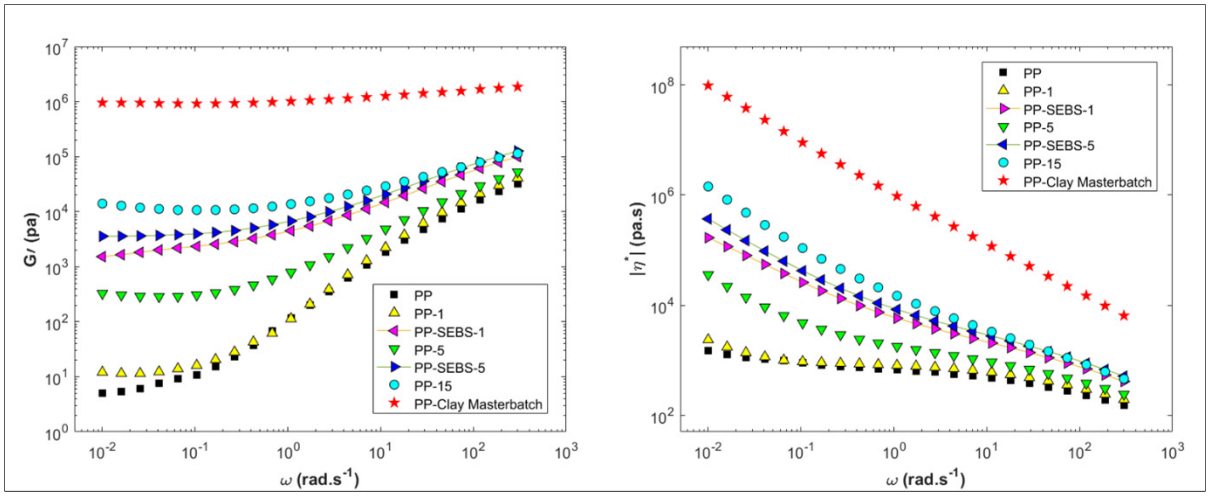

Figure 6-5 SAOS measurements of clay-reinforced nanocomposites: storage modulus (left) and complex viscosity (right) as function of angular frequency

6.3.4 Low-field Dielectric Measurements

As a non-polar low loss material, PP is expected to have frequency independent losses and not show any relaxation process over the temperature and frequency range of the measurement in

this work (Zhou, Hu et al. 2016). However, the dielectric behavior of PP is heavily affected by the presence of nanoclay. As an example, isothermal plots of dielectric loss for PP-5 are depicted in Figure 6-6.a as a function of frequency. A broad interfacial relaxation peak can be noticed at low frequencies moving towards higher frequencies with the increase in temperature showing a thermally activated behavior. This is anticipated due to the increase in the ionic conductivity along clay platelets at higher temperature resulting in lower relaxation times (Fréchette, Larocque et al. 2008). A double peak structure gradually develops in the nanocomposite representing two dielectric relaxation processes which is a common behavior in clay-filled plastic nanocomposites (Tomer, Polizos et al. 2011, David and Fréchette 2013). An example of fitting to HN at 90 ˚C is provided in Figure 6-6.b. The double peak structure appeared in all the binary nanocomposites (PP-n).

The first relaxation appeared at low frequency is most likely due to the charge trapping in the interface areas of nanoclay and PP which is known as Maxwell-Wagner-Sillars (MWS) polarization. The difference in conductivity of the two phases results in charge carriers to being trapped and then acting as large electric dipoles showing a dielectric relaxation process. The second relaxation peak at high frequency is most likely due to the orientation polarization associated with the polar domains of the organic intercalant that was used for surface treatment of clay layer. There is a nearly 4 decades' difference in relaxation times indicating that the orientation of the polar domains occur way faster than the movement of trapped charge carriers towards the PP/clay interface.

The evolution of dielectric loss for PP-15 with temperature and frequency, and an example of fitting are depicted in Figure 6-6.c&d. A consistent increase of dielectric loss towards low frequencies can be seen accompanied with the increase in the real permittivity (not shown here). This phenomenon is known as low frequency dispersion and consists of contributions of charge leakage through the specimen (dc conductivity) and charge blockage at the interface of the specimen and metal electrodes (electrode polarization). The contribution of the dc conductivity can be determined by the dc conductivity exponent which is the slope of the plot of imaginary permittivity versus frequency curve in log-scale. In case of ideal electronic

conductivity, the dc conductivity exponent is very close to unity, however, for PP-15 it is around 0.52 at 90˚C, which is the maximum value of the whole temperature range. This behavior is most likely due to the high nanofiller loading resulting in creation of a percolation network and is a common phenomenon in nanocomposites where the nanofiller is the main source of ionic conduction (Tanaka 2005).

A similar double peak structure was also witnessed for the nanocomposites with the blend matrix (PP-SEBS-n). The dielectric loss spectra of PP-SEBS-5 and an example of fitting at 90˚C are depicted in Figure 6-6.e&f. Comparing to the corresponding binary nanocomposite (PP-5), the two relaxations start to develop at lower frequencies which is an indication of the intramolecular interaction of nanoclay with the co-continuous structure and the intrinsic dielectric behavior of SEBS. Also, the level of dielectric loss is slightly higher which most probably due to the presence of MA polar groups in the SEBS. The blend nanocomposite becomes slightly conductive, especially at high temperatures exhibiting a low-frequency dispersion process with an exponent of 0.26 at 90 ˚C for the PP-SEBS-5 nanocomposite. This can be associated with the interaction of MA groups in the SEBS with functional groups on the surface of clay particles resulting in improved dispersion and slightly higher conductivity (Helal, Pottier et al. 2018).

Apart from the mentioned relaxation processes, a new relaxation mode is detected for the blend nanocomposite at higher frequencies which resulted in a broad and intensified high frequency peak. It is not expected to detect the segmental relaxation associated with the glass transition of the SEBS constituent. The segmental motion of the polystyrene (PS) is too slow and the one for the rubbery midblock (PEB) is too fast to be detected within the frequency and temperature range of this work. The origin of the new relaxation mode can be attributed to several phenomena such as the adsorbed water layer at the interface of nanofiller and polymer matrix (Glaskova and Aniskevich 2009), local motions inside EB blocks due to the presence of polar groups as a result of oxidative degradation (Panaitescu, Vuluga et al. 2013), molecular motions in the interface of SEBS domains (Chen, Hassan et al. 2011), and the local segment relaxation of rubber chains located at clay interface (Lin, Liu et al. 2015).

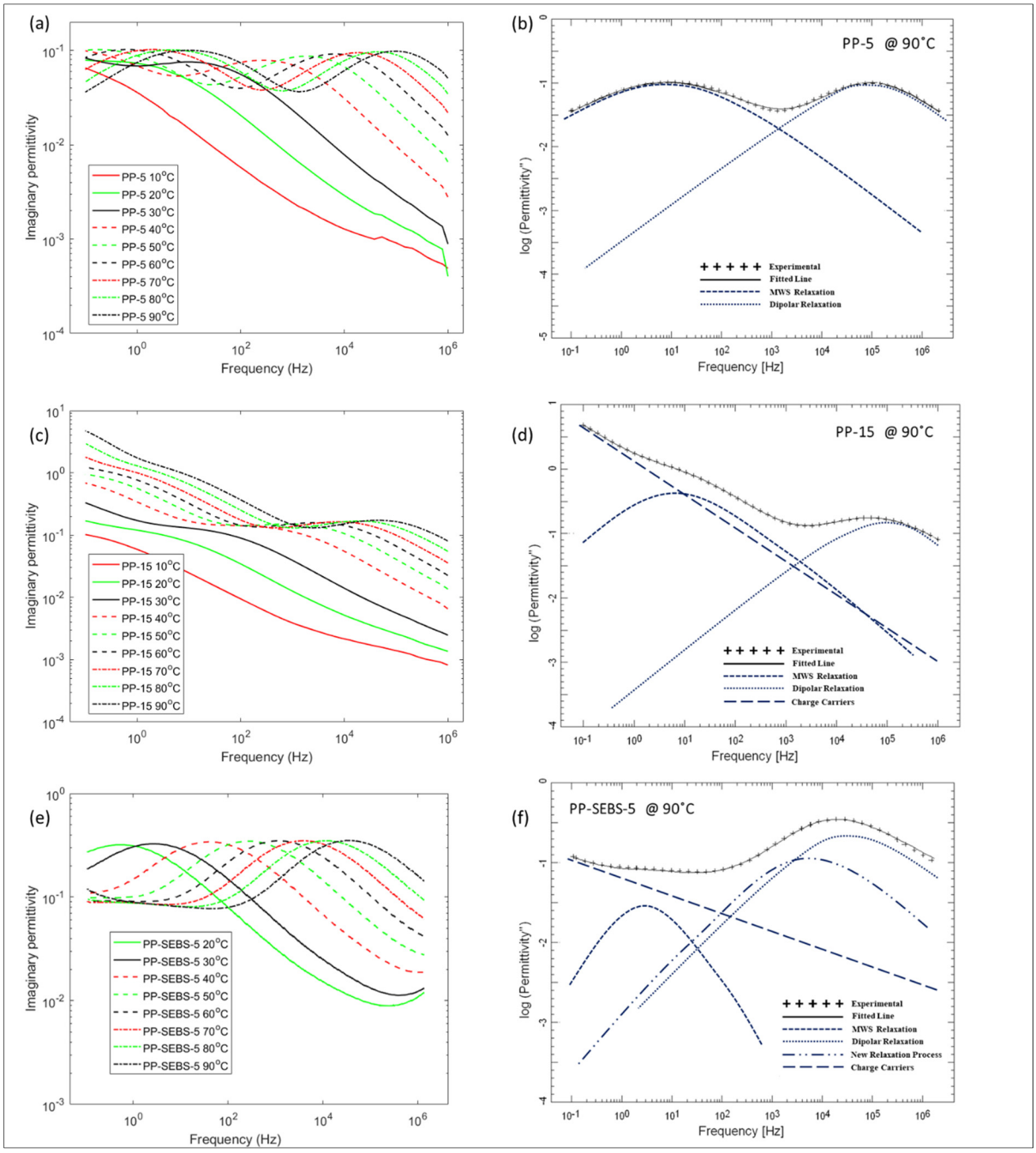

Figure 6-6 Dielectric loss (ϵ'') as a function of frequency and temperature for: a) PP-5, c) PP-15 and e) PP-SEBS-5. Fitting at 90 ˚C for b) PP-5, d) PP-15 and f) PP-SEBS-5

6.3.5 Space Charge Measurements

The time-dependent charge distribution profiles of PP, PP-5, PP-SEBS and PP-SEBS-5 are depicted in Figure 6-7 at 30 C and under poling electric field of 50 kV/mm. For PP a packet of positive charge is gradually injected from HV electrode which then disperses into the bulk. Simultaneously a thin layer of negative homocharge builds up close to LV electrode. For PP-5, however, a fairly thick layer of homocharges can be spotted close to LV electrode while low amount of positive charge is dispersed in the bulk of nanocomposite. The charge profiles for blends are stable and without any sign of charge injection from either of electrodes. In both cases low amount of positive charge is dispersed across the thickness. The suppression of space charge is slightly stronger for blend nanocomposite (PP-SEBS-5) which resulted in lower stored charge.

It appears that both blending and incorporation of nanoclay improves the ability of PP to suppress the accumulation of space charge. This could be related to the change in the microstructure and the introduction of deep traps. Traps can be introduced by the infinite surface area of the blend and also on the surface of clay layers which will then easily capture injected charges during the polarization process (Du, Xu et al. 2016, Andersson, Hynynen et al. 2017, Du, Li et al. 2017, Wang, Wu et al. 2017). While deep traps close to electrodes prevent the charge injection, the introduced shallow traps that are mostly responsible for conduction will allow for a portion of charge to gradually penetrates and get extracted at the opposite electrode. This is enhanced due to the high aspect ratio of clay layers and their accommodation in the interface area of the blend matrix. This mechanism prevents the charge injection under high electrical fields, keeps the charge profile stable and reduces the stored charge.

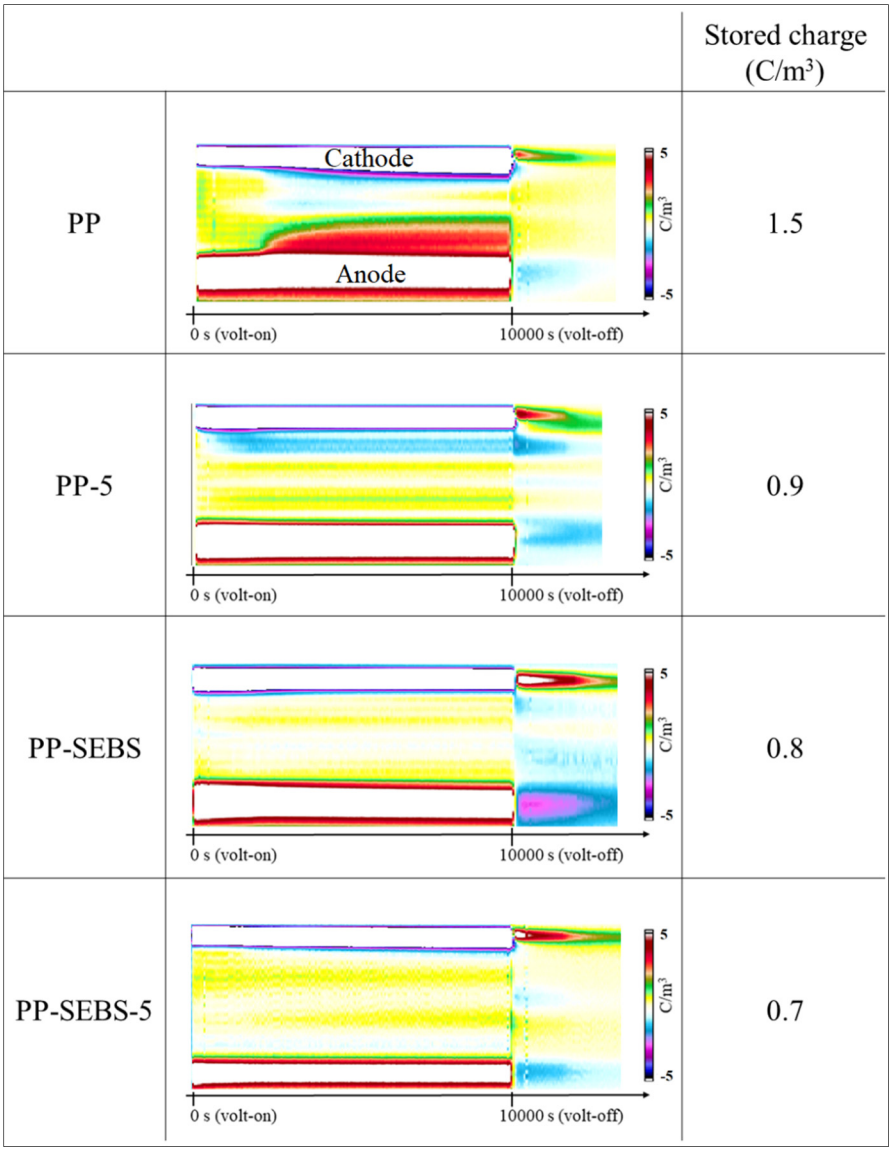

Figure 6-7 Space charge patterns for PP and its blend and nanocomposites at 30 ˚C and under 50 kV/mm of applied electric field (Stored charge was measured at the end of polarization period).

6.3.6 Short-term AC Breakdown Strength

The dielectric breakdown properties of nanocomposites were analyzed using a two-parameter Weibull distribution via a commercial software. The AC short-term breakdown strength data are displayed in Figure 6-8. The scale and shape parameters are embedded into the graph. The

shape parameter reflects the data scatter and the scale parameter is the characteristic breakdown strength at 63.2% cumulative breakdown. It can be seen that all nanocomposites show improved breakdown strength over the neat PP while having lower shape parameter. The characteristic breakdown strength goes up from 152 kV mm^{-1} for PP to 170 and 199 kV mm^{-1} upon addition of 1 and 5% nanoclay, respectively. At highest loading (15%) of nanoclay the scale parameter declines to 182 kV mm^{-1} but is still above PP. Due to the oscillation nature of AC condition, breakdown tends to initiate near the interface of the specimen and electrodes where charge trapping and accumulation most likely occur.

The improvement in AC breakdown strength of nanocomposites is probably originated from the interference of nanofiller with the charge transfer within the material. This is enhanced by the plate-like shape of clay stacks and platelets which makes it possible to form a tortuous path for charge carriers to travel across the thickness of nanocomposite (Fillery, Koerner et al. 2012). Other possible mechanisms include change of charge distribution and density around the interface of clay and polymer matrix (Zazoum, David et al. 2014), and nanoclay acting as scattering sites to reduce charge momentum (Thelakkadan, Coletti et al. 2011). The slightly diminished breakdown strength of nanocomposite with 15% loading of nanofiller is probably because of higher defect density due to the higher chance of particle agglomeration. Electric field around the agglomerates is enhanced which can eventually lead to breakdown (Nelson and Fothergill 2004). The sharp decrease in the shape parameter of nanocomposites comparing to neat PP is most likely due to the increase of sensitivity of the measurement to defects (i.e. clay tactoids) that accelerates the breakdown mechanism and increases the unreliability of the measurement. Regarding the AC breakdown strength of nanocomposites having blend matrix, they are expected to exhibit lower breakdown strength according to the rule of mixture for plastics since SEBS has a lower intrinsic breakdown strength due to its lower Young' modulus (Kollosche and Kofod 2010). However, no noticeable change can be spotted indicating that the improvement is mainly dominated and originated from the addition of nanoclay.

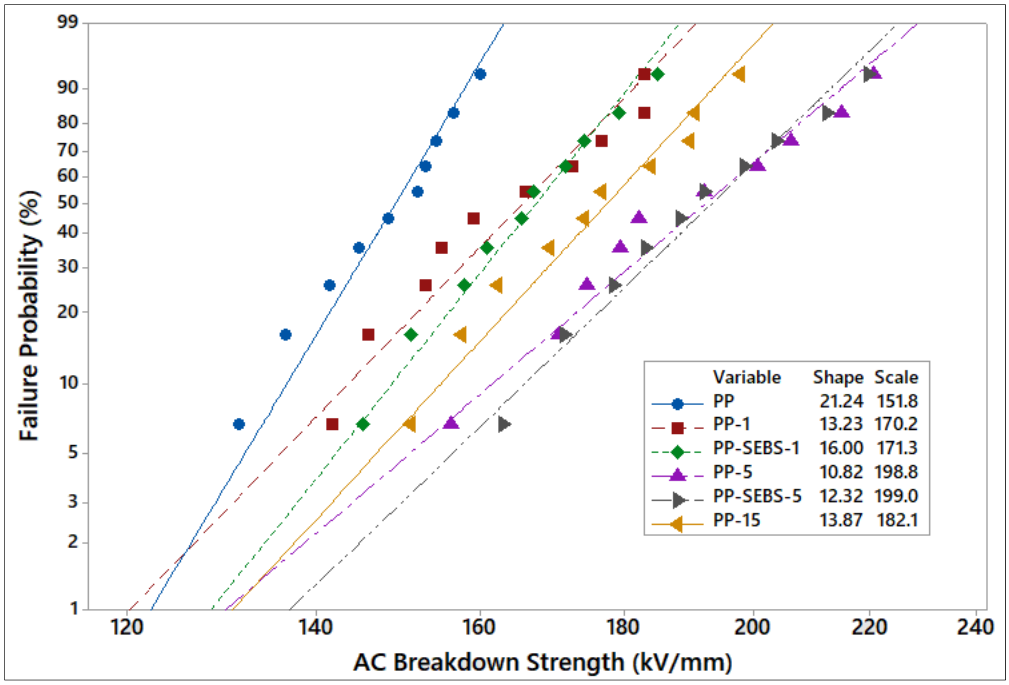

Figure 6-8 Weibull probability plots of PP/clay and PP/SEBS/clay nanocomposites (confidence intervals are removed for brevity)

Concluding Remarks

In this work the microstructure and dielectric properties of clay-containing PP nanocomposites have been investigated with the aim of evaluating the potentials of being used as insulating materials for HV cables. It was found out that clay is dispersed/distributed to good extent in the PP matrix, but fully dispersed in the blend matrix of PP and SEBS with equal weight percentage. This improvement was due to the migration of nanofiller from the polyolefin phase into the SEBS phase during the melt mixing process powered by the thermodynamic attraction of clay towards SEBS which resulted in more exfoliation of clay platelets and solid-like rheological behavior.

The incorporation of nanoclay significantly altered the electrical properties of PP. All nanocomposites have shown two unanimous peaks in their dielectric spectra that were absent in the neat PP: MWS relaxation at low frequencies representing the charge trapping in the polarized domains (MWS) and the dipolar orientation at high frequencies. A thermally

activated behavior was seen for nanocomposites as the dielectric spectra were moving towards higher frequencies with the increase in temperature. A new relaxation peak was observed for the blend nanocomposites that was at the origin of SEBS involvement.

Addition of nanoclay introduced deep traps that prevented the charge injection into the nanocomposite improving the space charge suppression of the material. The co-continuous structure of the blend also showed improved space charge patterns, especially when accompanied by the incorporation of nanofiller.

The short-term AC breakdown strength of PP was hugely enhanced when nanoclay was incorporated. Nanocomposites having 5% loading of nanoclay showed a 25% improvement in the characteristic breakdown strength, while lower improvements were reached for other loadings of nanofiller.

It seems that both addition of organomodified clay and using a co-continuous blend as the matrix have the potentials to make electrical properties of PP matrix superior/comparable to currently used XLPE-type cable insulation materials. The combination of the two phenomena led to the best results, where the difference in thermodynamic attraction of phases towards nanofiller and the sequence of feeding triggered clay particles to migrate into elastomer phase and thereby get stuck in the interface resulting in higher exfoliation rate.

CONCLUSION

In this section, a brief summary of all the findings will be presented. Materials prepared throughout this study can be classified into binary nanocomposites (LDPE/Clay and PP/Clay) and nanocomposites with polymer blend matrix (LDPE/SEBS/clay and PP/SEBS/Clay). The main findings for each of these materials are summarized below.

Clay-containing polyolefin nanocomposites

Series of nanocomposites containing different amount of nanoclay (1, 2.5, 5, 10 and 15%) were prepared based on LDPE and PP. A commercially available masterbatch was used as the source of nanoclay, comprising roughly of 50 wt% polyolefin, 31 wt% montmorillonite clay and 19 wt% organic modifiers. The masterbatch was then diluted to form nanocomposites with desired concentrations of nanofiller.

In both cases of LDPE/Clay and PP/Clay nanocomposites, it was shown that clay layers are well-dispersed and distributed into the polyolefin matrix. Stacks of clay were mostly intercalated by the polyolefin chains, but individual layers could be spotted separated from each other. The degree of dispersion was slightly higher when 5% of compatibilizer was used. Clay layers were seen to be oriented parallel to the surface of molded sheet, due to the high pressure condition of the molding process and very low thickness of the final sheet.

Addition of nanoclay significantly changed the rheological properties of polyolefin from a homopolymer-like terminal behavior to a solid-like behavior showing a plateau of storage modulus in low frequencies. This change in the rheological behavior was seen for all PP/clay nanocomposites but only visible for LDPE/Clay nanocomposites at high loading of nanofiller (10 and 15%). Clay tends to have a relatively weak interfacial interaction with LDPE, while forms a strong network in PP. However, the addition of compatibilizer slightly improved the solid-like behavior in LDPE/Clay nanocomposites.

The dielectric spectra regarding the binary nanocomposites fitted with Havriliak-Negami function unanimously showed two relaxation processes that were absent in the neat polyolefin. The first relaxation process occurred in the low frequencies at the origin of the charge trapping in the interface areas between nanofiller and the base polymer known as MWS relaxation. The second relaxation at relatively higher frequencies was attributed to the dipolar orientation of the polar domains of the organic intercalant that was used for surface treatment of clay layer. The dielectric response of nanocomposites was shown to be thermally activated as the dielectric loss spectra move towards higher frequencies as temperature increases.

Upon addition of nanoclay the DC characteristics of LDPE were changed significantly. All nanocomposites showed at least two orders of magnitude increase in the level of DC conductivity which was also directly related to the loading of nanofiller. It was also shown that the DC conductivity of the nanocomposites directly related to the applied electric field and temperature. This enhancement is believed to originate from the creation of the nanofiller network, which facilitates the movement of charge carriers. With regards to the space charge patterns of LDPE and its clay-containing nanocomposites, it was shown that the increased conductivity also help dispersing the accumulated space charge inside the material. For neat LDPE a highly distorted charge profile was observed, especially in higher electric fields while no significant charge accumulation was observed for nanocomposites. However, it was concluded that there is a threshold for this effect of nanoclay, above which massive injected charges heavily distorted the electric field distribution.

The AC breakdown strengths of polyolefin were significantly improved upon addition of clay. Optimum enhancement was observed for 5% incorporation of clay. This enhancement was attributed to the delaying in the process of charge transfer between electrodes through the material as a result of the creation of a tortuous path by clay network for charge carriers. However, the DC breakdown strength of LDPE nanocomposites were all diminished comparing the neat polymer due to the different mechanism involved and the thermal instability of nanocomposites.

Clay-containing blend nanocomposites

Two different grades of SEBS, pure and to which maleic anhydride was grafted (~2 wt%), both having 30% PS blocks, were used to form co-continuous blends with LDPE to host 5% of nanoclay (LDPE/SEBS/5C and LDPE/SEBS-MA-5C). The maleated SEBS was also used to form a blend with PP hosting 1 and 5% nanoclay (PP/SEBS-MA/1C and PP/SEBS/5C).

The co-continuous morphology of the blends was confirmed through scanning electron microscopy. While similar co-continuous morphology was observed for blend nanocomposites, the addition of clay took the co-continuity into smaller dimension. This downsizing effect was attributed to the prevention of coalescence induced by the presence of clay and compatibilizer. It was also concluded that nanoclay would migrate from the polyolefin phase into the block copolymer phase during the melt-mixing stage and thus clay would mostly have stuck in the interface of the two phases as was confirmed by TEM images.

The high level of heterogeneity in SEBS strongly affected the rheological behavior of blend nanocomposites and massively increases the storage modulus and complex viscosity especially in low frequencies to the point where it partially overshadowed the effect of nanofiller. Nonetheless, the nanofiller, mostly present in the interface of the two phases, helps suppressing the coalescence of the blend and enabling to form a network which strengthened the solid-like behavior.

The dielectric response of blend nanocomposites was fitted to HN function and a charge fluctuation term. In addition to the relaxation processes associated with the presence of clay, a new relaxation mode was observed in all blend nanocomposites and was related to the thermoplastic elastomer phase. The high frequency peak for blend nanocomposite with SEBS-MA was more intense than the one for SEBS. This was attributed to the higher compatibility of clay with maleated SEBS and overlaying a possible relaxation process assigned to localized fluctuations of the polar MA groups.

Regarding the short-term AC breakdown strength, the pure blends of SEBS with LDPE showed diminished breakdown strength as expected due to the inherent lower breakdown strength of SEBS. However, upon addition of clay, the characteristic breakdown strengths of blends significantly increased, similar to the result of binary nanocomposite. The same trend was observed for blend nanocomposites based on PP with even more enhance improvement.

RECOMMENDATIONS

This project evaluated several thermoplastic nanocomposites materials as possible candidates to substitute the current generation of insulating materials in HV application, particularly HV cable insulation. The incorporation of nanoclay seems to drastically improve certain electrical properties such as AC breakdown strength and space charge accumulation, but compromises a few other properties such as DC breakdown strength and the level of dielectric loss. At the same time clay offers a lot of advantages including availability, cheapness and ease of processing and the resultant material would still be recyclable.

Similar to what has been done in this work, clay can be compounded with base polymer via blending with a commercially available masterbatch without the need to modify the existing manufacturing lines. However, further studies are needed to have a more in-depth understanding of the role of nanoclay in improving the electrical performance of polyolefin such as LDPE, especially in cable geometry.

Other types of clay minerals can also be investigated as the nanoreinforcement. More precisely, non-swelling clays i.e. kaolinite can be of importance. Kaolinite is the purest of clays, meaning that it varies little in composition. It also does not absorb water and does not expand when it comes in contact with water.

Using a blend with a co-continuous morphology instead of a neat polyolefin enables to selectively accommodates the nanofiller showing promising improvements in electrical properties. This can be further investigated with different nanofillers and different blend constituents. Also morphologies other than co-continuous, i.e. droplet/matrix, can be interesting in some variations.

In this project equivalent amounts of SEBS and polyolefin were used to form the blends. Further studies can be placed to find the optimum weight percentage needed to create the co-

continuous morphology considering the relatively higher price of SEBS comparing to polyolefin.

Great results were achieved regarding electrical properties of nanocomposites especially short-term breakdown strength. To prove the reliability of the proposed materials, long-term measurements are necessary to conduct and will provide a more general view.

Also, a lot of aspects of electrical properties of the proposed materials can be modeled/simulated i.e. the dielectric permittivity. Theoretical studies can help further explaining the role of interface and its contribution to the final morphology of the nanocomposites which would ease up the path to deepen the understanding of structure-property relationships.

LIST OF BIBLIOGRAPHICAL REFERENCES

Agari, Y., A. Ueda and S. Nagai (1993). "Thermal conductivities of blends of polyethylene/SEBS block copolymer and polystyrene/SEBS block copolymer." Journal of applied polymer science **47**(2): 331-337.

Alateyah, A., H. Dhakal and Z. Zhang (2013). "Processing, properties, and applications of polymer nanocomposites based on layer silicates: a review." Advances in polymer technology **32**(4).

Albdiry, M., B. Yousif, H. Ku and K. Lau (2013). "A critical review on the manufacturing processes in relation to the properties of nanoclay/polymer composites." Journal of composite materials **47**(9): 1093-1115.

Alexandre, M. and P. Dubois (2000). "Polymer-layered silicate nanocomposites: preparation, properties and uses of a new class of materials." Materials Science and Engineering: R: Reports **28**(1): 1-63.

Alison, J. and L. Dissado (1996). Electric field enhancement within moulded samples of low density polyethene-a means of failure characterised by voltage ramp tests and space charge measurement. Dielectric Materials, Measurements and Applications, Seventh International Conference on (Conf. Publ. No. 430), IET.

Aloisi, G., F. Elisei, M. Nocchetti, G. Camino, A. Frache, U. Costantino and L. Latterini (2010). "Clay based polymeric composites: Preparation and quality characterization." Materials Chemistry and Physics **123**(2-3): 372-377.

Andersson, M. G., J. Hynynen, M. R. Andersson, V. Englund, P.-O. Hagstrand, T. Gkourmpis and C. Müller (2017). "Highly Insulating Polyethylene Blends for High-Voltage Direct-Current Power Cables." ACS Macro Letters **6**: 78-82.

As' habi, L., S. H. Jafari, B. Baghaei, H. A. Khonakdar, P. Pötschke and F. Böhme (2008). "Structural analysis of multicomponent nanoclay-containing polymer blends through simple model systems." Polymer **49**(8): 2119-2126.

Asai, S., K. Sakata, M. Sumita and K. Miyasaka (1992). "Effect of interfacial free energy on the heterogeneous distribution of oxidized carbon black in polymer blends." Polymer journal **24**(5): 415-420.

Bagheri-Kazemabad, S., D. Fox, Y. Chen, L. M. Geever, A. Khavandi, R. Bagheri, C. L. Higginbotham, H. Zhang and B. Chen (2012). "Morphology, rheology and mechanical properties of polypropylene/ethylene–octene copolymer/clay nanocomposites: effects of the compatibilizer." Composites Science and Technology **72**(14): 1697-1704.

Balsamo, V., A. T. Lorenzo, A. J. Müller, S. Corona-Galván, L. M. Fraga Trillo and V. R. Santa Quiteria (2006). "Structure, properties and applications of ABA and ABC triblock copolymers with hydrogenated polybutadiene blocks." Block Copolymers in Nanoscience: 367-389.

Beyer, G. (2002). "Nanocomposites: a new class of flame retardants for polymers." Plastics, Additives and Compounding **4**(10): 22-28.

Blythe, A. R. and D. Bloor (2005). Electrical properties of polymers, Cambridge University Press.

Böhning, M., H. Goering, A. Fritz, K.-W. Brzezinka, G. Turky, A. Schönhals and B. Schartel (2005). "Dielectric study of molecular mobility in poly (propylene-graft-maleic anhydride)/clay nanocomposites." Macromolecules **38**(7): 2764-2774.

Boudou, L., V. Griseri, J. Guastavino and L. Dissado (2004). Effect of temperature on space charge formation in low density polyethylene-role of antioxidant. Solid Dielectrics, 2004. ICSD 2004. Proceedings of the 2004 IEEE International Conference on, IEEE.

Bulinski, A., S. Bamji, M. Abou-Dakka and Y. Chen (2010). Dielectric properties of polypropylene containing synthetic and natural organoclays. Electrical Insulation (ISEI), Conference Record of the 2010 IEEE International Symposium on, IEEE.

Cao, Y., P. C. Irwin and K. Younsi (2004). "The future of nanodielectrics in the electrical power industry." IEEE Transactions on Dielectrics and Electrical Insulation **11**(5): 797-807.

Carastan, D. J., L. G. Amurin, A. F. Craievich, M. do Carmo Gonçalves and N. R. Demarquette (2013). "Morphological evolution of oriented clay-containing block copolymer nanocomposites under elongational flow." European Polymer Journal **49**(6): 1391-1405.

Carastan, D. J., L. G. Amurin, A. F. Craievich, M. d. C. Gonçalves and N. R. Demarquette (2014). "Clay-containing block copolymer nanocomposites with aligned morphology prepared by extrusion." Polymer International **63**(2): 184-194.

Carastan, D. J., N. R. Demarquette, A. Vermogen and K. Masenelli-Varlot (2008). "Linear viscoelasticity of styrenic block copolymers–clay nanocomposites." Rheologica Acta **47**(5-6): 521.

Cassagnau, P. (2008). "Melt rheology of organoclay and fumed silica nanocomposites." Polymer **49**(9): 2183-2196.

Chen, G., M. Hao, Z. Xu, A. Vaughan, J. Cao and H. Wang (2015). "Review of high voltage direct current cables." CSEE Journal of Power and Energy Systems **1**(2): 9-21.

Chen, G. and J. Zhao (2011). "Observation of negative differential mobility and charge packet in polyethylene." Journal of Physics D: Applied Physics **44**(21): 212001.

Chen, G., J. Zhao, S. Li and L. Zhong (2012). "Origin of thickness dependent dc electrical breakdown in dielectrics." Applied physics letters **100**(22): 222904.

Chen, H., M. K. Hassan, S. K. Peddini and K. A. Mauritz (2011). "Macromolecular dynamics of sulfonated poly (styrene-b-ethylene-ran-butylene-b-styrene) block copolymers by broadband dielectric spectroscopy." European polymer journal **47**(10): 1936-1948.

Choudalakis, G. and A. Gotsis (2009). "Permeability of polymer/clay nanocomposites: a review." European Polymer Journal **45**(4): 967-984.

Chow, W., A. A. Bakar, Z. M. Ishak, J. Karger-Kocsis and U. Ishiaku (2005). "Effect of maleic anhydride-grafted ethylene–propylene rubber on the mechanical, rheological and morphological properties of organoclay reinforced polyamide 6/polypropylene nanocomposites." European Polymer Journal **41**(4): 687-696.

Cole, K. S. and R. H. Cole (1941). "Dispersion and absorption in dielectrics I. Alternating current characteristics." The Journal of chemical physics **9**(4): 341-351.

Coleman, M. M., P. C. Painter and J. F. Graf (1995). Specific interactions and the miscibility of polymer blends, CRC Press.

Couderc, H., E. David, M. Frechette and A. Medjdoub (2013). Influence of water on PE—SiO 2 nanocomposites dielectric properties. Electrical Insulation and Dielectric Phenomena (CEIDP), 2013 IEEE Conference on, IEEE.

Crawford, R. J. (1998). Plastics engineering, Butterworth-Heinemann.

Darie, R. N., E. Pâslaru, A. Sdrobis, G. M. Pricope, G. E. Hitruc, A. Poiată, A. Baklavaridis and C. Vasile (2014). "Effect of nanoclay hydrophilicity on the poly (lactic acid)/clay nanocomposites properties." Industrial & Engineering Chemistry Research **53**(19): 7877-7890.

David, E. and M. Fréchette (2013). "Polymer nanocomposites-major conclusions and achievements reached so far." IEEE Electrical Insulation Magazine **29**(6): 29-36.

David, E., M. Fréchette, B. Zazoum, C. Daran-Daneau, A. D. Ngô and H. Couderc (2013). "Dielectric properties of PE/clay nanocomposites." Journal of Nanomaterials **2013**: 65.

David, E., B. Zazoum, M. Fréchette and F. Rogti (2015). Dielectric response of HDPE/clay nanocomposites containing 10% wt of organo-modified clay. Electrical Insulation and Dielectric Phenomena (CEIDP), 2015 IEEE Conference on, IEEE.

Davidson, D. W. and R. H. Cole (1951). "Dielectric relaxation in glycerol, propylene glycol, and n- propanol." The Journal of Chemical Physics **19**(12): 1484-1490.

De Lima, C. A., L. G. Amurin, N. R. Demarquette and E. David (2016). Morphological and electric properties of block copolymer/carbon nanotubes nanocomposites obtained by different methods. IEEE Electrical Insulation Conference (EIC), 2016, IEEE.

Debye, P. (1912). "Some results of kinetic theory of isolators.(preliminary announcement)." Physikalische Zeitschrift **13**: 97-100.

Degraeve, R., G. Groeseneken, R. Bellens, J. L. Ogier, M. Depas, P. J. Roussel and H. E. Maes (1998). "New insights in the relation between electron trap generation and the statistical properties of oxide breakdown." IEEE Transactions on Electron Devices **45**(4): 904-911.

Delbem, M. F., T. S. Valera, F. R. Valenzuela-Diaz and N. R. Demarquette (2010). "Modification of a Brazilian smectite clay with different quaternary ammonium salts." Química Nova **33**(2): 309-315.

Deshmukh, K., M. B. Ahamed, S. K. Pasha, R. R. Deshmukh and P. R. Bhagat (2015). "Highly dispersible graphene oxide reinforced polypyrrole/polyvinyl alcohol blend nanocomposites with high dielectric constant and low dielectric loss." RSC Advances **5**(76): 61933-61945.

Dissado, L. A. and J. C. Fothergill (1992). Electrical degradation and breakdown in polymers, IET.

Donth, E.-J. (1992). Relaxation and thermodynamics in polymers: glass transition, Akademie Verlag.

Du, B., J. Li and Y. Sekii (2017). "Effects of ZnO particles on space charge of EVA copolymer for HVDC cable accessory insulation." IEEE Transactions on Dielectrics and Electrical Insulation **24**(3): 1503-1510.

Du, B., H. Xu, J. Li and Z. Li (2016). "Space charge behaviors of PP/POE/ZnO nanocomposites for HVDC cables." IEEE Transactions on Dielectrics and Electrical Insulation **23**(5): 3165-3174.

Dumont, M. J., A. Reyna-Valencia, J. P. Emond and M. Bousmina (2007). "Barrier properties of polypropylene/organoclay nanocomposites." Journal of applied polymer science **103**(1): 618-625.

Durmuş, A., M. Woo, A. Kaşgöz, C. W. Macosko and M. Tsapatsis (2007). "Intercalated linear low density polyethylene (LLDPE)/clay nanocomposites prepared with oxidized

polyethylene as a new type compatibilizer: structural, mechanical and barrier properties." European Polymer Journal **43**(9): 3737-3749.

Eesaee, M., E. David, N. R. Demarquette and D. Fabiani (2018). "Electrical Breakdown Properties of Clay-Based LDPE Blends and Nanocomposites." Journal of Nanomaterials **2018**: 17.

Eesaee, M. and A. Shojaei (2014). "Effect of nanoclays on the mechanical properties and durability of novolac phenolic resin/woven glass fiber composite at various chemical environments." Composites Part A: Applied Science and Manufacturing **63**: 149-158.

Elias, L., F. Fenouillot, J.-C. Majesté, P. Alcouffe and P. Cassagnau (2008). "Immiscible polymer blends stabilized with nano-silica particles: Rheology and effective interfacial tension." Polymer **49**(20): 4378-4385.

Elias, L., F. Fenouillot, J.-C. Majesté and P. Cassagnau (2007). "Morphology and rheology of immiscible polymer blends filled with silica nanoparticles." Polymer **48**(20): 6029-6040.

Fabiani, D., A. Camprini, C. Vanga-Bouanga and M. Fréchette (2017). Optimization of space charge accumulation in LDPE nanocomposites containing graphene oxide. 2017 IEEE 17th International Conference on Nanotechnology (IEEE-NANO).

Fabiani, D., P. Mancinelli, C. Vanga-Bouanga, M. F. Fréchette and J. Castellon (2016). Effect of graphene-oxide content on space charge characteristics of PE-based nanocomposites. IEEE Electrical Insulation Conference (EIC), 2016, IEEE.

Fabiani, D., G. C. Montanari, L. A. Dissado, C. Laurent and G. Teyssedre (2009). "Fast and slow charge packets in polymeric materials under DC stress." IEEE Transactions on Dielectrics and Electrical Insulation **16**(1): 241-250.

Fang, Z., Y. Xu and L. Tong (2007). "Effect of clay on the morphology of binary blends of polyamide 6 with high density polyethylene and HDPE- graft- acrylic acid." Polymer Engineering & Science **47**(5): 551-559.

Filippone, G., N. T. Dintcheva, F. La Mantia and D. Acierno (2010). "Selective localization of organoclay and effects on the morphology and mechanical properties of LDPE/PA11 blends with distributed and co- continuous morphology." Journal of Polymer Science Part B: Polymer Physics **48**(5): 600-609.

Fillery, S. P., H. Koerner, L. Drummy, E. Dunkerley, M. F. Durstock, D. F. Schmidt and R. A. Vaia (2012). "Nanolaminates: increasing dielectric breakdown strength of composites." ACS applied materials & interfaces **4**(3): 1388-1396.

Fim, F. d. C., N. R. Basso, A. P. Graebin, D. S. Azambuja and G. B. Galland (2013). "Thermal, electrical, and mechanical properties of polyethylene–graphene nanocomposites obtained by in situ polymerization." Journal of Applied Polymer Science **128**(5): 2630-2637.

Fleming, R., A. Ammala, P. Casey and S. Lang (2008). "Conductivity and space charge in LDPE containing nano-and micro-sized ZnO particles." IEEE Transactions on Dielectrics and Electrical Insulation **15**(1).

Fleming, R., T. Pawlowski, A. Ammala, P. Casey and K. Lawrence (2005). "Electrical conductivity and space charge in LDPE containing TiO/sub 2/nanoparticles." IEEE transactions on dielectrics and electrical insulation **12**(4): 745-753.

Fortelný, I., J. Kovář and M. Stephan (1996). "Analysis of the phase structure development during the melt mixing of polymer blends." Journal of Elastomers & Plastics **28**(2): 106-139.

Fréchette, M., R. Larocque, M. Trudeau, R. Veillette, R. Rioux, S. Pelissou, S. Besner, M. Javan, K. Cole and M.-T. T. That (2008). "Nanostructured polymer microcomposites: A distinct class of insulating materials." IEEE Transactions on Dielectrics and Electrical Insulation **15**(1).

Fréchette, M. F., C. W. Reed and H. Sedding (2006). "Progress, understanding and challenges in the field of nanodielectrics." IEEJ Transactions on Fundamentals and Materials **126**(11): 1031-1043.

Garcıa-López, D., O. Picazo, J. Merino and J. Pastor (2003). "Polypropylene–clay nanocomposites: effect of compatibilizing agents on clay dispersion." European polymer journal **39**(5): 945-950.

Ghosh, S. K., W. Rahman, T. R. Middya, S. Sen and D. Mandal (2016). "Improved breakdown strength and electrical energy storage performance of γ-poly (vinylidene fluoride)/unmodified montmorillonite clay nano-dielectrics." Nanotechnology **27**(21): 215401.

Gilman, J. W., W. H. Awad, R. D. Davis, J. Shields, R. H. Harris, C. Davis, A. B. Morgan, T. E. Sutto, J. Callahan and P. C. Trulove (2002). "Polymer/layered silicate nanocomposites from thermally stable trialkylimidazolium-treated montmorillonite." Chemistry of Materials **14**(9): 3776-3785.

Glaskova, T. and A. Aniskevich (2009). "Moisture absorption by epoxy/montmorillonite nanocomposite." Composites Science and Technology **69**(15): 2711-2715.

Golberg, D., Y. Bando, Y. Huang, T. Terao, M. Mitome, C. Tang and C. Zhi (2010). "Boron nitride nanotubes and nanosheets." ACS nano **4**(6): 2979-2993.

Gong, G., J. Wu, Y. Lin, C. Chan and M. Yang (2009). "Dynamic rheological behavior of isotactic polypropylene filled with nano-calcium carbonate modified by stearic acid coating." Journal of Macromolecular Science® **48**(2): 329-343.

Graziano, A., S. Jaffer and M. Sain (2018). "Review on modification strategies of polyethylene/polypropylene immiscible thermoplastic polymer blends for enhancing their mechanical behavior." Journal of Elastomers & Plastics: 0095244318783806.

Guggenheim, S. and R. Martin (1995). "Definition of clay and clay mineral: joint report of the AIPEA nomenclature and CMS nomenclature committees." Clays and clay minerals **43**(2): 255-256.

Hakim, S., M. Nekoomanesh and A. Ali (2018). "Effects of Nanoclay Treatment with NH3/Methylaluminoxane/Dodecylamine on the Morphology and Properties of Polyethylene/Clay Nanocomposites Prepared by in-Situ Polymerization." Polyolefins Journal.

Hamzah, M. S., M. Jaafar, M. Jamil and M. Kamarol (2014). "Electrical insulation characteristics of alumina, titania, and organoclay nanoparticles filled PP/EPDM nanocomposites." Journal of Applied Polymer Science **131**(23).

Hands, A. and K. Ryden (2017). "Experimental Measurement of Low-Intensity and Long-Duration Internal Charging Behavior." IEEE Transactions on Plasma Science **45**(8): 1938-1946.

Hanley, T. L., R. P. Burford, R. J. Fleming and K. W. Barber (2003). "A general review of polymeric insulation for use in HVDC cables." IEEE Electrical Insulation Magazine **19**(1): 13-24.

Hasegawa, N. and A. Usuki (2004). "Silicate layer exfoliation in polyolefin/clay nanocomposites based on maleic anhydride modified polyolefins and organophilic clay." Journal of applied polymer science **93**(1): 464-470.

Havriliak, S. and S. Negami (1967). "A complex plane representation of dielectric and mechanical relaxation processes in some polymers." Polymer **8**: 161-210.

Heid, T., M. F. Fréchette and E. David (2015). "Functional epoxy composites for high voltage insulation involving c-BN and reactive POSS as compatibilizer." Journal of Materials Science **50**(16): 5494-5503.

Helal, E., L. Amurin, D. Carastan, R. de Sousa, E. David, M. Fréchette and N. Demarquette (2017). "Interfacial molecular dynamics of styrenic block copolymer-based nanocomposites with controlled spatial distribution." Polymer **113**: 9-26.

Helal, E., E. David, M. Fréchette and N. Demarquette (2017). "Thermoplastic elastomer nanocomposites with controlled nanoparticles dispersion for HV insulation systems: correlation between rheological, thermal, electrical and dielectric properties." European Polymer Journal.

Helal, E., E. David, M. Fréchette and N. R. Demarquette (2017). "Thermoplastic elastomer nanocomposites with controlled nanoparticles dispersion for HV insulation systems: Correlation between rheological, thermal, electrical and dielectric properties." European Polymer Journal **94**: 68-86.

Helal, E., N. R. Demarquette, L. Amurin, E. David, D. Carastan and M. Fréchette (2015). "Styrenic block copolymer-based nanocomposites: Implications of nanostructuration and nanofiller tailored dispersion on the dielectric properties." Polymer **64**: 139-152.

Helal, E., N. R. Demarquette, E. David and M. Fréchette (2016). Evaluation of dielectric behavior of polyethylene/thermoplastic elastomer blends containing zinc oxide (ZnO) nanoparticles for high voltage insulation. IEEE Electrical Insulation Conference (EIC), 2016, IEEE.

Helal, E., C. Pottier, E. David, M. Fréchette and N. Demarquette (2018). "Polyethylene/thermoplastic elastomer/Zinc Oxide nanocomposites for high voltage insulation applications: Dielectric, mechanical and rheological behavior." European Polymer Journal **100**: 258-269.

Hernández, M., J. Carretero-González, R. Verdejo, T. A. Ezquerra and M. A. López-Manchado (2009). "Molecular dynamics of natural rubber/layered silicate nanocomposites as studied by dielectric relaxation spectroscopy." Macromolecules **43**(2): 643-651.

Holden, G., H. R. Kricheldorf and R. P. Quirk (2004). Thermoplastic elastomers, Hanser Munich.

Hosier, I., M. Praeger, A. Holt, A. Vaughan and S. Swingler (2014). Effect of water absorption on dielectric properties of nano-silica/polyethylene composites. Electrical Insulation and Dielectric Phenomena (CEIDP), 2014 IEEE Conference on, IEEE.

Hosier, I., M. Praeger, A. Holt, A. Vaughan and S. Swingler (2015). "On the Effect of Functionaliser Chain Length and Water Content in Polyethylene/Silica Nanocomposites: Part I–Dielectric Properties and Breakdown Strength." IEEE Transactions on Dielectrics and Electrical Insulation: 1-10.

Huang, X., P. Jiang and T. Tanaka (2011). "A review of dielectric polymer composites with high thermal conductivity." IEEE Electrical Insulation Magazine **27**(4).

Huang, X., P. Jiang and C. U. Kim (2007). Electrical properties of polyethylene/aluminum nanocomposites.

Huang, X., F. Liu and P. Jiang (2010). "Effect of nanoparticle surface treatment on morphology, electrical and water treeing behavior of LLDPE composites." IEEE transactions on dielectrics and electrical insulation **17**(6): 1697-1704.

Huang, X., Z. Ma, Y. Wang, P. Jiang, Y. Yin and Z. Li (2009). "Polyethylene/aluminum nanocomposites: Improvement of dielectric strength by nanoparticle surface modification." Journal of applied polymer science **113**(6): 3577-3584.

Hui, L., L. S. Schadler and J. K. Nelson (2013). "The influence of moisture on the electrical properties of crosslinked polyethylene/silica nanocomposites." IEEE Transactions on Dielectrics and Electrical Insulation **20**(2): 641-653.

Ildstad, E., J. Sletbak, B. Nyberg and J. Larsen (2004). "Factors affecting the choice of insulation system for extruded HVDC Power Cables." paper D1-203, CIGRE Session.

Ishimoto, K., T. Tanaka, Y. Ohki, Y. Sekiguchi, Y. Murata and M. Gosyowaki (2008). Comparison of dielectric properties of low-density polyethylene/MgO composites with different size fillers. Electrical Insulation and Dielectric Phenomena, 2008. CEIDP 2008. Annual Report Conference on, IEEE.

Iyer, G., R. Gorur, R. Richert, A. Krivda and L. Schmidt (2011). "Dielectric properties of epoxy based nanocomposites for high voltage insulation." IEEE Transactions on Dielectrics and Electrical Insulation **18**(3).

Jiang, X., Q. Peng, W. Sima, P. Sun and M. Yang (2017). "Space charge behavior evolution of thermal-aged double-layered polyimide films." IEEE Transactions on Dielectrics and Electrical Insulation **24**(6): 3801-3810.

Jones, J., J. Llewellyn and T. Lewis (2005). "The contribution of field-induced morphological change to the electrical aging and breakdown of polyethylene." IEEE Transactions on Dielectrics and Electrical Insulation **12**(5): 951-966.

Jonscher, A. and R. Lacoste (1984). "On a cumulative model of dielectric breakdown in solids." IEEE transactions on electrical insulation(6): 567-577.

Jonscher, A. K. (1996). Universal relaxation law: a sequel to Dielectric relaxation in solids, Chelsea Dielectrics Press.

Kao, K. C. (2004). Dielectric phenomena in solids, Academic press.

Kar, G. P., S. Biswas, R. Rohini and S. Bose (2015). "Tailoring the dispersion of multiwall carbon nanotubes in co-continuous PVDF/ABS blends to design materials with enhanced electromagnetic interference shielding." Journal of Materials Chemistry A **3**(15): 7974-7985.

Khalf, A. and A. Ward (2010). "Use of rice husks as potential filler in styrene butadiene rubber/linear low density polyethylene blends in the presence of maleic anhydride." Materials & Design (1980-2015) **31**(5): 2414-2421.

Khatua, B., D. J. Lee, H. Y. Kim and J. K. Kim (2004). "Effect of organoclay platelets on morphology of nylon-6 and poly (ethylene-r an-propylene) rubber blends." Macromolecules **37**(7): 2454-2459.

Kiliaris, P. and C. Papaspyrides (2010). "Polymer/layered silicate (clay) nanocomposites: an overview of flame retardancy." Progress in Polymer Science **35**(7): 902-958.

Kim, H. and F. Shi (2001). "Thickness dependent dielectric strength of a low-permittivity dielectric film." IEEE Transactions on Dielectrics and Electrical Insulation **8**(2): 248-252.

Kindersberger, J., T. Tanaka and M. Frechette (2011). "Polymer nanocomposites-Fundamentals and possible applications to power sectors." Electra(254): 69-73.

Klein, N. and H. Gafni (1966). "The maximum dielectric strength of thin silicon oxide films." IEEE transactions on Electron Devices **13**(2): 281-289.

Kofod, G., S. Risse, H. Stoyanov, D. N. McCarthy, S. Sokolov and R. Kraehnert (2011). "Broad-spectrum enhancement of polymer composite dielectric constant at ultralow volume fractions of silica-supported copper nanoparticles." ACS nano **5**(3): 1623-1629.

Kollosche, M. and G. Kofod (2010). "Electrical failure in blends of chemically identical, soft thermoplastic elastomers with different elastic stiffness." Applied Physics Letters **96**(7): 071904.

Kozako, M., N. Fuse, Y. Ohki, T. Okamoto and T. Tanaka (2004). "Surface degradation of polyamide nanocomposites caused by partial discharges using IEC (b) electrodes." IEEE Transactions on Dielectrics and Electrical Insulation **11**(5): 833-839.

Krentz, T., M. M. Khani, M. Bell, B. C. Benicewicz, J. K. Nelson, S. Zhao, H. Hillborg and L. S. Schadler (2017). "Morphologically dependent alternating- current and direct- current breakdown strength in silica–polypropylene nanocomposites." Journal of Applied Polymer Science **134**(1).

Krueger, F. (1991). Industrial High Voltage Part I, Fields, dielectrics and constructions, Delft University Press.

Kuester, S., G. M. Barra, J. C. Ferreira Jr, B. G. Soares and N. R. Demarquette (2016). "Electromagnetic interference shielding and electrical properties of nanocomposites

based on poly (styrene-b-ethylene-ran-butylene-b-styrene) and carbon nanotubes." European Polymer Journal **77**: 43-53.

Kurahashi, K., Y. Matsuda, Y. Miyashita, T. Demura, A. Ueda and K. Yoshino (2006). "The application of novel polypropylene to the insulation of electric power cable (3)." Electrical Engineering in Japan **155**(3): 1-8.

Lan, T. and T. J. Pinnavaia (1994). "Clay-reinforced epoxy nanocomposites." Chemistry of materials **6**(12): 2216-2219.

Lau, K., M. Piah and K. Ching (2017). "Correlating the breakdown strength with electric field analysis for polyethylene/silica nanocomposites." Journal of Electrostatics **86**: 1-11.

Lau, K., A. Vaughan, G. Chen and I. Hosier (2012). Polyethylene nanodielectrics: The effect of nanosilica and its surface treatment on electrical breakdown strength. Electrical Insulation and Dielectric Phenomena (CEIDP), 2012 Annual Report Conference on, IEEE.

Lau, K., A. Vaughan, G. Chen, I. Hosier, A. Holt and K. Y. Ching (2014). "On the space charge and DC breakdown behavior of polyethylene/silica nanocomposites." IEEE Transactions on Dielectrics and Electrical Insulation **21**(1): 340-351.

Lawson, J. H. (2013). "The transition from paper-insulated, lead-covered cable to cross-linked polyethylene-insulated cable - a personal account." IEEE Electrical Insulation Magazine **29**(4): 16-23.

Le Roy, S., P. Segur, G. Teyssedre and C. Laurent (2003). "Description of bipolar charge transport in polyethylene using a fluid model with a constant mobility: model prediction." Journal of physics D: Applied physics **37**(2): 298.

Lee, H.-T. and L.-H. Lin (2006). "Waterborne polyurethane/clay nanocomposites: novel effects of the clay and its interlayer ions on the morphology and physical and electrical properties." Macromolecules **39**(18): 6133-6141.

Lee, W. D., S. S. Im, H.-M. Lim and K.-J. Kim (2006). "Preparation and properties of layered double hydroxide/poly (ethylene terephthalate) nanocomposites by direct melt compounding." Polymer **47**(4): 1364-1371.

Legge, N. R. (1987). "Thermoplastic elastomers, a comprehensive review." Hanser-Verlog.

Lewis, T. (1994). "Nanometric dielectrics." IEEE Transactions on Dielectrics and Electrical Insulation **1**(5): 812-825.

Lewis, T. (2004). "Interfaces are the dominant feature of dielectrics at the nanometric level." IEEE Transactions on Dielectrics and Electrical Insulation **11**(5): 739-753.

Lewis, T. (2014). "Charge transport in polyethylene nano dielectrics." IEEE transactions on dielectrics and electrical insulation **21**(2): 497-502.

Li, B., C. Camilli, P. Xidas, K. Triantafyllidis and E. Manias (2017). "Structured Polyethylene Nanocomposites: Effects of Crystal Orientation and Nanofiller Alignment on High Field Dielectric Properties." MRS Advances **2**(6): 363-368.

Li, S., L. Yang, W. Liu and W. Wang (2016). "Dielectric Breakdown of Polymer Nanocomposites."

Li, S., G. Yin, S. Bai and J. Li (2011). "A new potential barrier model in epoxy resin nanodielectrics." IEEE Transactions on Dielectrics and Electrical Insulation **18**(5).

Li, S., G. Yin, G. Chen, J. Li, S. Bai, L. Zhong, Y. Zhang and Q. Lei (2010). "Short-term breakdown and long-term failure in nanodielectrics: A review." IEEE Transactions on Dielectrics and Electrical Insulation **17**(5).

Li, S., G. Yin and J. Li (2012). Breakdown performance of low density polyethylene nanocomposites. Properties and Applications of Dielectric Materials (ICPADM), 2012 IEEE 10th International Conference on the, IEEE.

Liao, R., G. Bai, L. Yang, H. Cheng, Y. Yuan and J. Guan (2013). "Improved electric strength and space charge characterization in LDPE composites with montmorillonite fillers." Journal of Nanomaterials **2013**: 2.

Lin, Y., L. Liu, G. Xu, D. Zhang, A. Guan and G. Wu (2015). "Interfacial interactions and segmental dynamics of poly (vinyl acetate)/silica nanocomposites." The Journal of Physical Chemistry C **119**(23): 12956-12966.

Liu, J., V. Mhetar and J. Freestone (2011). Insulation containing styrene copolymers, Google Patents.

Liu, L., Y. Wang, F. Xiang, Y. Li, L. Han and Z. Zhou (2009). "Effects of functionalized multiwalled carbon nanotubes on the morphologies and mechanical properties of PP/EVA blend." Journal of Polymer Science Part B: Polymer Physics **47**(15): 1481-1491.

Liu, Y., H. Liu, L. Yu, Y. Li and L. Gao (2017). "Effect of thermal stress on the space charge distribution of 160 kV HVDC cable insulation material." IEEE Transactions on Dielectrics and Electrical Insulation **24**(3): 1355-1364.

Long, W. and S. Nilsson (2007). "HVDC transmission: yesterday and today." IEEE Power and Energy Magazine **5**(2): 22-31.

Luo, P., S. Wang, B. Feng, Q. Mu, M. Xu and Y. Xu (2016). AC breakdown strength and glass transition temperature of mesoporous silica/EP composite. High Voltage Engineering and Application (ICHVE), 2016 IEEE International Conference on, IEEE.

Ma, D., T. A. Hugener, R. W. Siegel, A. Christerson, E. Mårtensson, C. Önneby and L. S. Schadler (2005). "Influence of nanoparticle surface modification on the electrical behaviour of polyethylene nanocomposites." Nanotechnology **16**(6): 724.

Ma, Z., P. Jiang, L. Wang and J. Yang (2010). "Effect of styrene–ethylene–butadiene–styrene and its synergetic effect with ethylene vinyl acetate on the mechanical, thermal, dielectric, and water- treeing behaviors of crosslinked polyethylene." Journal of applied polymer science **118**(4): 2350-2357.

Maeno, T., T. Futami, H. Kushibe, T. Takada and C. Cooke (1988). "Measurement of spatial charge distribution in thick dielectrics using the pulsed electroacoustic method." IEEE transactions on Electrical Insulation **23**(3): 433-439.

Mancinelli, P., D. Fabiani, A. Saccani, M. Toselli and M. F. Fréchette (2015). "Electrical ac and dc behavior of epoxy nanocomposites containing graphene oxide." Journal of Applied Polymer Science **132**(18).

Manias, E., A. Touny, L. Wu, K. Strawhecker, B. Lu and T. Chung (2001). "Polypropylene/montmorillonite nanocomposites. Review of the synthetic routes and materials properties." Chemistry of Materials **13**(10): 3516-3523.

Mazzanti, G. and M. Marzinotto (2013). Extruded cables for high-voltage direct-current transmission: advances in research and development, John Wiley & Sons.

Mc Carthy, D. N., S. Risse, P. Katekomol and G. Kofod (2009). "The effect of dispersion on the increased relative permittivity of TiO2/SEBS composites." Journal of Physics D: Applied Physics **42**(14): 145406.

McAllister, I. W., G. C. Crichton and A. Pedersen (1996). Space charge fields in DC cables. Electrical Insulation, 1996., Conference Record of the 1996 IEEE International Symposium on, IEEE.

McPherson, J. (2016). On why dielectric breakdown strength reduces with dielectric thickness. Reliability Physics Symposium (IRPS), 2016 IEEE International, IEEE.

Messersmith, P. B. and E. P. Giannelis (1994). "Synthesis and characterization of layered silicate-epoxy nanocomposites." Chemistry of materials **6**(10): 1719-1725.

Milliere, L., K. Makasheva, C. Laurent, B. Despax, L. Boudou and G. Teyssedre (2014). Effects of a modified interface by silver nanoparticles/SiOC: H barrier layer against

space charge injection under HVDC. Electrical Insulation and Dielectric Phenomena (CEIDP), 2014 IEEE Conference on, IEEE.

Minkova, L., H. Yordanov, S. Filippi and N. Grizzuti (2003). "Interfacial tension of compatibilized blends of LDPE and PA6: the breaking thread method." Polymer **44**(26): 7925-7932.

Montanari, G. C., D. Fabiani, F. Palmieri, D. Kaempfer, R. Thomann and R. Mulhaupt (2004). "Modification of electrical properties and performance of EVA and PP insulation through nanostructure by organophilic silicates." IEEE Transactions on Dielectrics and Electrical Insulation **11**(5): 754-762.

Murakami, Y., M. Nemoto, S. Okuzumi, S. Masuda, M. Nagao, N. Hozumi, Y. Sekiguchi and Y. Murata (2008). "DC conduction and electrical breakdown of MgO/LDPE nanocomposite." IEEE Transactions on Dielectrics and Electrical Insulation **15**(1).

Murakami, Y., S. Okuzumi, M. Nagao, M. Fukuma, Y. Sekiguchi, M. Goshowaki and Y. Murata (2010). "Space Charge Measurement in MgO/LDPE Nanocomposite up to Breakdown under DC Ramp Voltage." IEEJ Transactions on Electrical and Electronic Engineering **5**(4): 395-399.

Murata, Y., Y. Sekiguchi, Y. Inoue and M. Kanaoka (2005). Investigation of electrical phenomena of inorganic-filler/LDPE nanocomposite material. Electrical Insulating Materials, 2005.(ISEIM 2005). Proceedings of 2005 International Symposium on, IEEE.

Nagao, M., T. Kimura, Y. Mizuno, M. Kosaki and M. Ieda (1990). "Detection of joule heating before dielectric breakdown in polyethylene films." IEEE transactions on electrical insulation **25**(4): 715-722.

Nelson, J. K. and J. C. Fothergill (2004). "Internal charge behaviour of nanocomposites." Nanotechnology **15**(5): 586.

Nelson, J. K., J. C. Fothergill, L. A. Dissado and W. Peasgood (2002). Towards an understanding of nanometric dielectrics. Electrical Insulation and Dielectric Phenomena, 2002 Annual Report Conference on, IEEE.

Nitta, K.-H., Y.-W. Shin, H. Hashiguchi, S. Tanimoto and M. Terano (2005). "Morphology and mechanical properties in the binary blends of isotactic polypropylene and novel propylene-co-olefin random copolymers with isotactic propylene sequence 1. Ethylene–propylene copolymers." Polymer **46**(3): 965-975.

Oskouyi, A. B. and P. Mertiny (2011). "Monte Carlo model for the study of percolation thresholds in composites filled with circular conductive nano-disks." Procedia Engineering **10**: 403-408.

Ouyang, B., H. Li, X. Zhang, S. Wang and J. Li (2017). "The role of micro-structure changes on space charge distribution of XLPE during thermo-oxidative ageing." IEEE Transactions on Dielectrics and Electrical Insulation **24**(6): 3849-3859.

Panaitescu, D. M., Z. Vuluga, P. V. Notingher and C. Nicolae (2013). "The effect of poly [styrene- b- (ethylene- co- butylene)- b- styrene] on dielectric, thermal, and morphological characteristics of polypropylene/silica nanocomposites." Polymer Engineering & Science **53**(10): 2081-2092.

Park, Y.-J., J.-H. Kwon, J.-Y. Sim, J.-N. Hwang, C.-W. Seo, J.-H. Kim and K.-J. Lim (2014). "DC conduction and breakdown characteristics of Al2O3/cross-linked polyethylene nanocomposites for high voltage direct current transmission cable insulation." Japanese Journal of Applied Physics **53**(8S3): 08NL05.

Paul, D. and S. Newman (1978). "Polymer blends, vol. 2." Academic, New York.

Paul, D. and L. M. Robeson (2008). "Polymer nanotechnology: nanocomposites." Polymer **49**(15): 3187-3204.

Pavlidou, S. and C. Papaspyrides (2008). "A review on polymer–layered silicate nanocomposites." Progress in polymer science **33**(12): 1119-1198.

Pawar, S. P. and S. Bose (2015). "Peculiar morphological transitions induced by nanoparticles in polymeric blends: retarded relaxation or altered interfacial tension?" Physical Chemistry Chemical Physics **17**(22): 14470-14478.

Peng, W., X. Huang, J. Yu, P. Jiang and W. Liu (2010). "Electrical and thermophysical properties of epoxy/aluminum nitride nanocomposites: Effects of nanoparticle surface modification." Composites Part A: Applied Science and Manufacturing **41**(9): 1201-1209.

Persson, A. L. and H. Bertilsson (1998). "Viscosity difference as distributing factor in selective absorption of aluminium borate whiskers in immiscible polymer blends." Polymer **39**(23): 5633-5642.

Pitsa, D. and M. G. Danikas (2011). "Interfaces features in polymer nanocomposites: A review of proposed models." Nano **6**(06): 497-508.

Pluta, M., J. Jeszka and G. Boiteux (2007). "Polylactide/montmorillonite nanocomposites: structure, dielectric, viscoelastic and thermal properties." European Polymer Journal **43**(7): 2819-2835.

Pötschke, P. and D. Paul (2003). "Formation of co-continuous structures in melt-mixed immiscible polymer blends." Journal of Macromolecular Science, Part C: Polymer Reviews **43**(1): 87-141.

Powell, C. E. and G. W. Beall (2007). Physical properties of polymer/clay nanocomposites. Physical properties of polymers handbook, Springer**:** 561-575.

Qu, M., F. Deng, S. M. Kalkhoran, A. Gouldstone, A. Robisson and K. J. Van Vliet (2011). "Nanoscale visualization and multiscale mechanical implications of bound rubber interphases in rubber–carbon black nanocomposites." Soft Matter **7**(3): 1066-1077.

Ray, S. S. and M. Okamoto (2003). "Polymer/layered silicate nanocomposites: a review from preparation to processing." Progress in polymer science **28**(11): 1539-1641.

Ray, S. S., S. Pouliot, M. Bousmina and L. A. Utracki (2004). "Role of organically modified layered silicate as an active interfacial modifier in immiscible polystyrene/polypropylene blends." Polymer **45**(25): 8403-8413.

Reichert, P., H. Nitz, S. Klinke, R. Brandsch, R. Thomann and R. Mülhaupt (2000). "Poly (propylene)/organoclay nanocomposite formation: influence of compatibilizer functionality and organoclay modification." Macromolecular Materials and Engineering **275**(1): 8-17.

Ren, J., A. S. Silva and R. Krishnamoorti (2000). "Linear viscoelasticity of disordered polystyrene− polyisoprene block copolymer based layered-silicate nanocomposites." Macromolecules **33**(10): 3739-3746.

Ritämaki, M., I. Rytöluoto, M. Niittymäki, K. Lahti and M. Karttunen (2016). Differences in AC and DC large-area breakdown behavior of polymer thin films. Dielectrics (ICD), 2016 IEEE International Conference on, IEEE.

Robeson, L. M. (2007). "Polymer blends." Hanser, Munich: 24-149.

Romeo, G., G. Filippone, A. Fernández-Nieves, P. Russo and D. Acierno (2008). "Elasticity and dynamics of particle gels in non-Newtonian melts." Rheologica acta **47**(9): 989-997.

Roy, M., J. Nelson, R. MacCrone, L. S. Schadler, C. Reed and R. Keefe (2005). "Polymer nanocomposite dielectrics-the role of the interface." IEEE Transactions on Dielectrics and Electrical Insulation **12**(4): 629-643.

Roy, M., J. K. Nelson, R. MacCrone and L. Schadler (2007). "Candidate mechanisms controlling the electrical characteristics of silica/XLPE nanodielectrics." Journal of Materials Science **42**(11): 3789-3799.

Ryan, H. M. (2001). High voltage engineering and testing, Iet.

Sánchez- Valdes, S., M. L. López- Quintanilla, E. Ramírez- Vargas, F. J. Medellín- Rodríguez and J. M. Gutierrez- Rodriguez (2006). "Effect of ionomeric compatibilizer on clay

dispersion in polyethylene/clay nanocomposites." Macromolecular Materials and Engineering **291**(2): 128-136.

Sarvestani, A. S. (2008). "Modeling the solid-like behavior of entangled polymer nanocomposites at low frequency regimes." European Polymer Journal **44**(2): 263-269.

Schönhals, A. and F. Kremer (2003). Analysis of dielectric spectra. Broadband dielectric spectroscopy, Springer**:** 59-98.

Scott, C. E. and C. W. Macosko (1995). "Morphology development during the initial stages of polymer-polymer blending." Polymer **36**(3): 461-470.

Sengers, W., O. Van den Berg, M. Wübbenhorst, A. Gotsis and S. Picken (2005). "Dielectric spectroscopy using dielectric probes: a new approach to study glass transition dynamics in immiscible apolar polymer blends." Polymer **46**(16): 6064-6074.

Sengwa, R., S. Sankhla and S. Choudhary (2010). "Dielectric characterization of solution intercalation and melt intercalation poly (vinyl alcohol)-poly (vinyl pyrrolidone) blend-montmorillonite clay nanocomposite films."

Shah, K., R. Jain, V. Shrinet, A. Singh and D. Bharambe (2009). "High density polyethylene (HDPE) clay nanocomposite for dielectric applications." IEEE Transactions on Dielectrics and Electrical Insulation **16**(3).

Shin, S.-Y. A., L. C. Simon, J. B. Soares and G. Scholz (2003). "Polyethylene–clay hybrid nanocomposites: in situ polymerization using bifunctional organic modifiers." Polymer **44**(18): 5317-5321.

Si, M., T. Araki, H. Ade, A. Kilcoyne, R. Fisher, J. C. Sokolov and M. H. Rafailovich (2006). "Compatibilizing bulk polymer blends by using organoclays." Macromolecules **39**(14): 4793-4801.

Siemens, A. (2011). "High voltage direct current transmission-proven technology for power exchange." Energy Sector, Germany. Accessed at http://www. siemens. com/sustainability/pool/en/environmental-portfolio/products-solutions/power-transmission-distribution/hvdc_proven_technology. pdf.

Song, W. L., P. Wang, L. Cao, A. Anderson, M. J. Meziani, A. J. Farr and Y. P. Sun (2012). "Polymer/boron nitride nanocomposite materials for superior thermal transport performance." Angewandte Chemie **124**(26): 6604-6607.

Song, Y. and Q. Zheng (2015). "Linear rheology of nanofilled polymers." Journal of Rheology **59**(1): 155-191.

Stoyanov, H., M. Kollosche, S. Risse, D. N. McCarthy and G. Kofod (2011). "Elastic block copolymer nanocomposites with controlled interfacial interactions for artificial muscles with direct voltage control." Soft Matter **7**(1): 194-202.

Sumita, M., K. Sakata, S. Asai, K. Miyasaka and H. Nakagawa (1991). "Dispersion of fillers and the electrical conductivity of polymer blends filled with carbon black." Polymer Bulletin **25**(2): 265-271.

Sune, J., D. Jimenez and E. Miranda (2001). "Breakdown modes and breakdown statistics of ultrathin SiO 2 gate oxides." International journal of high speed electronics and systems **11**(03): 789-848.

Takada, T., Y. Hayase, Y. Tanaka and T. Okamoto (2008). "Space charge trapping in electrical potential well caused by permanent and induced dipoles for LDPE/MgO nanocomposite." IEEE Transactions on Dielectrics and Electrical Insulation **15**(1).

Takala, M., H. Ranta, P. Nevalainen, P. Pakonen, J. Pelto, M. Karttunen, S. Virtanen, V. Koivu, M. Pettersson and B. Sonerud (2010). "Dielectric properties and partial discharge endurance of polypropylene-silica nanocomposite." IEEE Transactions on Dielectrics and Electrical Insulation **17**(4).

Tanaka, T. (2005). "Dielectric nanocomposites with insulating properties." IEEE Transactions on Dielectrics and Electrical Insulation **12**(5): 914-928.

Tanaka, T. (2010). Interface properties and surface erosion resistance. Dielectric Polymer Nanocomposites, Springer**:** 229-258.

Tanaka, T. (2016). Dielectric Breakdown in Polymer Nanocomposites. Polymer Nanocomposites, Springer**:** 113-137.

Tanaka, T., G. Montanari and R. Mulhaupt (2004). "Polymer nanocomposites as dielectrics and electrical insulation-perspectives for processing technologies, material characterization and future applications." IEEE transactions on Dielectrics and Electrical Insulation **11**(5): 763-784.

Thelakkadan, A., G. Coletti, F. Guastavino and A. Fina (2011). "Effect of the nature of clay on the thermo- mechanodynamical and electrical properties of epoxy/clay nanocomposites." Polymer Composites **32**(10): 1499-1504.

Theodosiou, K., I. Vitellas, I. Gialas and D. P. Agoris (2004). "Polymer films degradation and breakdown in high voltage AC fields." Journal of Electrical Engineering **55**(9-10): 225-2310.

Tiwari, R. R., D. L. Hunter and D. R. Paul (2012). "Extruder- made TPO nanocomposites. I. Effect of maleated polypropylene and organoclay ratio on the morphology and

mechanical properties." Journal of Polymer Science Part B: Polymer Physics **50**(22): 1577-1588.

Tjong, S., S. Bao and G. Liang (2005). "Polypropylene/montmorillonite nanocomposites toughened with SEBS- g- MA: Structure–property relationship." Journal of Polymer Science Part B: Polymer Physics **43**(21): 3112-3126.

Tokarský, J., L. Kulhánková, L. Neuwirthová, K. M. Kutláková, S. Vallová, V. Stýskala and P. Čapková (2016). "Highly anisotropic conductivity of tablets pressed from polyaniline-montmorillonite nanocomposite." Materials Research Bulletin **75**: 139-143.

Tomer, V., G. Polizos, C. Randall and E. Manias (2011). "Polyethylene nanocomposite dielectrics: implications of nanofiller orientation on high field properties and energy storage." Journal of Applied Physics **109**(7): 074113.

Ton- That, M. T., F. Perrin- Sarazin, K. Cole, M. Bureau and J. Denault (2004). "Polyolefin nanocomposites: formulation and development." Polymer Engineering & Science **44**(7): 1212-1219.

Vahedy, V. (2006). "Polymer insulated high voltage cables." IEEE Electrical Insulation Magazine **22**(3): 13-18.

Vaia, R. A. and E. P. Giannelis (1997). "Polymer melt intercalation in organically-modified layered silicates: model predictions and experiment." Macromolecules **30**(25): 8000-8009.

Vaughan, A. S., S. G. Swingler and Y. Zhang (2006). "Polyethylene nanodielectrics: the influence of nanoclays on structure formation and dielectric breakdown." IEEJ Transactions on Fundamentals and Materials **126**(11): 1057-1063.

Veenstra, H., P. C. Verkooijen, B. J. van Lent, J. van Dam, A. P. de Boer and A. P. H. Nijhof (2000). "On the mechanical properties of co-continuous polymer blends: experimental and modelling." Polymer **41**(5): 1817-1826.

Vo, L. T., S. H. Anastasiadis and E. P. Giannelis (2011). "Dielectric study of poly (styrene-co-butadiene) composites with carbon black, silica, and nanoclay." Macromolecules **44**(15): 6162-6171.

Wang, K. H., M. H. Choi, C. M. Koo, Y. S. Choi and I. J. Chung (2001). "Synthesis and characterization of maleated polyethylene/clay nanocomposites." Polymer **42**(24): 9819-9826.

Wang, S., S. Luo, Y. Tu, C. Wang and S. Qin (2017). "Effect of polarity reversal on space charge properties of CB/LDPE composite under DC field." IEEE Transactions on Dielectrics and Electrical Insulation **24**(3): 1349-1354.

Wang, V., J. Wu and Y. Yin (2017). "Nanostructures and space charge characteristics of MgO/LDPE nanocomposites." IEEE Transactions on Dielectrics and Electrical Insulation **24**(4): 2390-2399.

Wang, Y., G. Li, J. Wu and Y. Yin (2016). "Effect of temperature on space charge detrapping and periodic grounded DC tree in cross-linked polyethylene." IEEE Transactions on Dielectrics and Electrical Insulation **23**(6): 3704-3711.

Wang, Y., J. Wu and Y. Yin (2017). "Space charge behavior in low density polyethylene at low temperatures." IEEE Transactions on Dielectrics and Electrical Insulation **24**(6): 3860-3868.

Wang, Z., T. Iizuka, M. Kozako, Y. Ohki and T. Tanaka (2011). "Development of epoxy/BN composites with high thermal conductivity and sufficient dielectric breakdown strength part II-breakdown strength." IEEE Transactions on Dielectrics and Electrical Insulation **18**(6).

Wu, D., L. Wu, M. Zhang and Y. Zhao (2008). "Viscoelasticity and thermal stability of polylactide composites with various functionalized carbon nanotubes." Polymer Degradation and Stability **93**(8): 1577-1584.

Wu, K., Y. Wang, X. Wang, M. Fu and S. Hou (2017). "Effect of space charge in the aging law of cross-linked polyethylene materials for high voltage DC cables." IEEE Electrical Insulation Magazine **33**(4): 53-59.

Wu, S., Z. Tang, B. Guo, L. Zhang and D. Jia (2013). "Effects of interfacial interaction on chain dynamics of rubber/graphene oxide hybrids: a dielectric relaxation spectroscopy study." RSC Advances **3**(34): 14549-14559.

Xu, L., H. Nakajima, E. Manias and R. Krishnamoorti (2009). "Tailored nanocomposites of polypropylene with layered silicates." Macromolecules **42**(11): 3795-3803.

Yano, K., A. Usuki, A. Okada, T. Kurauchi and O. Kamigaito (1993). "Synthesis and properties of polyimide–clay hybrid." Journal of Polymer Science Part A: Polymer Chemistry **31**(10): 2493-2498.

Yin, Y., X. Dong, Z. Li and X. Li (2007). The effect of electrically prestressing on DC breakdown strength in the nanocomposite of low-density polyethylene/nano-SiOx. Solid Dielectrics, 2007. ICSD'07. IEEE International Conference on, IEEE.

Yuanxiang, Z., Z. Jiankang and L. Rui (2014). "Key technical analysis and prospect of high voltage and extra-high voltage power cable." High Voltage Engineering **40**(9): 2593-2612.

Zaikin, A., R. Karimov and V. Arkhireev (2001). "A study of the redistribution conditions of carbon black particles from the bulk to the interface in heterogeneous polymer blends." Colloid Journal **63**(1): 53-59.

Zaikin, A., E. Zharinova and R. Bikmullin (2007). "Specifics of localization of carbon black at the interface between polymeric phases." Polymer Science Series A **49**(3): 328-336.

Zakrevskii, V., N. Sudar, A. Zaopo and Y. A. Dubitsky (2003). "Mechanism of electrical degradation and breakdown of insulating polymers." Journal of applied physics **93**(4): 2135-2139.

Zazoum, B., E. David and A. D. Ngô (2013). "LDPE/HDPE/clay nanocomposites: effects of compatibilizer on the structure and dielectric response." Journal of Nanotechnology **2013**.

Zazoum, B., E. David and A. D. Ngô (2014). "Correlation between Structure and Dielectric Breakdown in LDPE/HDPE/Clay Nanocomposites." ISRN Nanomaterials **2014**.

Zazoum, B., E. David and A. D. Ngô (2014). "Structural and dielectric studies of LLDPE/O-MMT nanocomposites." Transactions on Electrical and Electronic Materials **15**(5): 235-240.

Zeller, H., P. Pfluger and J. Bernasconi (1984). "High-mobility states and dielectric breakdown in polymeric dielectrics." IEEE Transactions on Electrical Insulation(3): 200-204.

Zhang, D.-L., J.-W. Zha, C.-Q. Li, W.-K. Li, S.-J. Wang, Y. Wen and Z.-M. Dang (2017). "High thermal conductivity and excellent electrical insulation performance in double-percolated three-phase polymer nanocomposites." Composites Science and Technology **144**: 36-42.

Zhang, K., L. Li, L. Zhong, L. Cao, M. Xu, G. Chen and M. Fu (2016). DC dielectric properties of thermo-plastic polyolefin materials. Electrical Insulation and Dielectric Phenomena (CEIDP), 2016 IEEE Conference on, IEEE.

Zhang, Y., J. Lewiner, C. Alquie and N. Hampton (1996). "Evidence of strong correlation between space-charge buildup and breakdown in cable insulation." IEEE Transactions on Dielectrics and Electrical Insulation **3**(6): 778-783.

Zhou, Y., J. Hu, X. Chen, F. Yu and J. He (2016). "Thermoplastic polypropylene/aluminum nitride nanocomposites with enhanced thermal conductivity and low dielectric loss." IEEE Transactions on Dielectrics and Electrical Insulation **23**(5): 2768-2776.

Zhu, J., A. B. Morgan, F. J. Lamelas and C. A. Wilkie (2001). "Fire properties of polystyrene−clay nanocomposites." Chemistry of Materials **13**(10): 3774-3780.

Zou, C., J. C. Fothergill and S. W. Rowe (2007). A" water shell" model for the dielectric properties of hydrated silica-filled epoxy nano-composites. Solid Dielectrics, 2007. ICSD'07. IEEE International Conference on, IEEE.